Tao Zhang

INTELLIGENT ALGORITHMS OF A REDUNDANT ROBOT SYSTEM IN A FUTURE FUSION REACTOR

ACTA UNIVERSITATIS LAPPEENRANTAENSIS 965

Tao Zhang

INTELLIGENT ALGORITHMS OF A REDUNDANT ROBOT SYSTEM IN A FUTURE FUSION REACTOR

Dissertation for the degree of Doctor of Science (Technology) to be presented with due permission for public examination and criticism in Lappeenranta-Lahti University of Technology LUT, Lappeenranta, Finland on the 14th of May 2021, at noon.

The dissertation was written under a joint doctorate agreement between Lappeenranta-Lahti University of Technology LUT, Finland and the University of Science and Technology of China, China and jointly supervised by supervisors from both universities.

Acta Universitatis
Lappeenrantaensis 965

Supervisors Professor Heikki Handroos
LUT School of Energy Systems
Lappeenranta-Lahti University of Technology LUT
Finland

Adjunct professor Huapeng Wu
LUT School of Energy Systems
Lappeenranta-Lahti University of Technology LUT
Finland

Professor Yuntao Song
Institute of Plasma Physics
Chinese Academy of Science, China

Professor Biao Shen
Institute of Plasma Physics
Chinese Academy of Science, China

Reviewers Associate Professor Xuping Zhang
Department of Mechanical & Production Engineering
Aarhus University Denmark

Adjunct Professor Rainer Palm
School of Science and Technology
Örebro University Sweden

Opponents Associate Professor Xuping Zhang
Department of Mechanical & Production Engineering
Aarhus University Denmark

Adjunct Professor Rainer Palm
School of Science and Technology
Örebro University Sweden

ISBN 978-952-335-663-4
ISBN 978-952-335-664-1 (PDF)
ISSN-L 1456-4491
ISSN 1456-4491

Lappeenranta-Lahti University of Technology LUT
LUT University Press 2021

Abstract

Tao Zhang
Intelligent algorithms of a redundant robot system in a future fusion reactor
Lappeenranta 2021
67 pages
Acta Universitatis Lappeenrantaensis 965
Diss. Lappeenranta-Lahti University of Technology LUT
ISBN 978-952-335-663-4, ISBN 978-952-335-664-1 (PDF), ISSN-L 1456-4491, ISSN 1456-4491

A fusion reactor, also called a thermonuclear reactor, is a large-scale of size device to produce electrical power from the energy released in a nuclear fusion reaction, in which the environment is very hot and radioactive, requiring regular maintenance during the fusion process. A remote handling robotic system is an effective and economic device to promote quality and reduce the time needed for maintenance inside the reactor. This dissertation deliberated the intelligent algorithms to solve the deformation, kinematics and safety, which improves the performance of robotic systems during the maintenance process.

The maintenance robots designed normally have a redundant long mechanism. Due to the complex environment inside a fusion reactor, working within the reachable workspace and maintenance accuracy are highly demanding for the robot. The robotic problems in the fusion reactor environment are complicated, and free motion models are highly non-linear. Artificial intelligent algorithms are investigated in this study to find a solution for the problems. such as ant colony optimization (ACO), recurrent neural network (RNN) and perceptron, and finally a robot model is optimized to promote robot motion accuracy and prevent it from collision.

In order to work well within the robot's reachable workspace in fusion reactors, the robot is designed as a redundant mechanism with a long arm. The thesis focuses on three aspects of redundant long manipulators: deflection compensation, collision free and safe motion, and robot calibration. First, the flexible sag of the robot affects robot accuracy, and it is difficult to be modelled by a physical model. A feasible solution based on RNN for deformation compensation was developed as part of this thesis. The RNN has a "memory" function which can predict the deformation of the segment of the robot to reduce the error of the redundant robot motion. Second, the redundant robot's kinematics is a high-dimension and nonlinear problem, and an analytical method cannot solve this problem directly. A dynamic accuracy colony optimization (DAACO) method was designed, which refers to an evolution theory optimizing ACO by dynamic accuracy. This promotes the accuracy and speed of solving the nonlinear formulation of redundant robot kinematics. Furthermore, a collision detection algorithm to check whether the robot would collide with the fusion device was designed using grey information from the robot's section plane. Additionally, the motion safety of a double arm robot in the reactor vacuum is studied. A hybrid collision classifier was designed by the perceptron from the robot sensor/signal data such as the position, speed and current. The data used for the

training perceptron was pre-processed by using primary component analysis (PCA) and dimension reduction technology to simplify the classification in the perceptron. Third, the motion accuracy of the robot can be improved by calibrating the kinematic parameters. While the robot is planned in joint space independently, a specific trajectory of the slave robot's end frame forms a group of circle curves that can be fitted by a geometric algorithm to calibrate the kinematic parameters. This geometric calibration algorithm uses the least square method and 3σ rules to ensure the calibration result's uniqueness and optimality.

Keywords: gravity compensation, redundant heavy robot, dual arm robot, collision detection, ant colony optimization, robot kinematics, primary component analysis, perceptron

Acknowledgements

This study was carried out at the department of LUT School of the Energy System at Lappeenranta University of Technology (LUT), Finland and the University of Science and Technology of China (USTC), China from 2017 to 2020. I am extremely grateful that I have been accepted as a double degree student in these two schools, which are the world-famous. In LUT, I would like to extend my appreciation to the highly professional team in my lab and department.

Firstly, I would like to thank my two tutors in LUT , Huapeng Wu and Heikki Handroos. I am extremely grateful for their professional training in research work and for the practical hands on knowledge they taught me. Additionally, my tutor Huapeng Wu and his wife Mrs. Liu also helped me a lot in my daily life especially in my fresh days in Finland. Secondly, I would like to thank my Chinese tutor Yuntao Song. He encouraged me to apply to study in Finland and always encouraged me to do the lastest research. Thirdly, I would like to thank Roger in Race, UK. He gave me a great deal of professional advice for my research and papers although he is not my tutor in the common sense. Fourthly, I deeply appreciate Sari who is always kind. I am a foreign student at LUT and sometimes I am not familiar with the procedures about doctoral issues. She always gave me help patiently. Fifthly, I would like to thank Juha who was very kind and helped me a lot with the robot experiments and office issues in our lab. Moreover, I would like to thank all professors who taught me lessons, for example, Harri Eskelinen, Aki Mikkola, Jussi Sopanen, Lasse Lensu, Heikki Haario, Peter Jones, Rafal Jastrzebski and many more.

I would also like to express my sincere thanks to my colleagues and friends. I would especially like to mention my best friend in Finland, Chanyang Li. He was my student tutor when I came to LUT and sometimes cooked delicious meals for me. Secondly, I would like to mention my roommate Lauri, a Finnish gentleman. We discussed so many topics ranging from culture to food. It has been unforgettable time for me. Thirdly, I would like to mention my group of close friends which is Xinxin Yu, Libo Zhu, Meichun Wang, Marko, Ming Li, Yunxi Liu, Haibiao Ji, Ruochen Yin, Binyan Mao, Songxiong, Qifeng Hao, Chao Gao, Mingwei Sun, ans Xiaoyi Chen. I really miss the regular party on every Friday. Fourthly, I should appreciate my best Russian friend Victor. We talked about lots of different topics about life and philosophy. He is a handsome and brilliant man. Fifthly, I would like to mention my close friends Anya, Gloria, Mariona and Heloise. We always studied together to solve difficult tasks. Finally, I would like to mention my colleagues in our lab Amin Hekmatmannesh, Yashar Shabbouei Hagh, Hamid Roozbahani and Dmitrii Motorin.

Moreover, I would like to express my gratitude to my parents and my relatives. They have always stood with me to overcome any difficulties, no matter what in life and study. They encouraged me to be a better man.

Thanks.
Tao Zhang
August 2020
Hefei, China

To Dedication

This page is reserved for optional dedication. This page can be removed, if not used.
If this section is removed, then do not remove the section break at the end of the Acknowledgements.

Contents

List of publications

This dissertation is based on the following papers. The rights have been granted by publishers to include the papers in dissertation.

This dissertation contains material from the following papers. The rights have been granted by publishers to include the material in dissertation.

I. Zhang, Tao, Yong Cheng, Huapeng Wu, Yuntao Song, Sheng Yan, Heikki Handroos, Lei Zheng, Haibiao Ji, and Hongtao Pan. 2020. Dynamic accuracy ant colony optimization of inverse kinematic (DAACOIK) analysis of multi-purpose deployer (MPD) for CFETR remote handling. *Fusion Engineering and Design*, 156: 111522.

II. Zhang, Tao, Yuntao Song, Huapeng Wu, and Qi Wang. A novel method to identify DH parameters of the rigid serial-link robot based on a geometry model. *Industrial Robot: the international journal of robotics research and application*, 48: 157-167.

III. Tao, Zhang, Yuntao Song, Huapeng Wu, Lei Zheng, Yong Cheng, Heikki Handroos, Xuanchen Zhang, and Haibiao Ji. 2020. Hybrid collision detection perceptron of the robot in the fusion application. *Fusion Engineering and Design*, 160: 111800.

IV. Zhang, Tao, Yuntao Song, Huapeng Wu, Heikki Handroos, Yong Cheng, and Xuanchen Zhang. 2019. Deformation modeling of remote handling EAMA robot by recurrent neural networks. *Industrial Robot: the international journal of robotics research and application*, 46: 300-10.

Author's contribution

Publication I:

I am the principal author and investigator of this paper. The dynamic accuracy concept is designed to optimize the traditional ant colony optimization method both for the solving speed and accuracy. This original concept adopts the theory of evolution concept which is a bio-mimetic form of modelling. This algorithm is an appropriate application for non- linear problems.

Publication II:

I am the principal author and investigator of this paper. The robot's joint determines its motion features, for example rotation and prismatic movement. The specific motion or trajectory always includes some special geometric features which are related to the robot's kinematic parameters. Creating a mathematical model of the robot with these

geometric features together with the least squares method can determine the robot kinematic parameters uniquely. This method has no singularity and is faster at solving motion-related problems especially for the redundant robots.

Publication III:

I am the principal author and investigator of this paper. The hybrid perceptron is a model- free method basing on supervised machine learning. This method avoids complex dynamic modelling of the robot. It can detect collisions and has a big advantage in an un- known atmosphere.

Publication IV:

I am the principal author and investigator of this paper. The elastic joints and imperfection of assembly determine the flexibility of an EAMA robot. The motion transfer of segment is driven by corresponding cables. The cables deform when loaded with the force. How- ever, this deformation has a “memory function” based on an elastic mechanism. The recurrent neural network has large advantages concerning the “memory function” in the prediction problem. This modeling method can solve this deformation effectively.

Other scientific publications:

Liu, J., Lu, K., Pan, H., Cheng, Y., Zhang, T., Yao, Z. (2020). Vision-based tile recognition algorithms for robot grasping task in EAST. *Fusion Engineering and Design*, 152, 111422. doi:10.1016/j.fusengdes.2019.111422

Wu, J., Wu, H., Song, Y., Zhang, T., Zhang, J., Cheng, Y. (2018). Adaptive Neuro-fuzzy inference system based estimation of EAMA elevation joint error compensation. *Fusion Engineering and Design*, 126, 170-173. doi:10.1016/j.fusengdes.2017.11.025

Zhang, T., Zhang, X., Wang, L., Pan, H., Zheng, L., Cheng, Y., Wu, J. (2017). ASIPP remotely operated vehicle design (ROV) and feasibility study. *IOP Conference Series: Earth and Environmental Science*, 69, 012133. doi:10.1088/1755-1315/69/1/012133

Nomenclature

In the present work, variables and constants are denoted using *slanted style*, vectors are denoted using **bold regular style**, and abbreviations are denoted using regular style.

Latin alphabet

c_i^j	the choice of a solution component	–
$\mathcal{S}^p$	the partial solusion in p-dimension space	–
$\mathcal{R}$	component set	–
p	transition probabilities	–
$G(X)$	the cost function	–
f_i	the nonlinear restriction condition	–
X	the optimal solutions in ant colony optimization	–
χ	the input space	–
Y	the output space	–
$\mathcal{R}^k$	k-dimensional space	–
b	intercept	–
x	x-coordinate (width)	m
y	y-coordinate (depth)	m
z	z-coordinate (height)	m
T	the aim/requirement of accuracy	–
q	joint vector	deg
J	inertia of the robot dynamic equation	–
$C(q, \dot{q})$	Coriolis and centrifugal forces of the robot dynamic equation	–
$D(\dot{q})$	friction of the robot dynamic equation	–
$G(q)$	gravity of the robot dynamic equation	–
$f_{mod}(q, \dot{q})$	model of nonlinearities	–
$u(q, \dot{q}, \ddot{q})$	control law	–

Greek alphabet

α	(alfa) Euler angle in x axis
α	(alfa) the relative importance of pheromone value
β	(beta) Euler angle in y axis
β	(beta) the relative importance of heuristic information
γ	(gamma) Euler angle in z axis
θ	(theta) joint angle of robot
ω	(omega) weight vector
$\widehat{\omega}$	(omega) the orientation of coordinate frame i relative to coordinate frame j
τ_i^j	(tau) the pheromone trail parameter corresponding to flexible solutions c_i^j
η	(eta) heuristic information
τ	(tau) generalized forces

Abbreviations

CFETR	Chinese fusion engineering testing reactor
MM	manual maintenance
RH	remote handling
EAST	Experimental Advanced Superconducting Tokamak
EAMA	EAST articulated maintenance arm
ITER	International Thermonuclear Experimental Reactor
JET	Joint European Torus
VTT	Valtion Teknillinen Tutkimuskeskus
WEST	Tungsten (chemical symbol "W") Environment in Steady-state Tokamak
MPD	multi-purpose deployer
RP	research problem
DAACO	dynamic accuracy ant colony optimization
RMM	resolved motion method
EJM	extended Jacobian method
PSO	particle swarm optimization
NN	neural network
ACO	Ant Colony Optimization
AA	algorithm accuracy
II	iteration index
IN	iteration number
PCA	primary component analysis
PSD	position sensitive detectors
RNN	recurrent neural network
CPC	complete and parametrically continuous
POE	product of exponentials
BPNN	backpropagation neural network

1 Introduction

1.1 Research Background

The fusion reactor is a kind of magnetic-control confinement device. The fusion reaction with high temperature and high radiation will occur in the device, and may cause damage to the internal components of the device. Therefore, the regular maintenance is desperately needed. (Luo et al., 2007; Schlosser et al., 2005; Liu et al., 2020). However, manual repair is not efficient. Remote handling is important in the maintenance of devices.

Fusion reactors can be classified in three generations based on their level of technical maturity as: experimental fusion reactors, test fusion reactors and commercial fusion reactors (Buckingham and Loving, 2016; Raimondi, 1983; Rolfe et al., 1999; Rolfe, 1999; Rolfe and Team, 1998; Rolfe, 2007; David et al., 2005; Friconneau et al., 2011). The first generation are experimental fusion reactors that aim to explore the feasibility of the tokamak's engineering foundation. There are numerous fusion experimental reactors around the world, for example, J-Demo in Japanese, K-Demo in Korea, European DEMO, EAST in China and so on. With technology developing, a number of test reactors have been con- structed recently. ITER is a multi-party fusion device project, and the related research topics have been assigned to the corresponding member countries or organizations for design. The ITER organization (Council et al., 2008; Maruyama et al., 2015; Tada et al., 1998; Nakahira et al., 2009; Choi et al., 2015; Manuelraj et al., 2016; Noguchi et al., 2018; Chakraborty et al., 2010; Ferlay et al., 2013) is a transnational cooperation project that has a group of members including: the EU, the US, China, Japan, Indian, Korea and Russia, which aims to achieve sustainable fusion reactions and greater power from the device. At the same time, China is building its own fusion reactor named CFETR (Chinese Fusion Engineering Testing Reactor) (Zhuang et al., 2019). The testing reactor is a milestone for the commercial application of fusion technology. A commercial fusion re- actor is a future device, which will be a low radiation and clean nuclear reactor compared to fission reactors. However, the extreme conditions, such as the temperature, radiation, electromagnetism and vacuum require a complicated mechanism. The CFETR is designed as shown in Figure 1.1. The CFETR has six main components: a cryostat, cold shield, vacuum vessel, divertor, blanket and magnets and its functions are shown below.

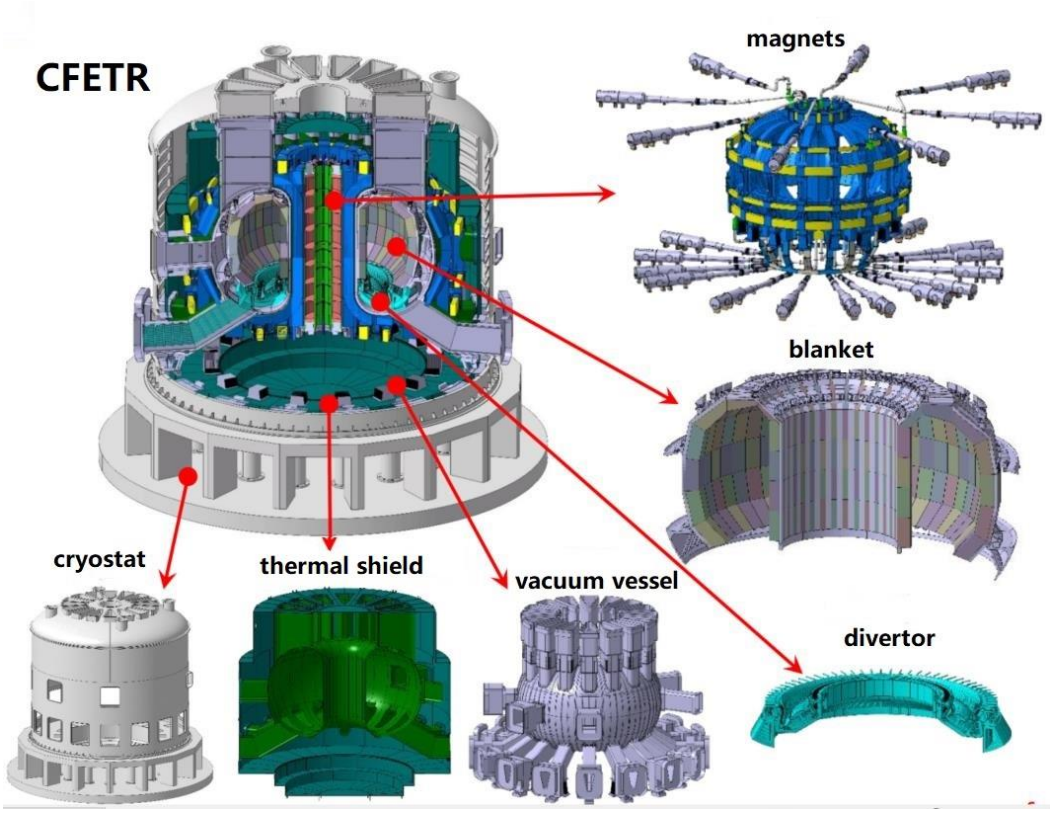

Figure 1.1: The CFETR and its components.

- cryostat: an external structural support for other components which is a vacuum shell and radiation shield between the inner reaction atmosphere and the outer surroundings;
- thermal shield: a cooling device which absorbs the reaction heat to control fusion experimental temperature conditions;
- vacuum vessel: a structural support for the device's ports which can shield some of the radiation from the reaction;
- divertor: a device to remove impurities from the plasma and remove helium ash;
- blanket: a device to achieve the tritium breeding and cool the device;
- magnets: a device to provide the necessary magnetic field of fusion reaction.

1.2 Status of Remote Handling System in Fusion Reactors

International studies on fusion remote handling maintenance were carried out at the beginning of this century and in the 1980s. This section will present the relevant fusion remote handling designs as well as their control methods and maintenance strategies of related organizations.

1.2.1 JET（Joint European Torus）Remote Handling System

The international remote handling system has an early start, dating back to the remote handling of the JET device in 1983. In 1998, the fusion remote handling device was firstly tested in the JET device. By upgrading the existing device and designing the mature first-generation robotic arm at the beginning of this century, the main arm is a hinged robotic arm with a total length of 10 m and 19 degrees of freedom, and the device is shown in Figure 1.2.

The device is equipped with a maintenance robot arm, Mascot, which is the core component of the JET robot arm and equipped with cameras, infrared light sources and hand claws to perform complex maintenance operations. Figure 1.3 shows a diagram of the Mascot unit, modular design, to cope with different remote handling requirements.

The Mascot device has also been updated to version 6, and intelligent algorithms have been added to optimize maintenance strategy, thus improving its safety and reliability. Mascot robots use the master-slave control (Figure 1.4), where the operator operates from control room and the slave robots inside the device move in response to the movement of the master robot. This approach is extremely demanding in terms of personnel operation with poor control and low intelligence.

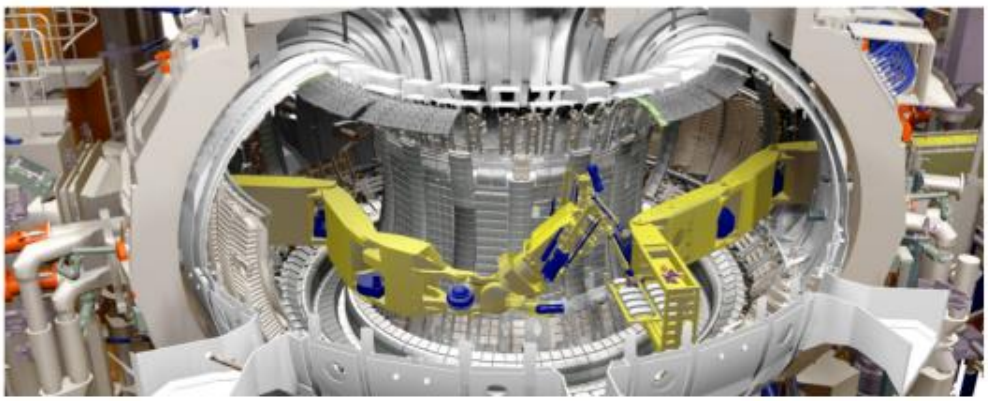

Figure 1.2: JET device remote handling system (Buckingham and Loving, 2016)

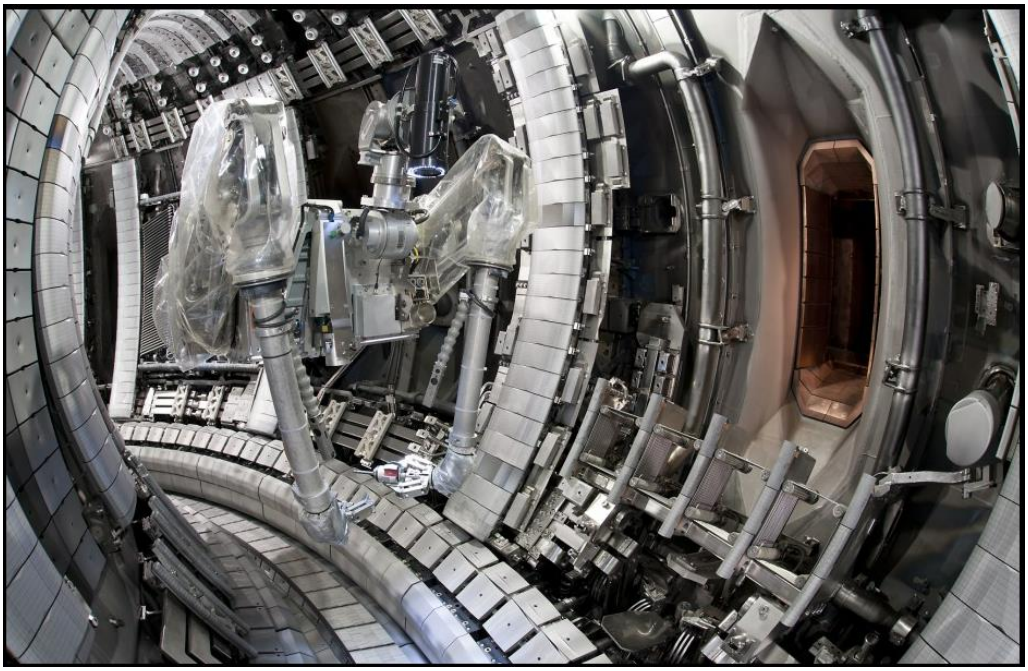

Figure 1.3: JET device end dual arm system Mascot (Wikipedia, 2021)

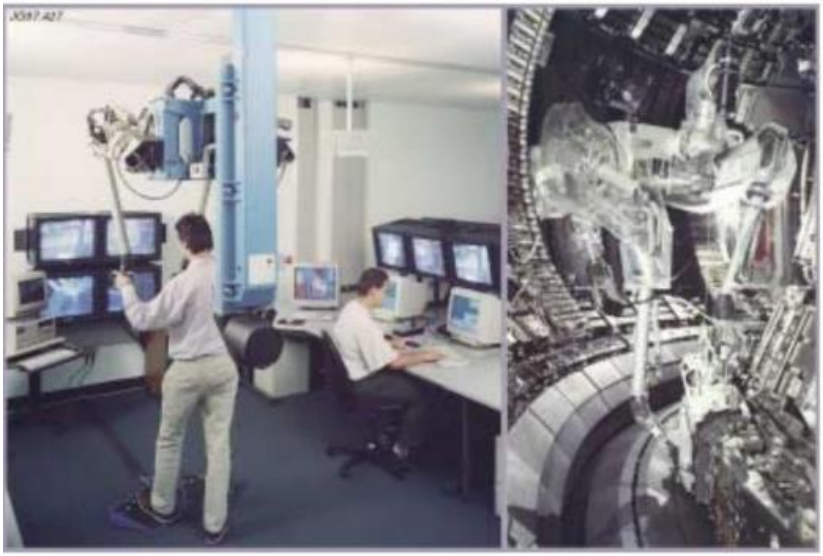

Figure 1.4: JET remote handling master-slave control mode (Rolfe, 1999)

1.2.2 ITER (International Thermonuclear Experimental Reactor) Remote Handling System

The ITER remote handling system is the world's largest existing remote handling system, and the requirements for the remote handling systems are very strict due to the complex structure of ITER. The design parameters of both ITER and JET remote handlings are shown in Table 1.1.

Table 1.1: Comparison of ITER and JET parameters (Pan, 2017)

	Manual maintenance (MM) mode	Remote handling (RH) mode
Working mode	Non-vacuum shutdown maintenance.	The inner peep is stopped under vacuum, other maintenance is stopped under non-vacuum conditions
Working environment	6m diameter vacuum, radiation dose 10mGy/h.	Vacuum with 12m diameter, radiation dose 10mGy/h.
Maintenance	All components in the vacuum.	All parts inside the vacuum, all parts inside the neutral beam and hot cell, parts inside the cryostat, and parts related to the transfer channel.
Remote handling tasks	Removal/replacement of parts (10g~350kg), 2D/3D measurement, visual and radiological detection, welding, cutting, cleaning, cable and pipe handling, fault recovery of teleoperated equipment, etc.	Removal/replacement of parts (1kg~11,000kg), 2D/3D measurement, visual and radiological detection, welding, cutting, cleaning, cable and pipe handling, fault recovery of remotely operated equipment, scrap packing.

The ITER remote handling system is a systematic remote handling system. As shown in Figure1.5, the current ITER remote handling systems include: the divertor RH system, the blanket RH system, the hot cell RH and the multi-purpose deployer system, the transfer cask system, the vessel viewing system, and the neutral beam cell RH system.

1.2.2.1 ITER Divertor Remote Handling System

The divertor directly faces the high-temperature plasma and provides a partial neutron shielding function. The remote handling system is led by VTT (Valtion Teknillinen Tutkimuskeskus), with the joint participation of the Intelligent Hydraulics and Automation Research Unit of Tampere University of Technology and Lappeenranta University of Technology from Finland. The robot is driven by water hydraulics to avoid

contamination of the unit by liquids in the event of a leak or pipe rupture. The project started in 1994, and the current composition of the remote handling system for the deflector is shown in Figure 1.6. The current divertor remote handling consists of the transfer cask system (TCS), the cassette multifunctional mover (CMM) and the cassettes toroidal mover (CTM). The remote handling and maintenance process of the divertor is as follows: the CTM enters the vacuum and removes the corresponding module to the RH Port using the ring track, carried by the CMM system, then to the TSC and to the hot cell for replacement.

The CMM system is the actuator for the remote handling of the deflector and consists of the front-end actuator, the SCEE, the auxiliary degree of freedom hydrodynamic robot arm WHMAN and the CMM body, as shown in Figure 1.7. The maintenance process is as follows: the WHMAN performs the corresponding dismantling work. After the dismantling is completed, the CMM robot performs the transfer, as shown in Figure 1.8. The CMM system uses rail for rough positioning, and the mainstream common maintenance strategy for industrial robots is used for fine maintenance.

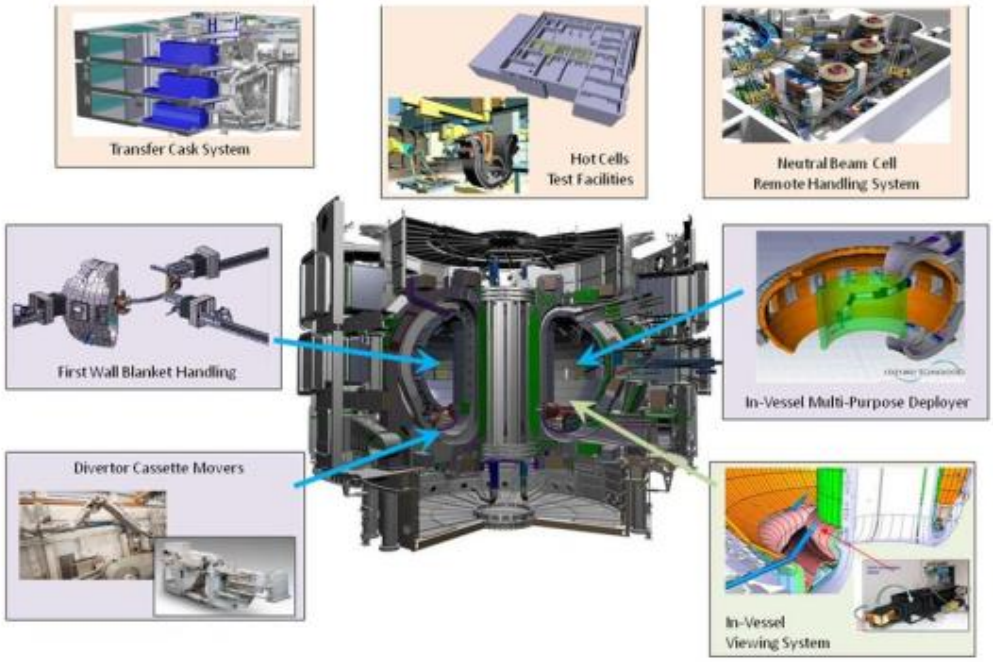

Figure 1.5: ITER remote handling system (Izard, 2013)

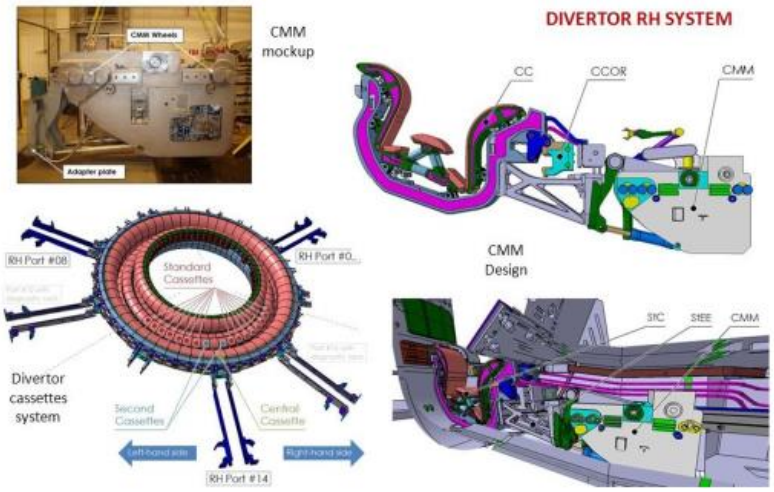

Figure 1.6: ITER divertor remote handling system. (Tesini, 2015)

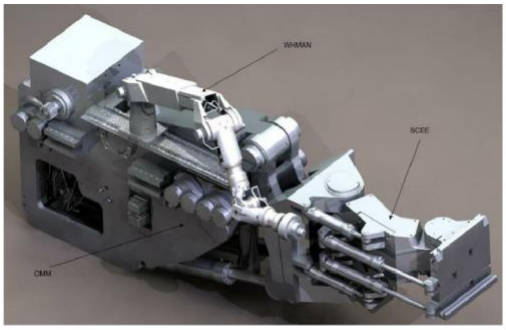

Figure 1.7: CMM system composition. (Siuko, 2021)

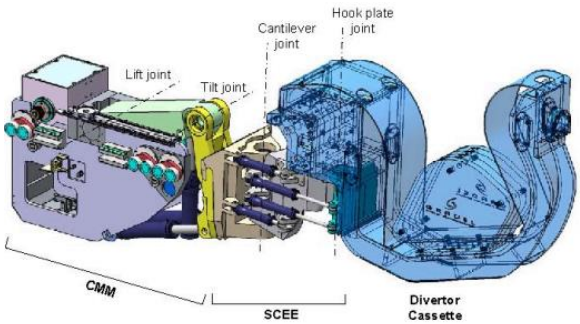

Figure 1.8: CMM system working principle. (Esque , 2007)

1.2.2.2 ITER Blanket Remote Handling System

The blanket is the component that provides the necessary elements such as neutrons and tritium for the fusion reaction to achieve multiplication. It has a large number of cooling circuits that can heat the fusion reaction out of the vacuum to cool the device. The blanket remote handling system was designed by the Japan atomic energy research institute and two technical lines are designed according to the size of the blanket module. The small blanket blocks are installed and removed using railcars and then transported out of the windows (Figure 1.9a). Large blanket modules are maintained by top lifting as shown in Figure 1.9b. Currently, the maintenance strategy of the blanket has been developed, but the control algorithms related to its maintenance strategy have not been designed, such as the lifting strategy and path planning for blanket maintenance replacement, and the algorithm for the cooperative maintenance strategy of multiple blankets.

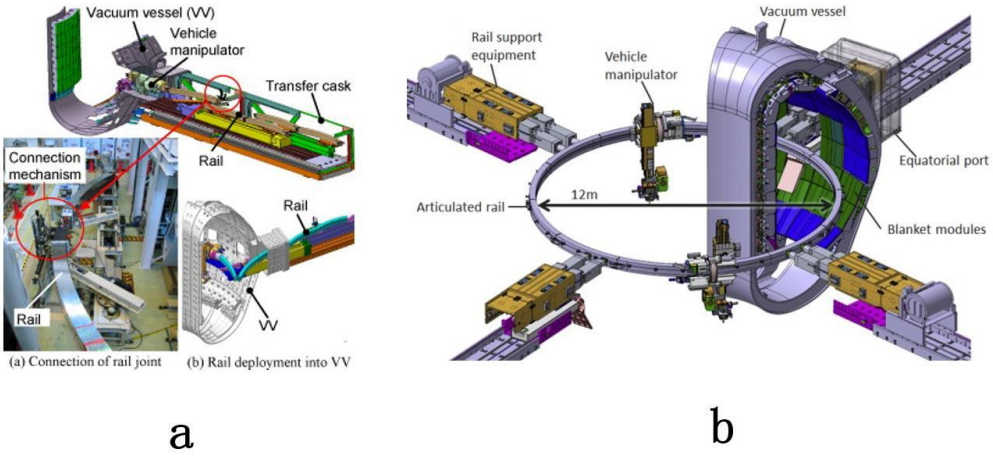

Figure 1.9: ITER blanket remote operating system - blanket solution. (Noguchi, 2018; Ribeiro, 2011)

1.2.2.3 Multi-Purpose Deployer

The multi-purpose deployer (MPD) is a multi-degree-of-freedom long-cantilever robot for the ITER remote handling. The cask unit and the dual-arm robot at the end of the MPD are deployed to perform maintenance on the ITER blanket and deflector (Figure 1.10). As shown in Figure 1.11, the MPD robot has nine rotary joints and one translational joint, with flanges at the end joints to connect the two-armed robot. The main maintenance of the MPD system includes the picking up vacuum debris, the replacing internal components, etc. The load is 2000 kg, the maximum speed is 100mm/s, and the end positioning accuracy is ±10mm, covering a section of the vacuum with a working range of ±60 degrees. The MPD system adopts the way of large arm to get the initial positioning and small arm to perform fine maintenance, which can reduce the difficulty of remote handling and maintenance. The MPD system is equipped with a camera at the end of the

robot to monitor the vacuum in time. The robot arm will be returned to the CASK and removed during shutdown to ensure the closed vacuum required for the discharge of the experimental device.

The MPD robot is a multi-degree-of-freedom tandem robot, and less research has been carried out on long-cantilever multi-degree-of-freedom robots. The research on trajectory and path planning, the obstacle avoidance, and the collision of MPD robots has been started at the ITER, but there is no published work on this topic so far.

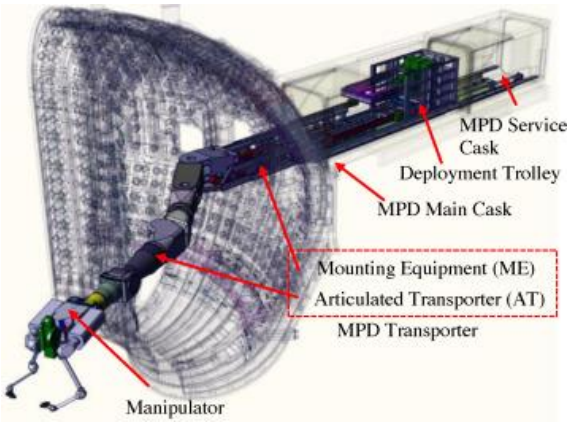

Figure 1.10: Multi-purpose deployer. (Choi et al., 2015)

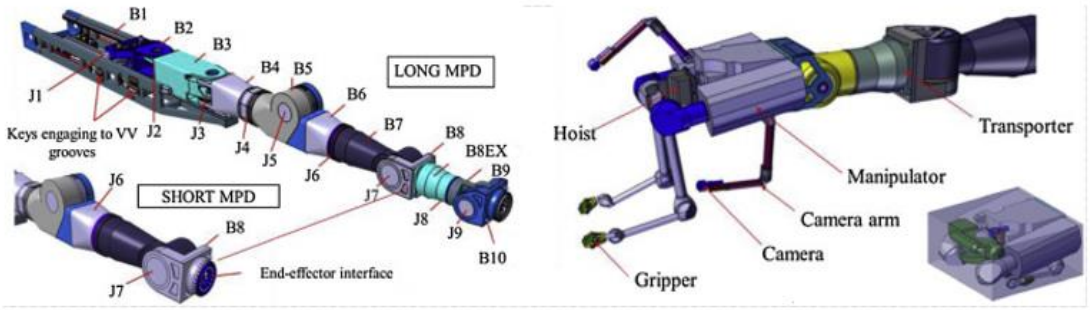

Figure 1.11: MPD and dual-arm robot. (Choi et al., 2015)

1.2.2.4 ITER Neutral Beam Remote Handling System

The neutral beam provides high power auxiliary heating and drive current to the tokamak unit. The neutral beam remote handling system is designed with a high capacity lifting mechanism and special robots for efficient maintenance of the device. Figure 1.12 shows the current remote handling scheme of the ITER neutral beam remote handling system. The remote handling and maintenance of the neutral beam currently adopts the manual

deployment of maintenance work, and no fully automated intelligent maintenance strategy has been designed. So, the degree of intelligence is low.

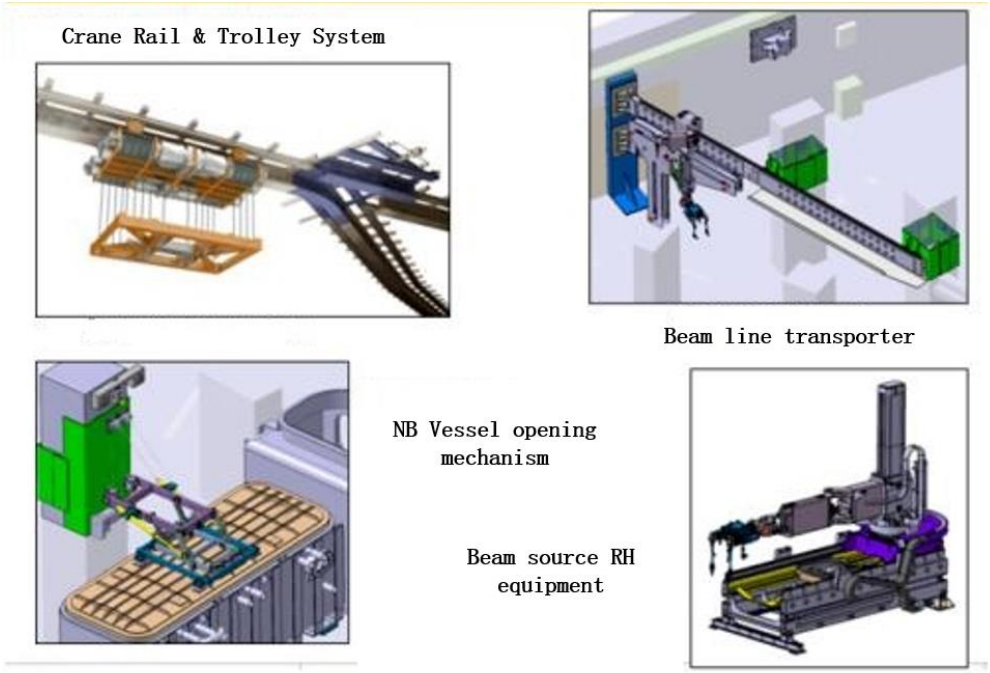

Figure 1.12: ITER neutral beam remote handling system. (Tesini, 2015)

1.2.2.5 ITER Hot cell Remote Handling System

The hot cell is an annex connected to the tokamak hall, and its main purpose is to provide a place for the refurbishment and the transfer of components inside the vacuum that may be activated. The hot cell is equipped with a variety of robots to clean and maintain the stored and disassembled radioactive internal components. The hot cell is essentially a large, low-radiation repair shop. The remote operation of the hot cell includes the AGV technology for the indoor positioning, the indoor drone technology for observation, and the robotic industrialization technology for cutting, the polishing equipment and the parts' replacement.

1.2.2.6 ITER Transfer Vehicle Remote Handling System

The transfer vehicle remote handling system is a mobile leak-proof device. When a corresponding part is removed from the vacuum window, the transfer vehicle will transfer the part to the maintenance point located in the hot room hall. The truck remote handling system consists of three subsystems: 1) a mobile cart equipped with an isolated box for loading the parts in order to avoid contact with the outside world; 2) a docking interface

for the internal parts transfer; and 3) an air transfer system for sending and receiving signals to drive the cart movement. The design concept of the teleoperated system of the transfer vehicle is shown in Figure 1.13. The nature of the transfer vehicle is an AGV system, which is mainly studied for the path planning and the trajectory planning in the environment of fusion industrial park. The geographic environment of the fusion industrial park is simpler than the outdoor city streets, so the intelligent algorithm design direction is safe and efficient path decision.

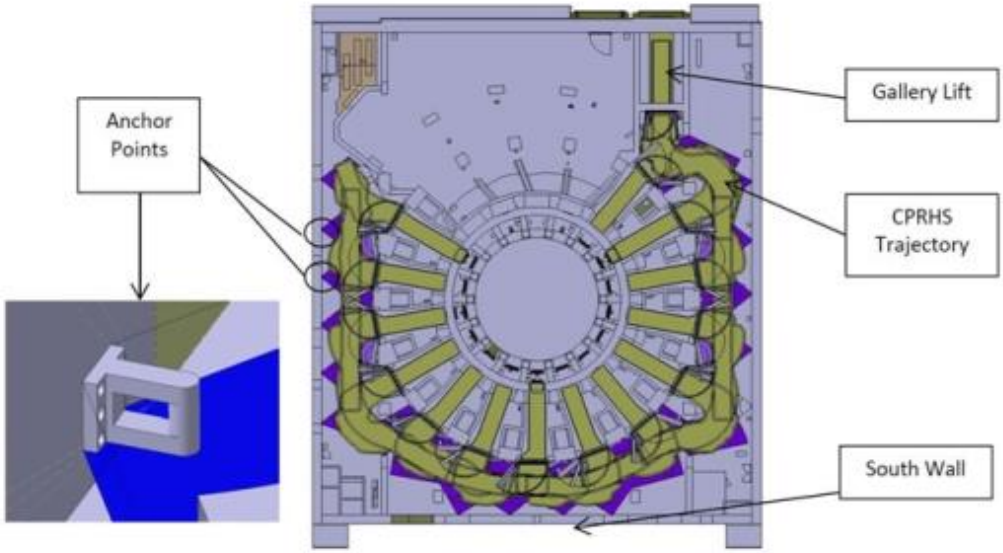

Figure 1.13 ITER transfer vehicle remote handling system. (Tesini, 2015)

1.2.3 Other Fusion Robots

The articulated inspection arm (AIA) is a hinged robot proposed by the French atomic and alternative energy commission (CEA), as shown in Figure 1.14. It is driven by a wire rope, has low positioning accuracy and is only used for internal inspection. The AIA has been used for the fusion device WEST (Tungsten (chemical symbol "W") Environment in Steady-state Tokamak) and the fusion device EAST (Experimental Advanced Superconducting Tokamak) endoscopy experiments. Because of the low motion accuracy, the motion planning is usually supplemented by automatic planning and dominated by manual remote control.

Figure 1.14 AIA remote handling robot. (Pan, 2017)

The AIA robot uses the vision-assisted manual remote control. The robot adopts a wire rope structure causes a large amount of flexible deformation. The gravity compensation algorithm designed by Energid company with open-loop compensation has an accuracy of 20 *mm*, and it is only used for manually controlled endoscopic inspection with a low degree of intelligence.

1.3 Related Platform about My Own Research

In the past, a manual maintenance mode was adopted to maintain the device, which is a time consuming and poorly effective method. Using intelligent computer methods, maintenance can be carried out using a remote handling mode (Song et al., 2014; Chen et al., 2014a; Wei et al., 2015; Zhao et al., 2019, 2015; Muhammad et al., 2007; Nieminen et al., 2009; Gonzalez Gutierrez et al., 2010). The features of the two different mode are shown in Table 1.2. RH mode can maintain devices in the vacuum conditions and it has a better economic performance for long-term experiments (Batistoni et al., 2017).

Table 1.2: The difference between RH and MM modes

	Manual maintenance (MM) mode	Remote handling (RH) mode
Working conditions	Repairmen need to go into the reactor to inspect and maintain it	A robot can inspect the device and do some maintenance
Vacuum Environment	Non-vacuum environment	Vacuum
effectiveness	Effectiveness	Highly effectiveness
Time cost	Long time	Short time
Financial cost	High cost of repair	High cost of designing RH robot but low cost of repair

In China, in the last 10 years, some researchers have also started to study robot and motion algorithms for EAST and CFETR maintenance (Lin et al., 2015; Yang et al., 2016b; Shi et al., 2016; Peng et al., 2010; Wang et al., 2017b; Zhang et al., 2019b; Wu et al., 2018, 2016; Pan et al., 2018). These algorithms have been applied in two robots: the EAST Articulated Maintenance Arm (EAMA) and the Multi-Purpose Deployer (MPD).

The EAMA is an inspection robot for the EAST device. This robot has 7 dofs in the main body which is equipped with a 3-DOF gripper as shown in Figure 1.15. Related parameters are listed in Table 1.3. Many parts in the robot result in an incorrect positioning, for example, the torsion of the motor axes, as well as friction, torsion and backlash in the gears, and elasticity of the links. The EAMA is a large, heavy, long but flexible beam arm. A deformation compensation algorithm is necessary to promote accuracy.

Table 1.3: The parameters of EAMA

Item	Parameters
Temperature	running: 80℃; baking 120℃
Dimension	radius: 160mm; length: 8.8m
DOF	1(base)+6(arm)+3(gripper)
Weight	< 100kg (arm)
Workspace	inspection:100%; maintenance:90%
Payload	20 kg for arm; 2kg for gripper

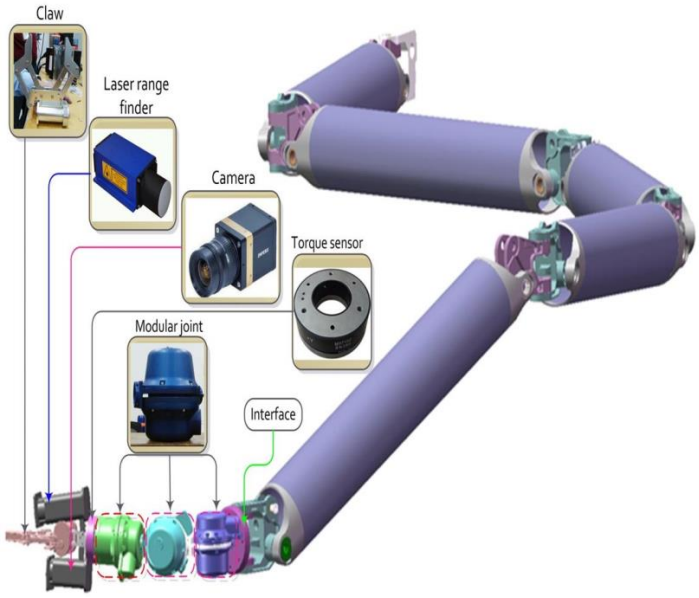

Figure 1.15: EAMA robot (Pan, 2017).

According to the mechanism of the CFETR, the researchers designed a multi-purpose deployer (MPD) system including two robots and other end effectors. A sketch map of system is shown in Figure 1.6. The dual arm effector does some maintenance operations such as grabbing, welding and so on. The dual arm's working space is limited because of its size so that the MPD supplies the main motion of the robot system. The CASK is a carriage for storing robots when the robots are out of work in Figure 1.6. The CASK has its own pathway. There is also a mobile shuttle vehicle. The MPD robot is connected with the shuttle by a binding mechanism to aid the robot going in or out of the CASK. At the end of the cask is a box which has some necessary tools for the dual arm effector to carry out different operations. Once the robot needs some inspection or other requirements, the mobile base can move the CASK together with robots to other places.

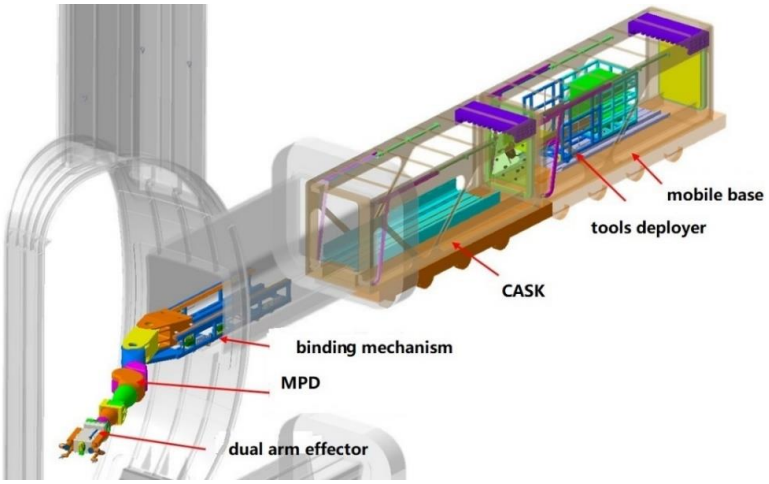

Figure 1.16: Sketch map of the MPD system.

The MPD is a 9-DOF robot as shown in Figure 1.17 whose joints are labelled from J3 to J10. Its driven mode is as shown in Table 1.4. The hybrid control mode can ensure accuracy and load at the same time. The joint which has a bigger load is designed with a hydraulic method because an electric system cannot match the mechanical or load requirements.

Table 1.4: The driven mode of MPD robot

Joint	J10	J9	J8	J7	J6	J5	J4	J3
Torque (kN · m)	24.3	24.3	69.3	69.3	157.0	157.0	-	-
Driven mode	E	E	E	E	H	H	E	E

(E: electric, H: hydraulic)

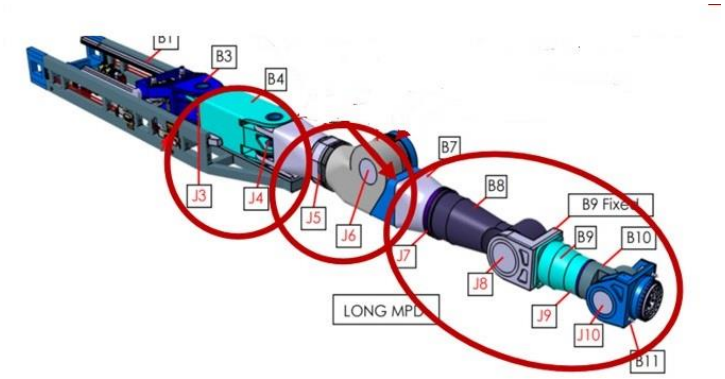

Figure 1.17: Driven mode of the MPD robot.

ALL in all, the EAMA and MPD are both fusion robots. However, the EAMA robot mainly inspects the fusion device and its accuracy of motion is low. As for the MPD, it has a big payload. Besides, the MPD together with the end effector will maintenance the device not only inspection but also some delicate tasks such as welding, assembling and so on, which requires the high accuracy of the robot.

1.4 Research Problem (RP)

The irregular working space restriction, redundant robot mechanism and ultra-working conditions in maintenance complicate the fusion robot system. Some fusion robots have a complicated redundant, long-beam mechanism, and traditional methods such as an analytical method cannot solve its kinematics. Meanwhile, the reactor has a complicated mechanism, as shown in Figure 1.1, so that there is high risk that the robot could collide with the device.

The robot dynamic equation is defined as Eq. 1.1

$$\mathrm{J} \cdot \ddot{q} + C(q, \dot{q}) \cdot \dot{q} + D(\dot{q}) + G(q) = \tau \tag{1.1}$$

where q is the joint vector, J is inertia, $C(q, \dot{q})$ is Coriolis and centrifugal forces, $D(\dot{q})$ is friction, $G(q)$ is gravity, and τ is generalized forces.

The generalized forces can be defined as Eq. 1.2

$$\tau = f_{mod}(q, \dot{q}) + u(q, \dot{q}, \ddot{q}) \tag{1.2}$$

where $f_{mod}(q, \dot{q})$ is model of nonlinearities, and $u(q, \dot{q}, \ddot{q})$ is control law.

For the fusion robot MPD system, the dynamical part is important but will be ignored below with the exception of the gravity part because of its low-speed motion while working.

Additionally, the high-quality maintenance needs the robot's motion accuracy. Taking these reasons into consideration, the research problem (RP) can be divided into four parts. **RP1** and **RP3** use the MPD robot to analyse the redundant robot kinematics and collision problems. **RP2** uses a lightweight robot to introduce a kinematic calibration which improves the accuracy of the fusion robot. **RP4** uses the EAMA robot to introduce the deformation compensation method.

1.4.1 Research Problem 1

The MPD moves in the CFETR so that the size of MPD is limited by the geometry of the CFETR. In order to demand its reachable workspace, the MPD was designed as a 9-DOF robot. Nevertheless, the redundant structure complicates its kinematics, and a traditional analytical method cannot solve this problem directly. A flexible solution of kinematics

which demands accuracy is important. The redundant robot has some redundant solutions, and not all solutions can require the collision free condition. For the safety of the reactor, the kinematic solutions should require that none of the robot's segments collide with the surroundings. Collision free and the redundant robot kinematics are bases for the MPD robot system.

1.4.2 Research Problem 2

The end effector is a dual arm robot which carries out maintenance tasks such as welding, screwing and so on. Hence, the kinematics accuracy of the robot determines the quality of robot maintenance. The conceptual design of a dual arm robot is shown in Figure 1.18. A dual arm robot can be regarded as a twin body robot with the same base frame shown in Figure 1.19. The motion of the dual arm can be regarded as two independent serial robots' motion planning. This planning can be modelled by the robot transformation frames' description. The parameters of the description are robot kinematic parameters which can be calibrated by experiment. The accuracy of the robot is related to the kinematic parameters. So the second task of the MPD robot system focuses on the kinematic parameters' identification to achieve effective maintenance.

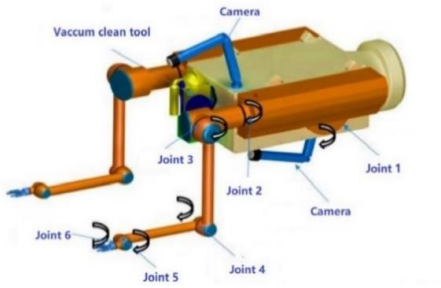

Figure 1.18: Conceptual design of a dual arm robot.

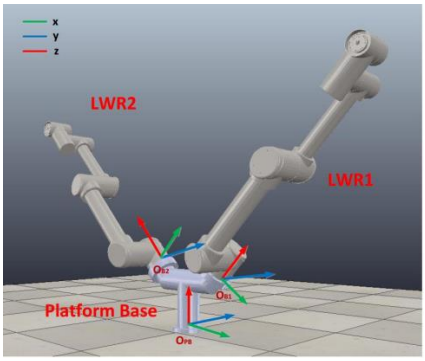

Figure 1.19: Mathematic model of a dual arm robot.

1.4.3 Research Problem 3

The inner structure of the CFETR is complicated and the inner, outer radius in equatorial plane and height are 4860mm and 9680mm and 9603mm, respectively, as shown in Figure 1.20. The dual arm effector is likely to collide with its surroundings especially in the space of divertor. It is essential to ensure the safety of robot for the MPD system.

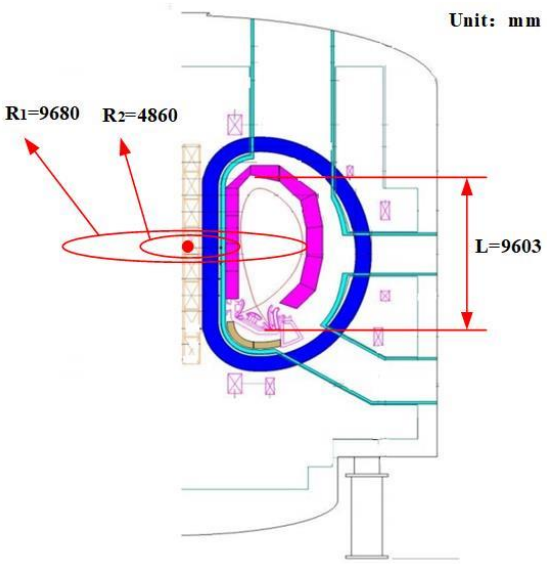

Figure 1.20: Maintenance workspace in the CFETR.

1.4.4 Research Problem 4

Because of the flexible joint design, imperfections in assembly and so on, the fusion robot has a deformation problem which influences its accuracy while working. A recurrent neural network model is studied for deformation compensation of this kind of the robot to enhance its accuracy. EAMA experiments show the error is accumulated so that the error is not independent in a different state. A detailed description is presented in **Publication IV**. This nonlinear position problem about the fusion robot in deformation compensation should be studied to eliminate the error.

1.4.5 Research Problem Summary

All in all, this dissertation focuses on some intelligent algorithms about fusion robots. There are five main algorithms which are introduced briefly for fusion remote handling: dynamic accuracy ant colony optimization of inverse kinematic (DAACOIK) for MPD, collision detection based on computer graphics, a hybrid collision detection perceptron for the robot, a novel method to identify the DH parameters of a rigid robot based on a

geometry model, a gravity compensation algorithm based on a recurrent neural network. The detailed presentations are shown in the appendix publications.

1.5 Thesis Contributions and Limitations

This dissertation focuses on motion planning for a redundant fusion robot system. The first point of the research focuses on the redundant robot's kinematics. **Publication I** introduces a dynamic accuracy ant colony optimization (DAACO) algorithm to solve the complex nonlinear formulas in kinematics. The dynamic accuracy mechanism accelerates the solving speed. Compared with traditional ant colony optimization, the accuracy is higher. Secondly, the MPD has a fixed geometric restriction as shown in Figure 1.20. By transforming the fixed geometric restriction into graphic problems, the graphic gray- scale information is used to check the segment's collision with itself and its surroundings. DAACO is a universal method for redundant robots with high speed and high accuracy in free space. Due to the complicated workspace of the MPD, collision detection based on computer graphics cannot ensure real-time accuracy for the kinematics. However, the motion planning for the complex fusion robot is offline. In other words, not the time sensitivity but the safety of the MPD is the key point for fusion remote handling. The third point is maintenance quality. Fusion robots should be calibrated before they are put into use. The traditional calibration is based on the gradient descent method to solve the kinematic parameters. However, this method would not be optimal and has singularity. Considering these problems, **Publication II** introduces a geometric method together with the least squares method to ensure the parameters are set uniquely and optimally. What's more, this geometric method also has no singularity for strange structures. Additionally, the algorithm is a universal calibration algorithm and it has a big advantage for redundant robots. However, the calibration should follow a designed trajectory to obtain more experimental data. For **Publication III**, a model-free method is illustrated. As we knew, building up a dynamic model for robots is time-consuming and difficult. A hybrid perceptron uses two key technologies: primary component analysis (PCA) to reduce the dimension of data, and a supervised machine learning method to optimize the perceptron. This method is a model-free method which refers to a non-physical model. This algorithm trains a great amount of data to obtain the model, and uses the model to detect collisions. In the simulation results, the hybrid collision detection perceptron can could successfully identify potential collisions over 98% of the time. However, the hybrid perceptron also has its shortcomings such as the accuracy influenced by the amount of training data, local minimum trap, overfitting, etc. As to the **Publication IV**, the deformation of fusion robot EAMA leads to a low position accuracy. This elastic deformation of the EAMA is a coupled and accumulated error. An RNN model is studied to predict the deformation, which has a memory function in fitting the coupled and accumulated error model. The paper uses a segment to verify the RNN model in an experiment. The testing results verified the model successfully.

1.6 Outline

This dissertation can be divided into four sections. The contents of these sections are summarized below.

Chapter 1 introduces the background of the research in fusion applications. By analysing the system of fusion devices, the chapter presents four topics in fusion remote handling which are research problems 1-4. Related methods are introduced briefly to solve these problems, The limitations of methods are introduced, which form the future work for the study. At the end of this section, the value of study is illustrated in the fusion robot research field.

Chapter 2 enumerates the related work or methods to solve these research problems. The characteristics of the methods are discussed in detail. Through the analysis, the advantages and details of the algorithms are illustrated scientifically.

Chapter 3 discusses the results based on simulations or experiments. Additionally, the advantages and innovation points of these algorithms are introduced further. The results and analysis of these research problems are discussed in detail.

Chapter 4 focuses on the algorithm conclusions of the research problems. The advantages and shortcoming of related methods in fusion remote handling are analysed. After summarizing the previous work or studies, future work suggestions are discussed.

2 State-of-the-Art Solution for a Redundant Robot System

This chapter will focus concerning the related work about the research problems mentioned in chapter 1. There are 4 main fields discussed: the kinematics, parameter identification/calibration, collision and deformation compensation in detail.

2.1 The Kinematics of a Redundant Robot System

In a narrow sense, the kinematic algorithm of a robot refers to the forward and inverse kinematics. The forward kinematics is a function which uses a series of joint values and the robot's kinematic parameters to calculate the end effector or tool frame of the robot in three-dimensional space. In other words, it is a mapping from the joint space to the Cartesian space for a robot. The inverse kinematics is reverse mapping which uses position and orientation information to calculate the values of the joints. More generally, authors define include motion planning, trajectory and position/speed/acceleration planning in kinematics.

Robot kinematics uses the rigid body kinematics conception, and the key to rigid body kinematics concentrates on the description of the pose of the body. Below are some typical methods for pose description.

- Euler Angles: For a minimal representation, the orientation of coordinate frame i relative to coordinate frame j can be denoted as a vector of three angles α,β,γ. These angles are known as Euler angles when each represents a rotation about an axis of a moving coordinate frame;
- Fixed Angles: A vector of three angles can also denote the orientation of coordinate frame i relative to coordinate frame j when each angle represents a rotation about an axis of a fixed reference frame;
- Angle-Axis: A single angle θ in combination with a unit vector $\hat{\omega}$ can also denote the orientation of coordinate frame i relative to coordinate frame j;
- Quaternions: The quaternion representation of orientation by Hamilton (Campa, 2008) is extremely useful for problems in robotics that result in representational singularities in the vector/matrix notation.

The kinematic problems of redundant robots are based on descriptions to find a solution between joint space and Cartesian space. The early research began in the 1980s and mainly focused on industrial robots. However, redundant robots have been widely applied in manufacturing recently ABB, KUKA, FANUC, and YASKAWA launched products such as 7-dof robots and snake-like robots. There is a binary classification according to

using the Jacobian matrix or not for the kinematics of a redundant robot: the Jacobian matrix method and the non-Jacobian matrix method.

2.1.1 Jacobian Matrix Method

The Jacobian matrix method refers to solving a kinematic solution by using the Jacobian matrix to represent the relationship in a rigid body description. Suh, Hollerbach (Suh and Hollerbach, 1987) came up with RMM (Resolved Motion Method) using a pseudo-inverse matrix that utilizes an extra vector as a restriction. Bailieul (Baillieul, 1987, 1985) studied an EJM (Extended Jacobian Method) with an extended Jacobian matrix to limit the position and orientation for end effectors, which is only suitable for a one-dof-redundant system. Chang (Chang, 1986) studied a closed-form method by combining the RMM and EJM with a Lagrangian multiplier for redundant kinematics.

2.1.2 Non-Jacobian Matrix Method

The non-Jacobian matrix method refers to modelling with an intelligent algorithm, which is a universal method in robot kinematic problems. Goldenberg (Goldenberg et al., 1985) studied a Newton-Raphson method for nonlinear kinematic problems. However, the accuracy and iteration were influenced severely by the initial values. Joey (Parker et al., 1989) came up with a genetic algorithm by designing a cost and fitness object function. Xia (Xia and Wang, 2001) used a quadratic optimization to design a dual network based on a recurrent neural network to solve redundant kinematics. Additionally, these are some other methods such as PSO (Particle Swarm Optimization), NN (Neural Network) and so on (Sancaktar et al., 2018; Kumar et al., 2011). Palm (Palm, 1992) designed a fuzzy control diagram to solve the redundant robot. Besides the fuzzy control can be used in obstacle avoiding which is a good tool for the redundant robot (Jun, 1993).

ACO (Dorigo et al., 1996) is a novel non-Jacobian method, which uses an intelligent method to solve the non- linear problem of a robot's kinematic problems. In ACO (Ant Colony Optimization), ants can be regarded as flexible solutions c_i^j in solution space $\mathcal{S}$. The solving procedure is just like ants searching for an optimal aim. In order to let most of solution step forward, a rule which simulates ants searching for food, is designed with some mathematic parameters such as a pheromone trail parameter, transition probabilities and so on. The pheromone trail parameter reflects an ant emitting a pheromone in a trail to tell his fellow ants to come along the same route for treasure. Transition probabilities reflect a parameter as to whether his fellow ants will receive his messages or not. The pheromone trail parameter which corresponding to c_i^j and transition probabilities $\mathrm{p}(c_i^j|\mathcal{S}^p)$can be represented as follows:

$$\tau_i^j \leftarrow (1-\rho)\cdot\tau_i^j + \sum_{c_k^l \in \mathcal{R}(\mathcal{S}^p)} \Delta\tau_i^j \qquad \forall c_k^l \in \mathcal{R}(\mathcal{S}^p) \tag{2.1}$$

where ρ is the evaporation rate, c_k^l is the choice of a solution component, $\mathcal{S}^p$ is a partial

solution, $\mathcal{R}(\mathcal{S}^p)$ is a feasible solution component set.

$$\mathrm{p}\left(c_i^j \middle| \mathcal{S}^p\right) = \frac{[\tau_i^j]^\alpha \cdot [\eta(c_i^j)]^\beta}{\sum_{c_i^j \in \mathcal{R}(\mathcal{S}^p)} [\tau_i^j]^\alpha \cdot [\eta(c_i^j)]^\beta} \quad \forall c_i^j \in \mathcal{R}(\mathcal{S}^p) \tag{2.2}$$

where α is the relative importance of pheromone value $\alpha > 0$, β is the relative importance of heuristic information $\beta > 0$, η is the heuristic information that assigns a component to each valid solution possibly depending on the current step.

However, the traditional ACO has some shortcomings such as its low problem solving speed, bad accuracy and so on. Inspired by the theory of evolution, a dynamic accuracy ant colony optimization (DAACO) for inverse kinematics was designed. There are two important parameters in DAACO which are a cost function $G(X)$ and heuristic information η(X). The DAACO procedure is shown below.

$$G(X) = \sum_{i=1}^{n} -\lambda_i \cdot f_i(X) \tag{2.3}$$

$$\eta = \frac{1}{G(X)} \tag{2.4}$$

where X is the feasible solution to ACO problems, λ_i is an arbitrary real positive number, and f_i is a nonlinear restriction condition. In a redundant robot kinematic problem, the X can be regarded as the feasible joint vector of robots. For example, the T_{total} is the transform matrix of MPD, and the t_{14} denotes the desired x-axis accuracy of T_{total}, which is equal to one of nonlinear restriction condition f_i.

Algorithm 1: Dynamic accuracy ant colony optimization

Input: the aim/requirement T , the range limitation of joints, the accuracy of the algorithm AA, the iteration index II, the iteration number IN

Output: the optimal solutions X

while $II <= IN$ **do**

  Initialize all parameters: X_i, τ_0; Update τ, p; Calculate the cost function G, heuristic information η **if** $G < AA \cdot \exp(IN - II)$ **then**

    if $IN - II = 0$ **then**

      $X \leftarrow X_i$

    else

      Using X_i which belongs to top 5 in G's value to generate new X_i by inheritance, variation and hybridization for the next iteration;

```
            end
        end
    end
end
```

In this algorithm, the $AA \cdot \exp(IN - II)$ is the dynamic accuracy of the DAACO method which is changeable with each iteration.

2.1.3 Discussion

An MPD robot is a redundant robot with a complex structure, and its kinematics cannot be solved by closed-form solutions. The ACO, a numerical method, is used for the kinematics of the MPD system. There are many criterion judging an algorithm such as speed, accuracy, complexity, iteration and so on. By optimizing the previous-mentioned ACO method, a dynamic accuracy mechanism that is named DAACO was designed. This is a universal and high accuracy method for solving a redundant robot's kinematics in fusion applications.

2.2 Parameter Identification/Calibration

An end effector robot consists of dual rigid robots that perform maintenance work such as welding, grasping and so on. Thus, the calibration, a kinematic parameters identification procedure, for the robot is necessary to ensure the quality of the maintenance. There are many factors influencing the robot accuracy such as abrasion, manufacture, gear clearance, and assembly. The robot accuracy can be promoted by calibrating the robot's kinematic parameters with an intrinsic hardware/configuration (Chen et al., 2014b). The parameters which are calibrated are used instead of the previous kinematic model (Lightcap et al., 2008; Li and Zhang, 2011; Li et al., 2011). The calibration method can be classified into two parts: non-parametric kinematics calibration and model-based kinematics calibration.

- Model-based kinematics calibration: based on an error model representing the error between the theoretical kinematic model and the actual end-effector pose. The errors of kinematic parameters can be compensated by calculating the error model and eliminating it.
- Non-parametric kinematics calibration: using intelligent algorithms to represent the relationship between Cartesian space and joint space instead of the formulas established by the kinematics parameters.

2.2.1 **Example of third level heading**

Model-based kinematics calibration has three elements which are model completeness, parameter minimality and model continuity (Schroer et al., 1997). There are five typical algorithms which are based on this theory: the DH method (Denavit and Hartenberg, 1955; Paul, 1981; Everett et al., 1987), the S model method (Stone, 1987), CPC (complete and parametrically continuous) model method (Zhuang and Roth, 1993, 1991), which is a robot kinematic modeling convention having no model singularities and allowing the modeling of the robot base and tool in the same manner by which the internal links are modeled. the zero reference system model (Zhong et al., 1996; Gupta, 1986) and the POE formula method (Okamura and Park, 1996; Brockett, 2006; Chen et al., 2001), which based on the product of exponentials (POE) formula are parametrically continuous and complete for the calibration of the kinematic parameters of serial robots.

The geometric method for calibration is a novel model-based kinematics method which has no singularity especially for redundant robots. This method can find the geometric features of the robot, such as revolution point and axis, by fitting a trajectory. In Figure 2.1, there are 6 trajectories as the corresponding joint moves independently for a six-revolution-DOF robot. These motion curves can be fitted to a circle in a mathematical model. Thus, based on these circles, the features of the robot, which are the revolution joint points and revolution axes, can be determined as shown in Figure 2.2.

In Figure 2.1, the geometric features of the fitting curves are the center of the circle and the normal of the circle. Using the corresponding fitting method together with the least squares method, these features can be determined uniquely. Then, the features coincide with the robot's DH model such as the centers and axes of rotation joint. Naturally, a fitting DH model according to the measurement points is built, and the robot kinematic parameters are deduced.

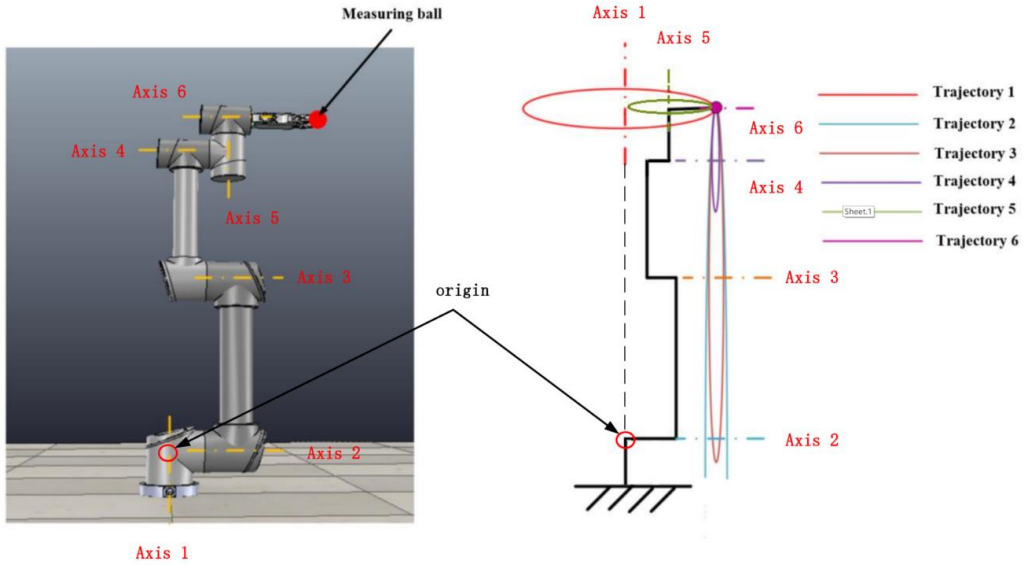

Figure 2.1: The relationship between the light weight robot and its calibration trajectories.

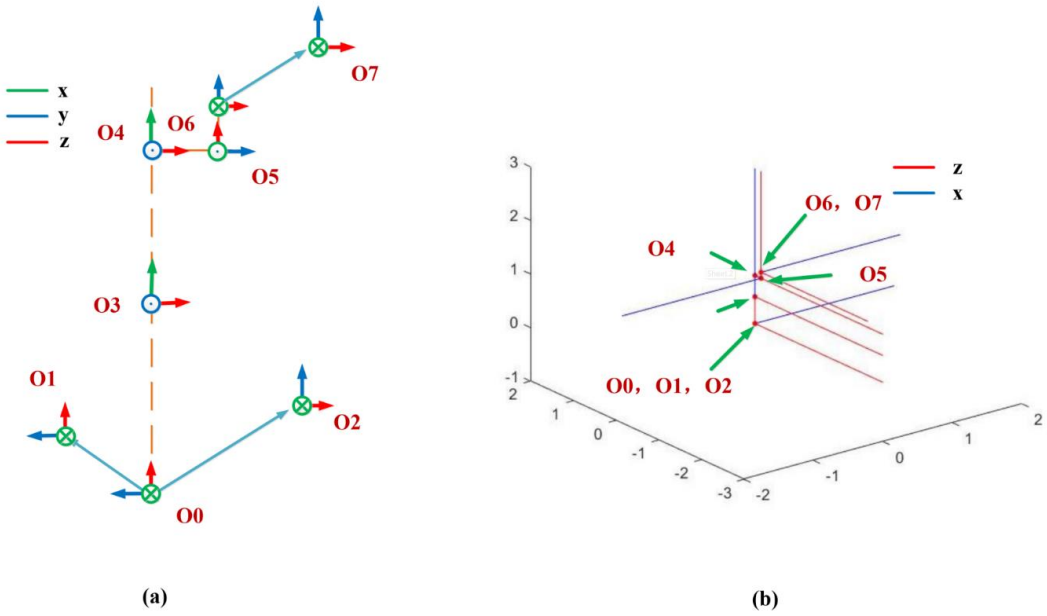

Figure 2.2: The geometry DH model of the robot.

2.2.2 Non-Parametric Kinematics Calibration

With the development of computing, the non-parametric kinematic calibration method has become widely used. There are two categories of this method: interpolation and neural network. Bilinear interpolation is a commonly used interpolation method in robot nonparametric kinematics calibration. It is assumed that the position errors of the end-effector follow a uniform distribution in bilinear interpolation (Motta et al., 2001). There is an another method called fuzzy interpolation (Motta et al., 2001) using fuzzy neuro networks. The other method uses a neuro network (NN) and takes advantage of the NN model instead of the robot kinematic model, for example, Pi-Sigma NN (Feijun et al., 1999), BPNN (backpropagation neural network)(Lewis et al., 1994), neural network and a camera-based measurement system (Wang et al., 2010) and so on.

2.2.3 Discussion

The non-parametric kinematics calibration usually has some shortcomings such as local minimum, iteration, singularity, or speed problems. In this dissertation a geometric model with LSM (least squares method) is designed which identical to the model-based form on kinematics calibration. Moreover, this method has no singularity problem because it builds up the model based on the geometric model not the DH model of the robot. Additionally, it is suitable for redundant robots.

2.3 Collision

It is likely that a robot will collide with known and unknown obstacles. The research on collision mainly focuses on two aspects: obstacle avoidance and collision detection. The former uses sensor information or geometric information to plan the safe trajectory of robots. The other senses the collision immediately the robot has a slight collision with an obstacle.

2.3.1 Discussion Obstacle Avoidance

The study of obstacle avoidance dates back to early robot research. It can be divided into two parts which are single step planning and multi-step planning.

Single step planning has two branches which are heuristic methods and physical analogies.

The heuristic method uses autologous sensor signals to help the robot motion avoid an obstacle. Vladimir (Lumelsky and Stepanov, 1987) designed a tactile sensor to perceive surroundings. Masafumi (Uchida and Ide, 1995) used computer graphics and vector analysis to perceive obstacles. Gouzenes (Gouzenes, 1984) came up with an intrinsic tree structure to analyze the atmosphere. Single step planning is a simple way which is widely used in logistics robots, service robots, military robots and so on (Zhang et al., 2019a; Khan et al., 2019; Yang et al., 2016a; BenAri and Mondada, 2018; Budakova et al., 2019).

Physical analogies simulate various physical theories to aid the safe motion of a robot, for instance, potential field methods (Khatib, 1985; Krogh and Thorpe, 1986; Borenstein and Koren, 1989), virtual diffusion (Azarm and Schmidt, 1994) and circulatory fields (Singh et al., 1996).

Multi step planning aims to plan the steps of the robot towards the determined aims of the task, for example, a robot completing an inspection task. The most popular method is to use a vector field histogram (Borenstein and Koren, 1991) which detects a safe distance with a sensor and uses differential information to drive the robot. There are also other methods such as the obstacle restriction method (Minguez, 2005), hierarchical architecture (Feiten et al., 1994) and so on (Fox et al., 1997; Shiller, 1998; Simmons, 1996; Wang et al., 2017a).

The MPD adopts a multi-step planning method which uses fixed geometric boundaries, and a CFETR model, to avoid obstacles. When the MPD moves in the CFETR, the next several steps can be predicted by forward kinematics. Figure 2.3, there are 4 collision cases. Rows 1 and 2, rows 3 and 4 show the collision in the main body and cask of the CFETR respectively. By rendering the section plane, there could be some difference in column a and d. In cases 2 and 4 (row 2 and 4), it is obvious that the MPD collides with the fusion device. Based on the computer graphics method, the collision can be detected more effectively than by solving nonlinear geometric equations.

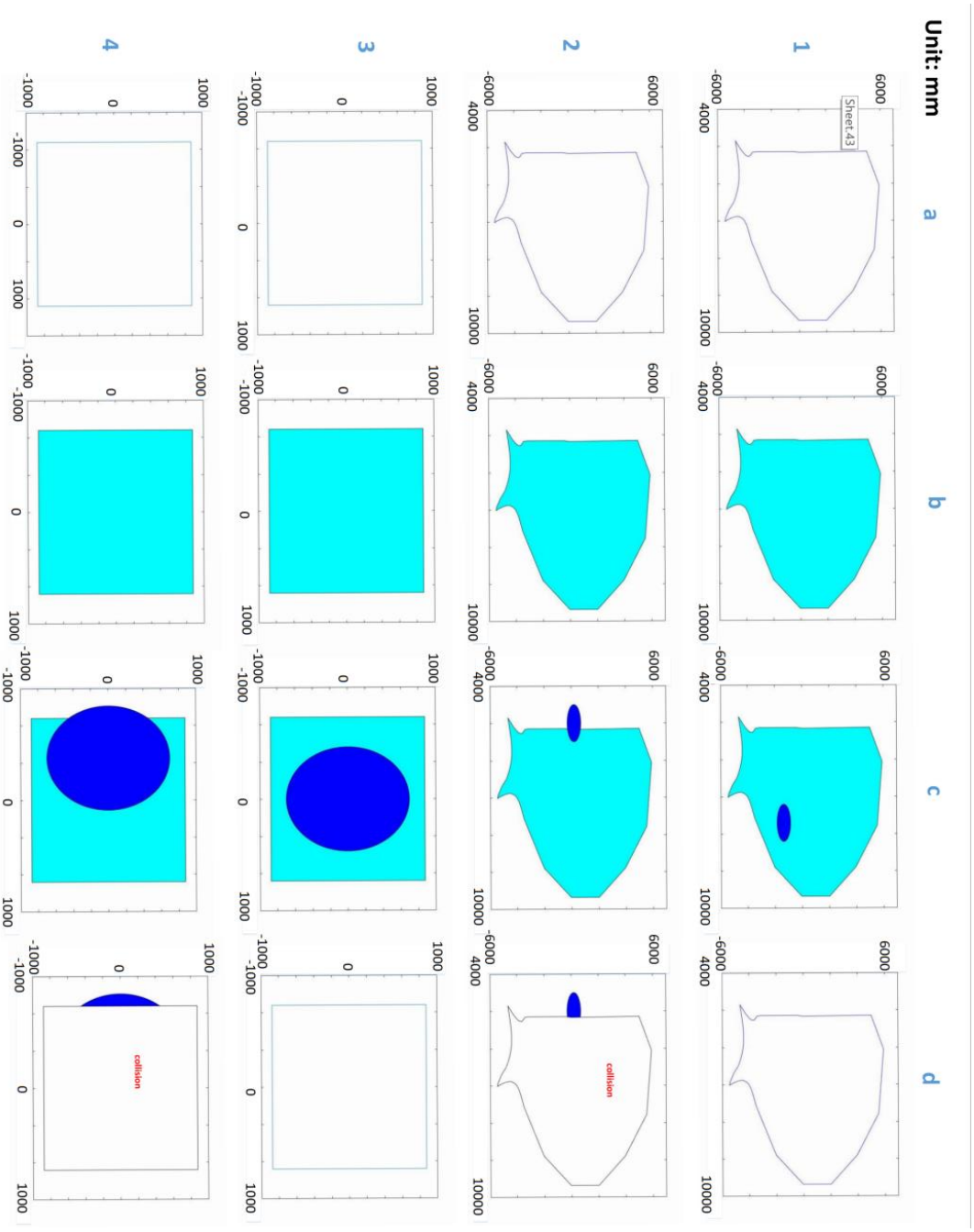

Figure 2.3: The section plane of collision

2.3.2 Discussion Collision Detection

With the development of the robot, the need for collaboration between human beings and robots is necessary. This requires that the robot can stop immediately when it feels some obstacle so that the safety of human beings or device can be ensured. The Haddain (Haddadin et al., 2017) came up a collision event pipeline with seven steps as shown in Figure 2.4.

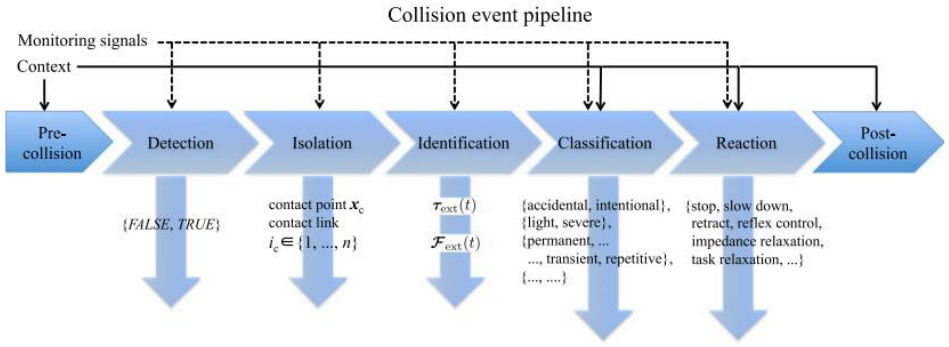

Figure 2.4: The collision event pipeline (Haddadin et al., 2017).

In industrial robots, there are five main ways to detect collisions.

- The current loop: calculating the generalized force and comparing it with the current message to detect a collision, e.g., the Yumi robot;
- The flexible joint: using torque sensors and encoders to estimate the generalized force to detect a collision, e.g., the iiwa robot;
- The dual encoder: designing an algorithm based on a model of the encoder and harmonic reducer information to detect a collision, e.g., the UR robot;
- The electric skin: using a skin sensor to detect collision;
- The base torque sensor: designing a perceptron to detect collision based on a base sensor instead of a joint torque sensor, e.g., the Fanuc robot.

Collision detection can be interpreted as a binary problem. An intelligent algorithm has obvious advantages in classification problems. When a robot collides, its instinct signals will be changed, such as its position, velocity and current information. However, as for a six-dof robot, the dimension of the data is 18 (six joint with its own parameters: position, velocity, acceleration or current), which is difficult to analyze. Based on this case, a design for a hybrid collision detection machine is shown in Figure 2.5. In this hybrid collision detection algorithm, PCA (Primary Component Analysis), a classical dimension

reduction method can preprocess the data of the robot to reveal its features to simplify the identification of the collision.

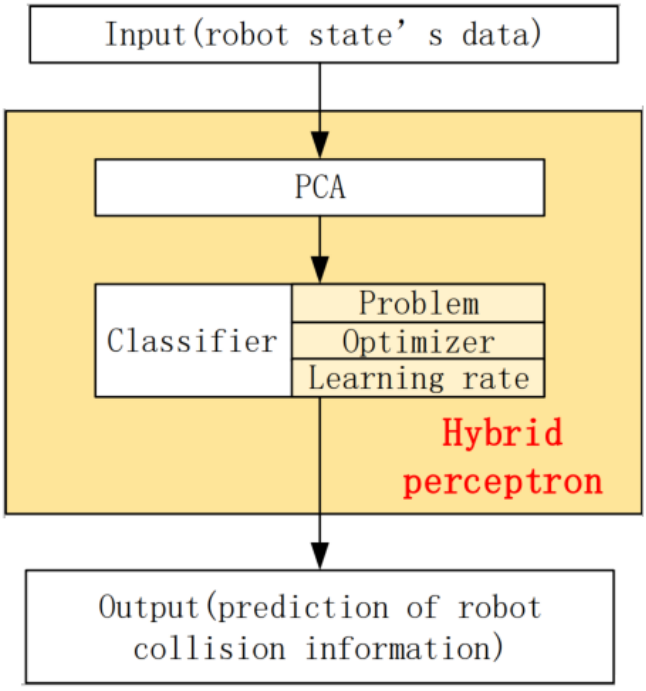

Figure 2.5: The hybrid collision detection machine.

The classifier aims to calculate the separating plane to distinguish a collision in Figure 2.6. The input space and output space are $\chi \subseteq \mathcal{R}^k$ and $Y = \{y_1 = +1, y_2 = -1\}$respectively (+1 means safe and -1 means collision) where k is the number of data features. The input vector $x \in \chi$ denotes a sample which can be classified by the perceptron. The hyperplane $\omega^T \cdot x + b = 0$ is a separating hyperplane that can classify the high dimension space into 2 parts: collision space and safe space. The ω and b are weights and intercept respectively. Figure 2.6 shows a physical model in 2 dimensions of the perceptron. The weight vector ω which is also a normal vector of the hyperplane can form a border between the collision space and safe space. The norm of $\frac{b}{|\omega|}$ shows the Euclidean distance between the origin and the hyperplane. The size of the weight vector ω and input vector x are both k dimensions. In the perceptron, a weight vector ω may not be unique because there might be many separating hyperplanes. However, uncertainty usually of the weight vector ω will not influence the accuracy if the data is separable. The weight vector ω can be trained by the machine learning algorithm.

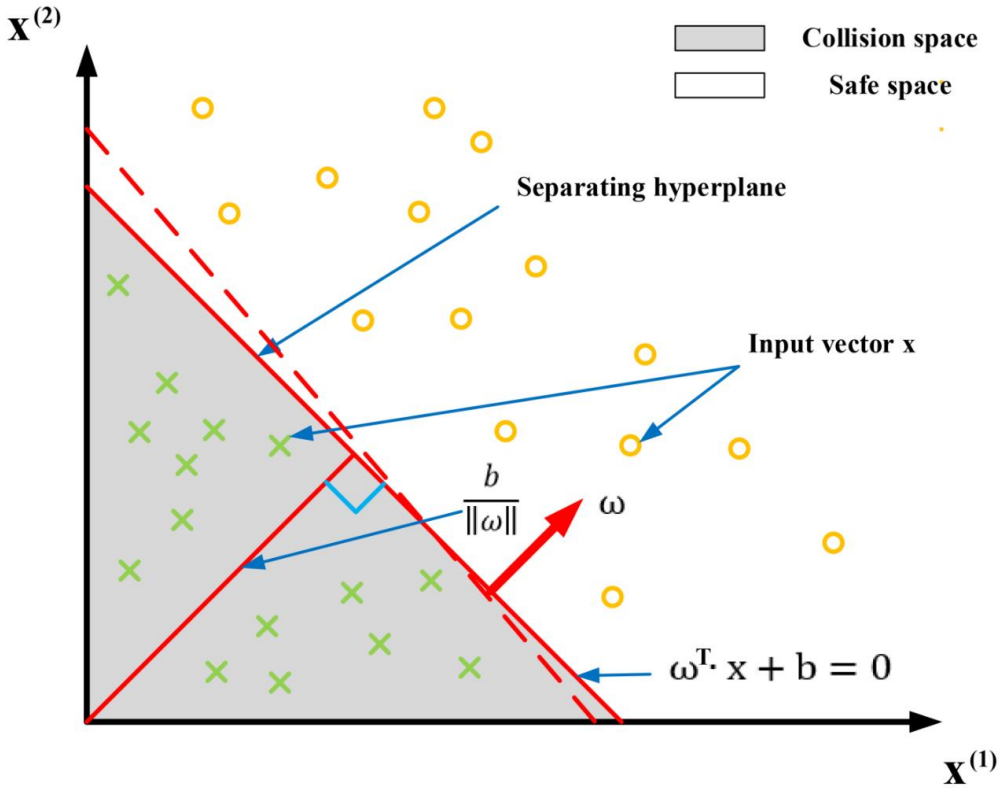

Figure 2.6: The separating plane for detecting a collision.

2.3.3 Discussion

There are two aspects of this research: obstacle avoidance and collision detection. The MPD has a fixed restriction which is the MPD's workspace, and the vacuum of the CFETR. The MPD adopts an offline simulation to plan the robot's movements, and the trajectory can be calculated in advance. Based on the geometric restrictions, the candidate solution can be filtered to optimize a flexible solution further by using computer graphics. For the end effector, it is likely to collide with a divertor in the CFETR. Considering the safety of the fusion devices and robots, a collision detection algorithm should be designed. A hybrid perceptron is a model-free method based on the current, speed and position loop. Training the data, a perceptron can be determined to identify a collision to ensure the safety of the robot.

2.4 Deformation Compensation

Previous researches has focused on increasing the position accuracy by kinematic calibration and modelling the manipulator, which is not enough for increasing the accuracy in some complex processes such as milling, welding and so on because of rigid model hypothesis of the robot. Many parts in the robot can induce an incorrect position and orientation, for example, torsion of the motor axes, friction, torsion and backlash in the gears, elasticity of the links, especially for a redundant, long, heavy but flexible robot. It is necessary to develop some algorithms to compensate for the motion accuracy for high precision maintenance such as welding, assembling and grasping. There are lots of hypothesis concerning deformation models, such as the spring model, stiffness model, neural network model and so on. There is a universal classification of deformation compensation which is model-based deformation compensation and sensor-based (Schneider et al., 2014).

2.4.1 Model-Based Deformation Compensation

Model-based compensation uses a model to predict the robot deformation, and then modifies the robot position reference accordingly. Feroen (De Backer and Bolmsjo, 2014) regarded that the external forces/payload would influence the position accuracy of the robot. He designed a spring model between the external force/moment and joint deviation, building a deflection model in the controller to reduce the motion error for robotic friction stir welding. Ulrich Schneider (Schneider et al., 2014) created a stiffness model to relate the compliant displacement of the end effector and external wrench of the robot. By minimizing the error of wrench force and calculating force with the stiffness model, stiffness coefficients can be calibrated, which are applied to the robot controller. Wang (Wang et al., 2009) also designed a stiffness model to reduce its error of deformation. All in all, the model-based method mainly adopts an open loop mode to compensate for the error of deformation (Sun et al., 2019).

Fusion robots are redundant, long, heavy but flexible because of their huge maintenance working space. For example, the EAMA robot is 7-dof fusion robot which is 10 m in length. It is designed with a cable joint structure and titanium alloy mechanism to reduce the weight of the robot. However, joint flexibility, imperfect assembly and other errors can influence the accuracy of the robot's positioning. The deformation of fusion robots is nonlinear so that the linear model cannot predict the sag effectively. RNN is an intelligent model which has a memory function to predict coupled nonlinear problems. It has 3 main layers: an input layer, a hidden layer and an output layer. In the hidden layer, every neuron has a recurrent function or memory function which connect its own input and output.

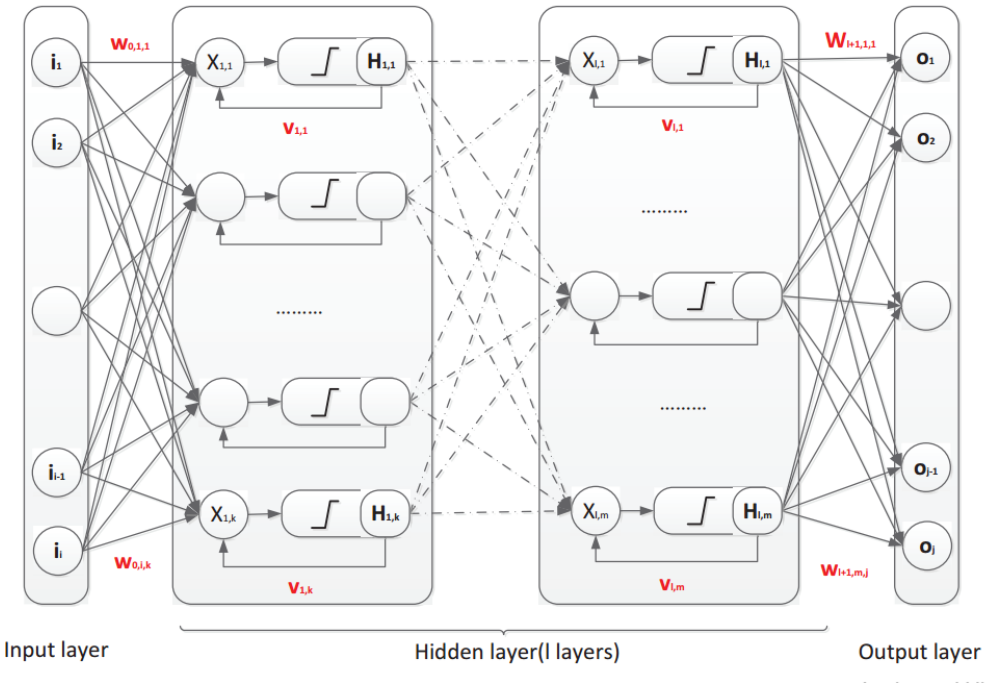

Figure 2.7: A diagram of the RNN model.

2.4.2 Sensor-Based Deformation Compensation

The sensor-based methods measure the deformation inducing position error in either the joint space or the Cartesian space and then adjust the position reference accordingly, which needs more hardware and data processing. Xu (Xu et al., 1997) used three position sensitive detectors (PSD) at the other end of the link to build a laser-optical sensing system, which was proposed for the measurement of the deflections of each individual flexible link. The positioning inaccuracies of the robot can be measured with a sensor based deflection model and finally compensated for in real time by adjusting joint variables. Li (Li et al., 2018) used dual quaternion algebra to create a stiffness model and calibrate the related parameters by using a torque sensor and laser tracker. A sensor-based method is more precise because of using a more accurate device to detect or calibrate parameters.

2.4.3 Discussion

Deflection compensation is important because the accuracy of the robot influences the quality of remote handling. However, deformation is always a nonlinear problem although some of researchers use a spring model, which is a linear model to improve accuracy. The RNN (recurrent neural network), a nonlinear optimization, has some

recurrent functions which can memorize the previous deformation, which would be suitable for a cable structure model such as EAMA. An open-loop controller designed using the RNN can improve the accuracy of the robot for monitor tasks.

3 Publication Summary and Discussion

3.1 Redundant Robot Kinematics (RP1)

The redundant robot's kinematics is a hot topic in research because its kinematics require is a high dimension and nonlinear formula. For a redundant robot, this is usually divided into multiple parts, and kinematics problems are solved in each subpart respectively. In **Publication I**, the MPD is divided into two parts to reduce the complexity of the robot kinematics. For each subpart, the geometric restriction and kinematics accuracy are coupled with each other. A middle joint is chosen whose position is a stochastic point obeying geometric requirements, which is also break joint for dividing the robot into sub parts. An analytical method is a common way to solve some robot kinematics. While the joint's configuration does not follow a special structure, this method is difficult to be deduced especially for redundant robots. So it is more suitable to choose a numerical method to solve redundant robot kinematics. However, a redundant robot's kinematics is a high dimension nonlinear problem. In the dimension reduction of a high-order system is important to accelerate the solving procedure. A multi-part analysis is a simple and efficient method to reduce data dimensions. Each part's kinematics is also a complex nonlinear formula, and the ACO algorithm is applied to solve it. The solution plane is a convex plane that has a countable or countless local maxima and minima. It is easier for the ACO to escape from a local maximum or minimum. In order to improve the algorithm's accuracy, a filter mechanism is designed, which is a different level accuracy target in every cost function and is named dynamic accuracy. The accuracy target is promoted with each generation of the solved flexible solution space in every iteration. Additionally , the new candidates who have the same accuracy as the solved flexible solution. This procedure is inspired by the theory of evolution which simulates the competition mechanism to optimize the solution. However, robot collision should be checked in complex surroundings further. Graphic gray-scale information which shows the section plane's relation between the MPD and the CFETR can be used to check for collisions. 100 groups have be evaluated and the maximum position and orientation error is 0.6381mm and 0.1071deg. The detailed results and procedures are illustrated in **Publication I**. Calculating the redundant robot's kinematics in complex surroundings using dynamic accuracy ant colony optimization (DAACO) is an effective method for nonlinear redundant kinematics.

However, this algorithm is a time-consuming method because it uses graphic gray-scale information to check for collisions. The check time is related to the number of section plane figures. Although this computer graphics method avoids building up the complex geometric boundary formula of the CFETR, the collision figures should be rendered by a computer, which needs some time to generate the collision render graphs. These shortcomings could be solved in the future when the GPU performance improves. However, it will not influence the MPD's motion because fusion robot remote handling uses an offline

method, which can simulate the robot in advance to ensure the safety of the CFETR and robots.

3.2 Calibration of Kinematic Parameters (RP2)

The kinematic parameters influence the accuracy of rigid robot kinematics, which is a hot topic in robot kinematics research. However, some strange robot structure or redundant robots are hard to calibrate because of its high dimensionality and nonlinearity which are discussed in Chapter 2's related work, for example, the gradient descent local minimum. The geometric model in **Publication II** for calibrating robots is a universal method for all robots. It presents a specific trajectory for the robot's motion to avoid singularity of robot structure. The modelling procedure together with LSM ensures unique and optimal calibration results, and the accuracy has big advantages compared to other methods. The maximum position error is 0.00056048mm which is higher than the universal industrial robot, for example, UR robot's 0.005mm, which is an ultra-lightweight, compact collaborative industrial robot, ideal for table-top applications by Denmark Universal Robots company. Finally, the unique geometric model reduces the iteration procedures so that the calculation speed is higher.

The shortcoming of this algorithm is that some simple structural robots do not need too many points to calibrate the kinematic parameters. The specific trajectory of the geometric method always needs enough points to calibrate the model which is five to ten measuring points for each joint, for example, 20 points for a four-DOF robot at least. The reason for this is some points can fit some geometric features better. For example, the more points in a quasi-circle curve to fit a circle, the more precisely the model will be constructed

3.3 Hybrid Perceptron of Collision Detection (RP3)

Collision detection always takes advantages of the dynamic model. As we know, a dynamic model of a robot can be built by the Newton-Euler or Lagrange method, which is a complex and model-based method. A dynamic model is a nonlinear model that can be replaced equivalently by another nonlinear modelling method such as machine learning. The collision problem can be defined as a binary classification problem, and machine learning would have big advantages in this kind of problem. However, the information needed for robotics is huge, for example, the 7-DOF robot has 21 items (current, velocity, and position for each of joint). Such high dimension data is difficult to analyse. A PCA method can be adopted to achieve the dimension reduction. Combined with supervised machine learning, a hybrid perceptron for collision detection can be designed. The results show its effectiveness and flexibility, and 98% of collisions can be detected successfully.

Nevertheless, there are some shortcoming of this perceptron which are also a weakness of machine learning. First of all, a great amount of data would be needed to train the

model. Secondly, although many experiments would be done, there is still some probability that classifications could occur. In the future, another collision detection perceptron based on different mechanisms should be designed to enhance the collision safety.

3.4 **Deflection Compensation for Long Beam Redundant Robots (RP4)**

The structure, backlash in the gears and elasticity of the links lead to flexibility of the robot, which influence the accuracy of the motion. This paper studied a recurrent neural network model according to the robot deformation features which is the current state deformation influenced by the previous states. This mechanism acts similarly to a memory function. The recurrent neural network has big advantages in memory and nonlinear problems because it has recurrent neurons in its networks. This algorithm improves the accuracy greatly and the maximum position error is 0.8mm compared to the previous 6mm. The behaviour of this algorithm is suitable for monitoring maintenance tasks for fusion reactors.

Nevertheless, the EAMA robot is only used to monitor device because of its low accuracy when compared with the industrial robots. This RNN model is an open-loop method which reduces the sag but does not eliminating the error caused by flexibility. Because it is not an industrial class application, this method cannot be used for some delicate maintenance directly.

4 Publication Summary and Discussion

4.1 Conclusions

This dissertation focuses on the kinematic accuracy, kinematics planning and safety for robots used in fusion reactors. **Publication I** to **Publication IV** introduce the redundant robot kinematics, the kinematic parameters calibration, the collision detection and avoidance algorithms, and deformation compensation, which are the fundamentals of the research for robots used in fusion reactors.. Through the study of remote handling in a fusion reactor, problems were revealed in maintenance work. The dissertation summarizes the research problems which are listed in Chapter 1 and aims to model nonlinear problems affecting fusion robots by means of a diverse intelligent algorithm to solve these problems. Through delicate investigation of related work in Chapter 2, novel and suitable methods were studied. The results demonstrate advantages both in accuracy, solving speed, and the complexity of the algorithms in each publication. Finally, the critical comments of the features of the methods were discussed in detail in Chapter 3.

All in all, there are four algorithms which were used to solve nonlinear problems common to fusion robots: the dynamic accuracy ant colony optimization in a redundant robot's kinematics (**Publication I**), the geometric method for calibrating the parameters of the robot (**Publication II**), the hybrid collision detection perceptron of the robot (**Publication III**) and a recurrent neural network for the robot's deformation compensation (**Publication IV**).

4.1.1 Dynamic Accuracy Ant Colony Optimization in a Redundant Robot Kinematics

This algorithm systematically investigates a kinematic algorithm for a robot with multiple degrees of freedom with fixed constraints, by improving the original ant colony algorithm, combining the concept of dynamic accuracy and gray-scale value information to guarantee the safety and validity of the robot solution, and finally performing a simulation to verify its main advantages as follows:

- The concept of dynamic accuracy is innovatively proposed to solve the nonlinear kinematic problems of multi-degree-of-freedom robots by improving the existing ant colony algorithm, and the accuracy and the speed of the solution are improved.
- For the robot kinematics problem with fixed constraints, a computer graphics-based collision detection algorithm is proposed to avoid solving complex geometric equations for robot-environment interference and to improve the speed of redundant solution screening for robot inverse kinematics.

The DAACO algorithm is a general robot kinematics algorithm for fixed constraint environments with complex robot configurations.

4.1.2 Geometric Method for Calibrating the Parameters of the Robot

In this section, a geometric feature-based kinematic parameter calibration algorithm is investigated by fitting a normal plane, a circle and a common normal feature, and using these features to assist in building a robot DH model and solving robot-related kinematic parameters. The algorithm was tested by building a calibration platform for a light-weight robot, Ruban. The maximum position error was 5.604842e−4, which verifies the high accuracy and effectiveness of the algorithm. The geometric feature-based kinematic parameter calibration algorithm has the following main advantages:

- Based on the robot motion trajectory, the algorithm combines the least squares method and the 3σ rule to ensure the optimality of the algorithm.
- Compared with some intelligent algorithms, such as PSO and NN, this algorithm does not need to set initial values, does not have the problem of sensitivity to initial values, does not have a systematic error in the algorithm, and does not need to iterate, the algorithm space complexity is low, and the solution speed is fast.

The geometric feature-based kinematic parameter calibration algorithm is a general algorithm for robot kinematic parameter calibration, which is suitable for robots with a high degree of stiffness.

4.1.3 Hybrid Collision Detection Perceptron of the Robot

In this section, a hybrid perceptron is proposed to sense robot collisions without establishing complex dynamics equations by means of PCA downscaling and perceptron algorithms. Its main advantages are as follows:

- By downscaling the PCA data, the data features related to the robot dynamics are enlarged to make the difference between robot collision and safety data relatively obvious, which helps the perceptron to classify the collision;
- Using logistic regression to analyze the problem, different optimizers such as Adam, SGD, and Adagrad, are designed with different combinations of learning rates to form 12 different hybrid collision perceptron to predict collisions without establishing complex dynamics equations, with prediction accuracy of 98.80%.

The PCA collision perceptron is a supervised learning algorithm based on data analysis that can predict robot collisions more accurately and help robots operate safely.

4.1.4 Recurrent Neural Network for the Robot's Deformation Compensation

This dissertation studies a recurrent neural network model for a fusion robot's deformation compensation. In a mechanics performance experiment, the relationship between the different loads and corresponding deformation of the end effector was measured. The RNN model instead of linear model was used to fit this procedure.

- A recurrent neural network has a "memory" function, which can well perceive the cumulative impact of the previous error on the current error.
- It is a nonlinear problem that the deformation of the robot varies with its mechanical properties. Compared with the linear fitting model, the recursive neural network model has higher accuracy, with a final accuracy of 4.96596mm.

RNN is a nonlinear intelligent algorithm with a simple model and high prediction accuracy for robot deformation compensation, which is especially suitable for flexible static deformation.

4.2 Future Work

The future work of this research will mainly concentrate on the following aspects:

Firstly, **RP1** and **RP3** have only been tested by the simulation individually. These two research problems are coupled to the MPD system motion safety. A coupled test with two algorithms should be simulated together.

Secondly, in **RP3**, the model is trained by the joint force information. In actual application, the current message not force would be used to train the hybrid perceptron. In actual perceptron training, the algorithm system parameters should be modified according to the actual physical model.

Thirdly, a universal fusion robot algorithm architecture has not been built yet. For example, the open motion planning library (OMPL) is a universal motion planning library. In the future, the universal algorithm API which is suitable for future fusion robot should be normalized so that it can accelerate the remote handling research in fusion applications. The standardization of plug-ins is a key point of this research.

Finally, in **RP2**, the geometric model should be built by manual operation. As we knew, the urdf file is a universal robot description file that includes lots of joint, transformation, and mechanic features. This information can be read by the computer automatically so that the mathematical geometric model can be built immediately.

While a mathematical geometric model is done, the designed trajectory of the robot is generated, and the calibration work will be committed automatically. The calibration parameters will replace the nominal parameters so that the accuracy of the robot would be promoted directly to ensure the effective robot mission.

References

Azarm, K. and Schmidt, G. (1994). Integrated mobile robot motion planning and execution in changing indoor environments. *In Proceedings of IEEE/RSJ International Conference on Intelligent Robots and Systems (IROS 94)*, pp. 298 – 305 vol.1.

Baillieul, J. (1985). Kinematic Programming Alternatives for Redundant Manipulators. *In: IEEE International Conference on Robotics and Automation*, vol. 2, pp. 722 – 728.

Baillieul, J. (1987). A constraint oriented approach to inverse problems for kinematically redundant manipulators. *In: IEEE International Conference on Robotics and Automation*, pp. 1827 – 1833.

Batistoni, P., et al. (2017). Technical preparations for the in-vessel 14 MeV neutron calibration at JET. *Fusion Engineering and Design*, 117, pp. 107–114. doi: 10.1016/j.fusengdes.2017.01.023.

BenAri, M. and Mondada, F. (2018). Local Navigation Obstacle Avoidance. *In: Elements of Robotics*, pp. 111–126.

Borenstein, J. and Koren, Y. (1989). Real-Time Obstacle Avoidance for Fast Mobile Robots. *IEEE Transactions on Systems, Man and Cybernetics*, 19, pp. 1179 – 1187. doi:10.1109/21.44033.

Borenstein, J. and Koren, Y. (1991). The Vector Field Histogram - Fast Obstacle Avoidance For Mobile Robots. *IEEE Transactions on Robotics and Automation*, 7, pp. 278– 288. doi:10.1109/70.88137.

Brockett, R. W. (1984). Robotic manipulators and the product of exponentials formula. In *Mathematical Theory of Networks and Systems*, edited by P. A. Fuhrmann, 120-29. Berlin, Heidelberg: Springer Berlin Heidelberg. Buckingham, R. and Loving, A. (2016). Remote-handling challenges in fusion research and beyond. *Nature Physics*, 12, pp. 391–393. doi:10.1038/nphys3755.

Budakova, D., Pavlova, G., Trifonov, R., and Chavdarov, I. (2019). Obstacle avoidance algorithms for mobile robots. *In: Proceedings of the 20th International Conference on Computer Systems and Technologies*, pp. 78–83.

wikipedia. 2021. *RACE (Remote Applications in Challenging Environments) From Wikipedia, the free encyclopedia*. Viewed 22 February 2021, <https://en.wikipedia.org/wiki/RACE_(Remote_Applications_in_Challenging_Environments)>.

Chakraborty, A., et al. (2010). Diagnostic Neutral Beam for ITER – Concept to Engineering. *IEEE Transactions on Plasma Science*, 38, pp. 248 – 253. doi: 10.1109/TPS.2009.2035809.

Chang, P. (1986). A Closed Form Solution for Control of Manipulators with Kinematic Redundancy. *In: IEEE International Conference on Robotics and Automation*, vol. 1, pp. 9 – 14.

Chen, C., et al. (2014a). An electro-hydraulic servo control system research for CFETR blanket RH. *Fusion Engineering and Design*, 89(11), pp. 2806–2813.

Chen, G., et al. (2014b). Review on Kinematics Calibration Technology of Serial Robots. *International Journal of Precision Engineering and Manufacturing*, 15, pp. 1759– 1774. doi:10.1007/s12541-014-0528-1.

Chen, I., Yang, G., Tan, C., and Song, H. (2001). Local POE model for robot kinematic calibration. *Mechanism and Machine Theory – MECH MACH THEORY*, 36. doi: 10.1016/S0094-114X(01)00048-9.

Choi, C.H., et al. (2015). Multi-purpose deployer for ITER in-vessel maintenance. *Fusion Engineering and Design*, 98. doi:10.1016/j.fusengdes.2015.06.156.

Council, N., et al. (2008). Plasma Science: Advancing Knowledge in the National Interest, Physics 2010. *National Academies Press*. ISBN 9780309109437.

David, O., et al. (2005). Operational experience feedback in JET Remote Handling. *Fusion Engineering and Design*, 75, pp. 519–523. doi:10.1016/j.fusengdes.2005.06.161.

De Backer, J. and Bolmsjo, G. (2014). Deflection model for robotic friction stir welding. *Industrial Robot: An International Journal*, 41, pp. 365–372. doi:10.1108/IR-01-2014-0301.

Denavit, J. and Hartenberg, R. (1955). A Kinematic Notation for Lower-Pair Mechanisms. *ASME Journal of Applied Mechanics*, 22, pp. 215–221.

Esque , S., H. Saarinen, A. Muhammad, Likui Zhai, J. Tammisto, J. Seppala, J. Mattila, T. Virvalo, M. Linjama, and M. Vilenius. 2007. ITER Divertor Maintenance: Development of a Control System for the Remote Handling of the Divertor Cassette Mover, *2007 IEEE 22nd Symposium on Fusion Engineering*: 1-6.

Everett, L., Driels, M., and Mooring, B. (1987). Kinematic Modeling for Robot Calibration. *In: IEEE International Conference on Robotics and Automation*, vol. 4, pp. 183 – 189.

Feijun, S., S. M., S., and C. G., R. (1999). A fuzzy logic controller design methodology for 4D systems with optimal global performance using enhanced cell state space based best estimate directed search method. In: IEEE SMC'99 Conference Proceedings. 1999 IEEE International Conference on Systems, Man, and Cybernetics (Cat. No.99CH37028), vol. 6, pp. 138–143 vol.6.

Feiten, W., Bauer, R., and Lawitzky, G. (1994). Robust Obstacle Avoidance in Unknown and Cramped Environments. *In: 1994 IEEE International Conference on Robotics and Automation*, pp. 2412–2417.

Ferlay, F., et al. (2013). First analysis of remote handling maintenance procedure in the hot cell for the ITER ICH and CD antenna aˆ C“ RVTL replacement. *In: Fusion Engineering and Design*, vol. 88, pp. 1924–1928.

Fox, D., Burgard, W., and Thrun, S. (1997). The Dynamic Window Approach to Collision Avoidance. *Robotics and Automation Magazine, IEEE*, 4, pp. 23 – 33. doi: 10.1109/100.580977.

Friconneau, J.P., et al. (2011). ITER remote maintenance system configuration model overview. *Fusion Engineering and Design - FUSION ENG DES*, 86, pp. 1903–1906. doi:10.1016/j.fusengdes.2011.01.118.

Goldenberg, A.A., Benhabib, B., and Fenton, R. (1985). A Complete Generalized Solution to the Inverse Kinematics of Robots. *IEEE International Journal on Robotics and Automation*, 1, pp. 14 – 20. doi:10.1109/JRA.1985.1086995.

Gonzalez Gutierrez, C., et al. (2010). ITER Transfer Cask System: Status of design, issues and future developments. *Fusion Engineering and Design - FUSION ENG DES*, 85, pp. 2295–2299. doi:10.1016/j.fusengdes.2010.09.010.

Gouzenes, L. (1984). Strategies for Solving Collision-Free Trajectory Problems for Mobile and Manipulator Robots. *The International Journal of Robotics Research*, 3, pp. 51–65. doi:10.1177/027836498400300403.

Gupta, K. (1986). KINEMATIC ANALYSIS OF MANIPULATORS USING THE ZERO REFERENCE POSITION DESCRIPTION. *International Journal of Robotic Research- IJRR*, 5, pp. 5–13. doi:10.1177/027836498600500202.

Haddadin, S., Luca, A., and Albu-Schaffer, A. (2017). Robot Collisions: A Survey on Detection, Isolation, and Identification. *IEEE Transactions on Robotics*, PP, pp. 1–21. doi:10.1109/TRO.2017.2723903.

Hamilton, W. (2009). XLII. On quaternions; or on a new system of imaginaries in algebra. *Philosophical Magazine Series 3*, 34. doi:10.1080/14786444908646233.

Campa, R., Camarillo-Gómez, K. (2008). Unit Quaternions: A Mathematical Tool for Modeling, *Path Planning and Control of Robot Manipulators*. 10.5772/6197.

Izard, Jean-Baptiste. 2013. Development of Remote Handling Technologies Tolerant to Operation Ready Fusion Reactor Conditions.

Khan, M.M., Nabi, A., Nahid, A., and Ali, M. (2019). Temperature Sensed Obstacle Avoiding Robot. *In: 2019 International Conference on Electrical, Computer and Communication Engineering (ECCE)*, pp. 1–6.

Khatib, O. (1985). Real-Time Obstacle Avoidance for Manipulators and Mobile Robots. *In: 1985 IEEE International Conference on Robotics and Automation*, vol. 1, pp. 500–505.

Krogh, B. and Thorpe, C. (1986). Integrated path planning and dynamic steering control for autonomous vehicles. *In: 1986 IEEE International Conference on Robotics and Automation*, vol. 3, pp. 1664 – 1669.

Kumar, N., et al. (2011). Neural network-based nonlinear tracking control of kinematically redundant robot manipulators. *Mathematical and Computer Modelling*, 53, pp. 1889–1901. doi:10.1016/j.mcm.2011.01.014.

Lewis, J., Zhong, X., and Rea, H. (1994). A neural network approach to the robot inverse calibration problem. *In: Second International Conference on Intelligent Systems Engineering*, pp. 342 – 347.

Li, G., Zhang, F., Fu, Y., and Wang, S. (2018). Joint Stiffness Identification and Deformation Compensation of Serial Robots Based on Dual Quaternion Algebra. *Applied Sciences*, 9, p. 65. doi:10.3390/app9010065.

Li, T., Sun, K., Xie, Z.w., and Liu, H. (2011). Optimal measurement configurations for kinematic calibration of six-DOF serial robot. *Journal of Central South University of Technology*, 18, pp. 618–626. doi:10.1007/s11771-011-0739-x.

Li, X. and Zhang, B. (2011). Toward general industrial robot cell calibration. *In: IEEE Conference on Robotics, Automation and Mechatronics, RAM Proceedings*, pp. 137– 142.

Lightcap, C., Hamner, S., Schmitz, T., and Banks, S. (2008). Improved Positioning Accuracy of the PA10-6CE Robot with Geometric and Flexibility Calibration. *IEEE Transactions on Robotics*, 24, pp. 452 – 456. doi:10.1109/TRO.2007.914003.

Lin, L.L., et al. (2015). Computer vision system RD for EAST Articulated Maintenance Arm robot. *Fusion Engineering and Design*, 100, pp. 254–259. doi: 10.1016/j.fusengdes.2015.06.017.

Liu, J., et al. (2020). Vision-based tile recognition algorithms for robot grasp- ing task in EAST. *Fusion Engineering and Design*, 152, p. 111422. doi: 10.1016/j.fusengdes.2019.111422.

Lumelsky, V. and Stepanov, A. (1987). Path-Planning Strategies for a Point Mobile Automaton Moving Amidst Unknown Obstacles of Arbitrary Shape. *Algorithmica*, 2, pp. 403–430. doi:10.1007/BF01840369.

Luo, G.N., et al. (2007). Directly-cooled VPS-W/Cu limiter and its preliminary results in HT-7. *Journal of Nuclear Materials*, 363-365(none), pp. 1241–1245.

Manuelraj, M., et al. (2016). Structural analysis of ITER multi-purpose deployer. *Fusion Engineering and Design*, 109. doi:10.1016/j.fusengdes.2015.12.039.

Maruyama, T., Noguchi, Y., Takeda, N., and Kakudate, S. (2015). Availability analysis of the iter blanket remote handling system. *Plasma and Fusion Research*, 10, pp. 1–4. doi:10.1585/pfr.10.3405010.

Minguez, J. (2005). The Obstacle Restriction Method (ORM): Obstacle Avoidance in Difficult Scenarios. *In: IEEE International Conference of Intelligent Robot System*.

Motta, J., Carvalho, G., and McMaster, R. (2001). Robot calibration using a 3D vision-based measurement system with a single camera. *Robotics and Computer-Integrated Manufacturing*, 17, pp. 487–497. doi:10.1016/S0736-5845(01)00024-2.

Muhammad, A., et al. (2007). Development of Water Hydraulic Remote Handling System for Divertor Maintenance of ITER. *In: 2007 IEEE 22nd Symposium on Fusion Engineering*, pp. 1–4.

Nakahira, M., et al. (2009). Design progress of the ITER blanket remote handling equipment. *Fusion Engineering and Design - FUSION ENG DES*, 84, pp. 1394–1398. doi: 10.1016/j.fusengdes.2009.03.006.

Nieminen, P., et al. (2009). Water hydraulic manipulator for fail safe and fault tolerant remote handling operations at ITER. *Fusion Engineering and Design - FUSION ENG DES*, 84, pp. 1420–1424. doi:10.1016/j.fusengdes.2008.12.002.

Noguchi, Y., Saito, M., Maruyama, T., and Takeda, N. (2018). Design progress of ITER blanket remote handling system towards manufacturing. *Fusion Engineering and Design*, 136. doi:10.1016/j.fusengdes.2018.03.068.

Okamura, K. and Park, F. (1996). Kinematic calibration using the product of exponentials formula. *Robotica*, 14, pp. 415 – 421. doi:10.1017/S0263574700019810.

Pan, H., 2017. Research on Compliance Control System of Remote Handling Robot for Graphite Tile of EAST PFC. Hefei, China: University of Science and Technology of China.

Pan, P., et al. (2018). Design and implementation of 3-DOF gripper for maintenances tasks in EAST vacuum vessel. *Fusion Engineering and Design*, 127, pp. 40–49. doi: 10.1016/j.fusengdes.2017.12.026.

Parker, J., Khoogar, A., and Goldberg, D. (1989). Inverse kinematics of redundant robots using genetic algorithms. *In: IEEE International Journal on Robotics and Automation*, pp. 271 – 276 vol.1. ISBN 0-8186-1938-4.

Paul, R. (1981). The Computer Control of Robot Manipulators. *Robot manipulators: mathematics, programming, and control*.

Peng, X., Lei, M., and Li, G. (2010). Conceptual design of EAST flexible in-vessel inspec- tion system. *Fusion Engineering and Design - FUSION ENG DES*, 85, pp. 1362–1365. doi:10.1016/j.fusengdes.2010.03.043.

Raimondi, T. (1989). The jet experience with remote handling equipment and future prospects. *Fusion Engineering and Design*, 11: 197-208. Rolfe, A. and Team, T. (1998). *The exchange of JET divertor modules using remote handling techniques*. ISBN JETP(98)15, 15-24 p.

Rolfe, A. C (1999). Experiences from the first ever remote handling operations at JET.' in, Proceeding of the International Conference : Remote techniques for Hazardous Environments. Rolfe, A.C., et al.. A report on the first remote handling operations at JET. *Fusion Engineering and Design*, 46(2-4), pp. 299–306.

Rolfe, A. (2007). A perspective on fusion relevant remote handling techniques. *Fusion Engineering and Design*, 82, pp. 1917–1923. doi:10.1016/j.fusengdes.2007.04.049.

Palm, R. （1992）. Control of a redundant manipulator using fuzzy rules. *Fuzzy Sets and Systems*, 45, 279-298.

Sancaktar, I., Tuna, B., and Ulutas, M. (2018). Inverse kinematics application on medical robot using adapted PSO method. *Engineering Science and Technology, an International Journal*, 21. doi:10.1016/j.jestch.2018.06.011.

Jun, Z., G. V. S. Raju. (1993). Fuzzy rule-based approach for robot motion control in the presence of obstacles. *Proceedings of IEEE Systems Man and Cybernetics Conference - SMC*, 4, pp. 662-667. doi: 10.1109/ICSMC.1993.390791.

Dorigo, M., Maniezzo, V., Colorni, A. (1996). Ant system: optimization by a colony of cooperating agents. *IEEE Transactions on Systems, Man, and Cybernetics*, Part B (Cybernetics), 26, 29-41.

Schlosser, J., et al. (2005). Technologies for ITER divertor vertical target plasma facing components. *Nuclear Fusion*, 45(6), pp. p.512–518.

Schneider, U., Momeni-K, M., Ansaloni, M., and Verl, A. (2014). *Stiffness Modeling of Industrial Robots for Deformation Compensation in Machining*.

Schroer, K., Albright, S., and Grethlein, M. (1997). Complete, minimal and model-continuous kinematic models for robot calibration. *Robotics and Computer Integrated Manufacturing*, 13, pp. 73–85. doi:10.1016/S0736-5845(96)00025-7.

Shi, S., et al. (2016). Conceptual design main progress of EAST Articulated Maintenance Arm (EAMA) system. *Fusion Engineering and Design*, 104, pp. 40–45.

Shiller, Z. (1998). Motion planning in dynamic environments using velocity obstacles. *The International Journal of Robotics Research*, 17, p. 760.

Simmons, R. (1996). The curvature velocity method for local obstacle avoidance. *In: 1996 IEEE International Conference on Robotics and Automation*, pp. 3375 – 3382 vol.4.

Singh, L., Stephanou, H., and Wen, J. (1996). Real-time robot motion control with circulatory fields. *In: Proceedings of the 1996 IEEE Intemational Conference on Robotics and Automation*, vol. 3, pp. 2737 – 2742 vol.3.

Siuko, Mikko, Jorma Järvenpää, Jouni Mattila, C. Damiani, and J. Palmer. 2021. IT/P7-19 DTP2 – Verifying The Divertor Remote Handling Equipment For ITER.

Song, Y., et al. (2014). Concept design on RH maintenance of CFETR Tokamak reactor. *Fusion Engineering and Design*, 89(9-10), pp. 2331–2335.

Stone, H. (1987). *Kinematic Modeling, Identification, and Control of Robotic Manipulators*, vol. 29.

Suh, K. and Hollerbach, J. (1987). Local Versus Global Torque Optimization of Redundant Manipulators. *In: IEEE International Conference on Robotics and Automation*, vol. 2, pp. 619 – 624.

Sun, Y., et al. (2019). Model-based spinal deformation compensation in robot- assisted decompressive laminectomy. *Mechatronics*, 59, pp. 115–126. doi: 10.1016/j.mechatronics.2019.03.008.

Tada, E., et al. (1998). Development of remote maintenance equipment for ITER blankets. *Fusion Engineering and Design*, 42, pp. 463–471. doi:10.1016/S0920-3796(98)00125- 2.

Tesini, A.(2015). *Maintence & Remote Handling*, <https://slideplayer.com/slide/4911527/>

Uchida, M. and Ide, H. (1995). Path Planning by SPM Method and its Application to Mobile Robot System. *IEEJ Transactions on Electronics Information and Systems*, 115, pp. 785–791.

Wang, D., Bai, Y., and Zhao, J. (2010). Robot manipulator calibration using neural network and a camera-based measurement system. *Transactions of The Institute of*

Measurement and Control - TRANS INST MEASURE CONTROL, 32. doi: 10.1177/0142331210377350.

Wang, J., Zhang, H., and Fuhlbrigge, T. (2009). *Improving Machining Accuracy with Robot Deformation Compensation*. pp. 3826 – 3831.

Wang, K., et al. (2017a). Inverse kinematics research using obstacle avoidance geometry method for EAST Articulated Maintenance Arm (EAMA). *Fusion Engineering and Design*, 119, pp. 1–11. doi:10.1016/j.fusengdes.2017.04.054.

Wang, Y., et al. (2017b). Accuracy improvement studies for remote maintenance manipulators. *Fusion Engineering and Design*. doi:10.1016/j.fusengdes.2017.04.097.

Wei, J., et al. (2015). Conceptual design of Blanket Remote Handling System for CFETR. *Fusion Engineering and Design*, 100(NOV.), pp. 190–197.

Wu, J., et al. (2016). Genetic algorithm trajectory plan optimization for EAMA: EAST Articulated Maintenance Arm. *Fusion Engineering and Design*, 109-111. doi: 10.1016/j.fusengdes.2016.02.015.

Wu, J., et al. (2018). Adaptive Neuro fuzzy inference system based estimation of EAMA elevation joint error compensation. *Fusion Engineering and Design*, 126, pp. 170–173. doi:10.1016/j.fusengdes.2017.11.025.

Xia, Y. and Wang, J. (2001). A dual neural network for kinematic control of redundant robot manipulators. *IEEE Trans- actions on Systems, Man, and Cybernetics, Part B: Cybernetics*, 31, pp. 147 – 154. doi:10.1109/3477.907574.

Xu, P., Tso, S., Wang, X., and Zhang, J. (1997). Sensor-based deflection modeling and compensation control of flexible robotic manipulator. *Mechanism and Machine Theory-MECH MACH THEOR*, 33, pp. 3780 – 3785 vol.4. doi:10.1109/ICSMC.1997.633258.

Yang, C., Ma, H., and Fu, M. (2016a). Obstacle Avoidance for Robot Manipulator. *In:Advanced Technologies in Modern Robotic Applications*, pp. 231–256.

Yang, Y., et al. (2016b). Visual servo simulation of EAST articulated maintenance arm robot. *Fusion Engineering and Design*, 104, pp. 28–33.

Zhang, J., Zhang, S., and Gao, R. (2019a). Discrete-time predictive trajectory tracking control for nonholonomic mobile robots with obstacle avoidance. *International Journal of Advanced Robotic Systems*, 16, p. 172988141987731. doi: 10.1177/1729881419877316.

Zhang, T., et al. (2019b). Deformation modeling of remote handling EAMA robot by recurrent neural networks. *Industrial Robot: the international journal of robotics research and application*, 46, pp. 300–310. doi:10.1108/IR-08-2018-0171.

Zhao, W., et al. (2015). Concept design of the CFETR divertor remote handling system.*Fusion Engineering and Design*, 98-99(OCT.), pp. 1706–1709.

Zhao, W., et al. (2019). Reliability based assessment of remote maintenance system for CFETR divertor. *Fusion Engineering and Design*, 146(Part B), pp. 2777–2780.

Zhong, X.L., Lewis, J., and L.N.-Nagy, F. (1996). Autonomous robot calibration using a trigger probe. *Robotics and Autonomous Systems*, 18, pp. 395–410. doi:10.1016/0921-8890(96)00011-5.

Zhuang, G., et al. (2019). Progress of the CFETR design. *Nuclear Fusion*, 59(11), p. 112010. doi:10.1088/1741-4326/ab0e27.

Zhuang, H. and Roth, Z. (1991). A closed form solution to the kinematic parameter identification of robot manipulators. *In: Proceedings - IEEE International Conference on Robotics and Automation*, vol. 3, pp. 2682 – 2688 vol.3.

Zhuang, H. and Roth, Z. (1993). Linear solution to the kinematic parameter identification of robot manipulators. *IEEE Transactions on Robotics and Automation*, 9, pp. 174 – 185. doi:10.1109/70.238281.

NOGUCHI, Y., SAITO, M., MARUYAMA, T. & TAKEDA, N. (2018). Design progress of ITER blanket remote handling system towards manufacturing. *Fusion Engineering and Design*, 136, 722-728.

RIBEIRO, I., DAMIANI, C., TESINI, A., KAKUDATE, S., SIUKO, M. & NERI, C. (2011). The remote handling systems for ITER. *Fusion Engineering and Design*, 86, 471-477.

CHOI, C.-H., TESINI, A., SUBRAMANIAN, R., ROLFE, A., MILLS, S., SCOTT, R., FROUD, T., HAIST, B. & MCCARRON, E. 2015. Multi-purpose deployer for ITER in-vessel maintenance. *Fusion Engineering and Design*, 98-99, 1448-1452.

Publication I

Zhang, T., Cheng, Y., Wu, H., Song, Y., Yan, S., Handroos, H., Zheng, L., Ji, H., and Pan, H.

Dynamic accuracy ant colony optimization of inverse kinematic (DAACOIK) analysis of multi-purpose deployer (MPD) for CFETR remote handling

Reprinted with permission from
Fusion Engineering and Design
Vol.156: 111522, 2020

Fusion Engineering and Design 156 (2020) 111522

Contents lists available at ScienceDirect

Fusion Engineering and Design

journal homepage: www.elsevier.com/locate/fusengdes

Dynamic accuracy ant colony optimization of inverse kinematic (DAACOIK) analysis of multi-purpose deployer (MPD) for CFETR remote handling

Tao Zhang[a,b,c], Yong Cheng[a,d,*], Huapeng Wu[c], Yuntao Song[a], Sheng Yan[a,b], Heikki Handroos[c], Lei Zheng[a], Haibiao Ji[a,c], Hongtao Pan[a,d]

[a] Institute of Plasma Physics Chinese Academy of Sciences (ASIPP), Chinese Academy of Sciences, He'fei, 230000, China
[b] University of Science and Technology of China, He'fei, 230000, China
[c] Lappeenranta University of Technology (LUT), Lappeenranta, Finland
[d] Huainan New Energy Research Center, Anhui Provincial Key Laboratory of Special Welding, Huai'nan, 232000, China

ARTICLE INFO

Keywords:
Multi-Purpose Deployer (MPD)
Inverse kinematics (IK)
Ant colony optimization (ACO)

ABSTRACT

The Chinese Fusion Engineering Testing Reactor (CFETR) is a superconducting Tokamak device that needs delicate maintenance. The Multi-Purpose Deployer (MPD), a redundant and heavy robot for remote handling (RH), is used to repair and monitor the device. For a redundant robot doing maintenance in complicated surroundings, the accurate and efficient Inverse Kinematics (IK) calculating is necessary for the motion control. In this paper, a new method that uses a Dynamic Accuracy Ant Colony Optimization (DAACO) solving redundant IK of MPD is developed. The result shows that this method has an excellent performance in kinematics to control the MPD to complete the RH task in future fusion engineering construction.

1. Introduction

The Chinese Fusion Engineering Testing Reactor (CFETR) is a superconducting Tokamak device [1] shown in Fig. 1. The vacuum vessel, a container of the fusion reaction, which would possibly be damaged during experiments by high-temperature baking or radiation, should be maintained at halt mode by RH systems [2,3]. Thus, a nine-degrees of freedom (DOF)long and heavy robot, equipping with a lightweight end effector, has been developed to commit the complex maintenance tasks inside of the complicated structure of CFETR [4]. Meanwhile, the motion trajectory of MPD should be planned very precisely and its kinematics must satisfy geometric and collision-free constraints [5].

The MPD is a redundant robot that has complicated mechanic structure, eight rotation joints and one prismatic joint shown in Fig. 2. The prismatic track is supported by a cask to store, transports the device and offers a linear motion. The redundant kinematics problems have been widely studied in the word [6], which are important to control the redundant robot especially in fusion applications.

There are two main methods to solve redundant inverse kinematics problems, which are the analytic method and numerical method. The former one calculates the joint's analytic equations. By contrast, the second one mainly solves the inverse kinematics solution of joints by iterations. The analytic method studies the equations of the transformation matrix of joints [7]. And a method that analyzes the geometric model of a robot to calculate analytic equations is introduced in the reference [8]. The other methods are studied by Liegeois [9] and Klein [10], those methods are categorized into the Jacobian matrix method [11]. Klein is the earliest researcher, who studies IK of redundant robots. However, the Jacobian method has some singularity problems. Yoshihiko developed an IK method with singularity robustness in 1986 [12]. He modified the SR-inverse Jacobian matrix to reduce singularity. With the increased computational power, many intelligent algorithms have developed, and various numerical methods are developed in actual applications. With the intelligent algorithms, complicated formulas of a robot can be easily solved. Many techniques focus on evolutionary approaches [13–15]. Patrick Beeson [15] created an IK library with generic algorithms that imitate the genetic theory of creatures to search optimization solutions. Ahmed R. J. Almusawi came up with an artificial neural network (ANN) to solve the IK. However, the process of training network is time-consuming and difficult [16]. The particle swarm optimization (PSO) is also a good way to solve a nonlinear optimization problem [17,18]. However, The PSO's model is quite complicated. These intelligent methods regard the IK problem as an optimization problem. As we knew, the ant colony optimization (ACO) has good advantages in an optimization problem especially for solving nonlinear equations. So a metabolic ant colony optimization,

* Corresponding author at: Institute of Plasma Physics Chinese Academy of Sciences (ASIPP), Chinese Academy of Sciences, He'fei, 230000, China.
E-mail address: chengyong@ipp.ac.cn (Y. Cheng).

https://doi.org/10.1016/j.fusengdes.2020.111522
Received 19 September 2019; Received in revised form 2 February 2020; Accepted 2 February 2020
Available online 06 March 2020
0920-3796/

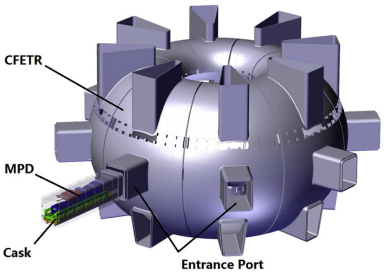

Fig. 1. Whole view of MPD together with CFETR.

which is called DAACO, is studied in this paper. It is a more accurate method comparing to the ACO.

In this paper, Section 1 introduces some background and the related work about the MPD. The mathematics model of MPD with the standard Denavit–Hartenberg (DH) method and reconstruction model of the CFETR have been studied in Section 2. Section 3 lays emphasis on dynamic accuracy ant colony optimization. In Section 4, the procedure of the MPD's IK is introduced in detail, such as forward kinematics, inverse kinematics and collision. The results and conclusions are shown in Section 5.

2. Kinematic modeling of robot MPD and CFETR

2.1. Mathematic model of robot MPD

The fundamental analysis of a robot is building up coordinate systems by the Denavit–Hartenberg (DH) convention and find the DH parameters [19]. There are 2 branches : the standard DH method and the modified DH method. The difference between them is the sequence defining α, a, d, and θ, which are the DH parameters of a robot. Using the standard DH method, the coordination of MPD can be established in Fig. 3, and its DH parameters are listed in Table 1. Accordingly, a relationship in adjacent coordinates (coordinate i bonded to joint i and coordination i-1 bonded to joint i-1) can be given by a homogenous transformation matrix A_i

$$A_i = \begin{bmatrix} \cos\theta_i & -\sin\theta_i\cos\alpha_i & \sin\theta_i\sin\alpha_i & a_i\cos\theta_i \\ \sin\theta_i & \cos\theta_i\cos\alpha_i & -\cos\theta_i\sin\alpha_i & a_i\sin\theta_i \\ 0 & \sin\alpha_i & \cos\alpha_i & d_i \\ 0 & 0 & 0 & 1 \end{bmatrix} \tag{1}$$

where θ_i, a_{i-1}, d_i, and α_{i-1} are link parameters of joint i.

2.2. Geometric model of CFETR

The CFETR's geometric model can be rebuilt by the point cloud. This point cloud would be measured by a laser device (Leica Absolute Tracker AT960 and FARO Laser Scan Arm), and a measuring method is introduced by Haibiao Ji [20]. In his study, the 3D model's point cloud is replaced by the measuring for the simulation. Hundreds of points on the CFETR's section plane were measured to fitting curves of a blanket. There is a transformation ${}^{CFETR}_{MPD}T$ between CFETR's and MPD's origin as shown in Eq. 2. The model of CFETR is shown in Fig. 4. Fig. 4a shows a relation between the CFETR and the MPD in top view. Points P_1 and P_2 represent two typical points in the main body of the CFETR and in the tunnel respectively. At the same time, Fig. 4a, 4c and 4d show the geometric positions of P_1 and P_2 in the top view and sectional view respectively. Eqs. 3 and 4 show the relation by analyzing the geometric features of them. By using CFETR's 3D model, a mathematical 3D model has been built up with the help of MATLAB's robotic tools in Fig. 4b.

$${}^{CFETR}_{MPD}T = \begin{bmatrix} 1 & 0 & 0 & 0 \\ 0 & 1 & 0 & -d_{CM} \\ 0 & 0 & 1 & 0 \\ 0 & 0 & 0 & 1 \end{bmatrix} \tag{2}$$

where d_{CM} is the distance between the CFETR's origin and the MPD's origin.

$$\begin{cases} x_{D1} = \sqrt{x_1^2 + y_1^2} \\ y_{D1} = z_1 \end{cases} \tag{3}$$

$$\begin{cases} x_{D2} = x_2 \\ y_{D2} = z_2 \end{cases} \tag{4}$$

3. Dynamic accuracy ant colony optimization (DAACO)

There are some methods about the inverse kinematics of the redundant robot. Compared to the PSO algorithm, the ACO is more efficient in global optimization. Moreover, the ACO algorithm is a stochastic searching procedure as same as and rapidly exploring random tree (RTT). However, the former one has lower space complexity. To improve its performance, the dynamic accuracy is introduced comparing to the fixed accuracy of traditional ACO in Section 3.2. The central component of ACO is the pheromone model, which is used to probabilistically sample the search space [21].

3.1. Introduction to ACO

The ACO is a system that has lots of choices of solution components c_i^j in solution space $\mathscr{S}$, which simulate ants searching for optimal solutions. This process is designed with mathematic parameters such as pheromone trail parameter, transition probabilities and so on. Pheromone trail parameters reflect an ant emitting some pheromone in trail to tell its fellows to come along this route for treasure. And transition probabilities indicate whether its fellows can receive his messages. The pheromone trail parameter τ_i^j, which is corresponding to c_i^j and transition probabilities $p(c_i^j|\ s^p)$, can be represented as follow:

$$\tau_i^j \longleftarrow (1-\rho)\cdot\tau_i^j + \sum_{c_k^l \in \Re(s^p)} \Delta\tau_i^j, \quad , \ \forall\ c_k^l \in \Re(s^p) \tag{5}$$

where ρ is an evaporation rate, c_i^j is the choice of a solution component, s^p is a partial solution, $\Re(s^p)$ is a feasible solution component set.

$$p(c_i^j|\ s^p) = \frac{[\tau_i^j]^\alpha \bullet [\eta(c_i^j)]^\beta}{\sum_{c_k^l \in \Re(s^p)} [\tau_k^l]^\alpha \bullet [\eta(c_k^l)]^\beta}, \ \forall\ c_i^j \in \Re(s^p) \tag{6}$$

where α is the relative importance of pheromone value ($\alpha > 0$). β is the relative importance of heuristic information ($\beta > 0$). η is heuristic information that assigns to each valid solution component possibly depending on the current step.

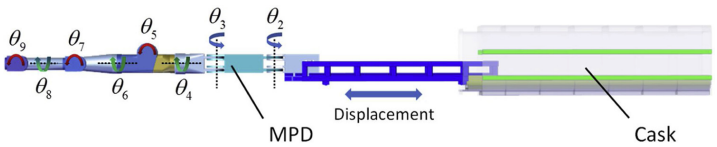

Fig. 2. 3D model of MPD.

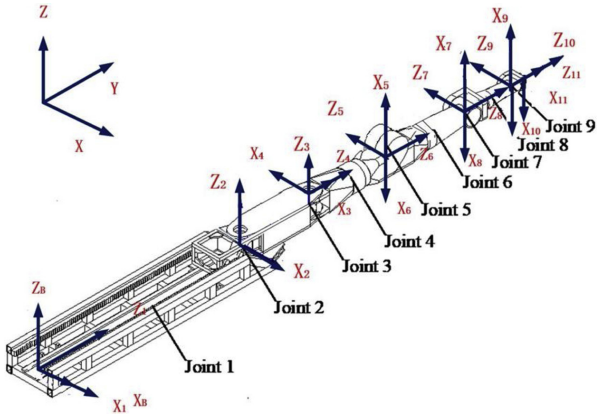

Fig. 3. DH coordinate system established for MPD.

Table 1
DH parameters of MPD.

Index	α (deg)	a(mm)	θ(deg)	d(mm)	Range from initial value	Initial value of joint
1	−90	0	0	0	None	None
2	90	0	0	d_1	[−1965,4455]	0
3	0	1750	θ_2	0	[90,270]	90
4	90	0	θ_3	0	[−90,90]	90
5	90	0	θ_4	1965	[−90,270]	90
6	90	0	θ_5	0	[0,180]	180
7	90	0	θ_6	2000	[0,360]	180
8	90	0	θ_7	0	[90,270]	180
9	90	0	θ_8	1600	[0,360]	180
10	90	0	θ_9	0	[90,270]	180
11	0	0	0	435	None	None

3.2. DAACO of MPD's IK

The IK problem can be regarded as a case that is solving some nonlinear equations as Eq.7 [22]. And the solutions of $F(X) = 0$ is equal to find the solutions of a cost function $G(X) = 0$. The $G(X)$ can be written as shown in Eq. 8.

$$F(X) = \begin{cases} f_1(X) \\ f_2(X) \\ \cdots \\ f_n(X) \end{cases} \tag{7}$$

where X is a vector of variables, f_i is a nonlinear function position or orientation restriction condition.

$$G(X) = \sum_{i=1}^{n} - \lambda_i f_i^2 \tag{8}$$

where λ_i is an arbitrary real positive number.

In the MPD's IK, the c_i^j can be regarded as a possible solution X_i of IK and the $G(X)$ represents an index of result. Moreover, Heuristic information can be designed as shown in Eq. 9.

$$\eta = \frac{1}{G(X)} \tag{9}$$

The DAACO has a dynamic accuracy that is changeable together with iteration index (II). When II approaches the iteration number (IN), the dynamic accuracy would be closer to the desired algorithm accuracy. This dynamic accuracy algorithm would search in solution space more precisely, and won't trap into a local minimum.

4. Kinematics of MPD

4.1. Forward kinematics

The kinematics of a robot is the foundation for robot control. According to the DH method, the homogeneous matrix ${}_i^jT$ represents the relation of j^{th} joint to i^{th} joint, which can be also denoted as a matrix A_i. The forward kinematics of MPD can be easily calculated from Eq. 10.

$${}_i^jT = A_j \quad s.t. \quad j = i + 1 \tag{10}$$

$${}_{11}^{0}\mathrm{T} = A_1 \bullet A_2 \bullet\bullet\bullet\bullet\bullet\bullet\bullet A_9 \bullet A_{10} \bullet A_{11} \tag{11}$$

There is a position restriction of cask for 1st, 2nd and 3rd joint in Table 3. And these cases map different geometric situations shown in Fig. 5a, 5b and 5c respectively. In Case 1 (Fig. 5a), a prismatic joint restriction of the cask leads to a result that joint 2 and joint 3 cannot have any rotation. When the 1st joint goes forward and the 3rd joint goes into the vacuum vessel completely, the 3rd joint can rotate without any restriction in Case 2 (Fig. 5b). And in Case 3 (Fig. 5c), there is no geometric restriction on the 2nd and 3rd joint, and both joints can move in the workspace freely.

Thus, the MPD is a redundant robot that can 'freely' position and orient an object in the Cartesian workspace [23]. Some DOF restrictions, such as self-collision free and surrounding collision-free, should be considered so that solutions can be reasonable. To simplify the model, a novel method, which is dividing the whole arm into two parts, analyzes the MPD's inverse kinematics (Fig. 7).

4.2. Inverse kinematics

The redundant inverse kinematics model is a nonlinear, and it's hard to calculate the analytic equations. There are lots of methods to find the solution, such as the Newton algorithm (NA), Muller algorithm (MA), Levenberg-Marquardt algorithm (LMA), rapid-exploring random trees (RRT) and so on. The NA algorithm adopts a differential method to calculate solutions with the shortcoming of local minimum, i.e., possibly it cannot find a solution when the step size is not small enough [24]. The MA is less efficient in solving multivariable of nonlinear equations [25]. The LMA is a good method for solving nonlinear equations, but it depends on the initial searching points. Generally, an IK problem is always a hyperplane problem and hard to guess the initial

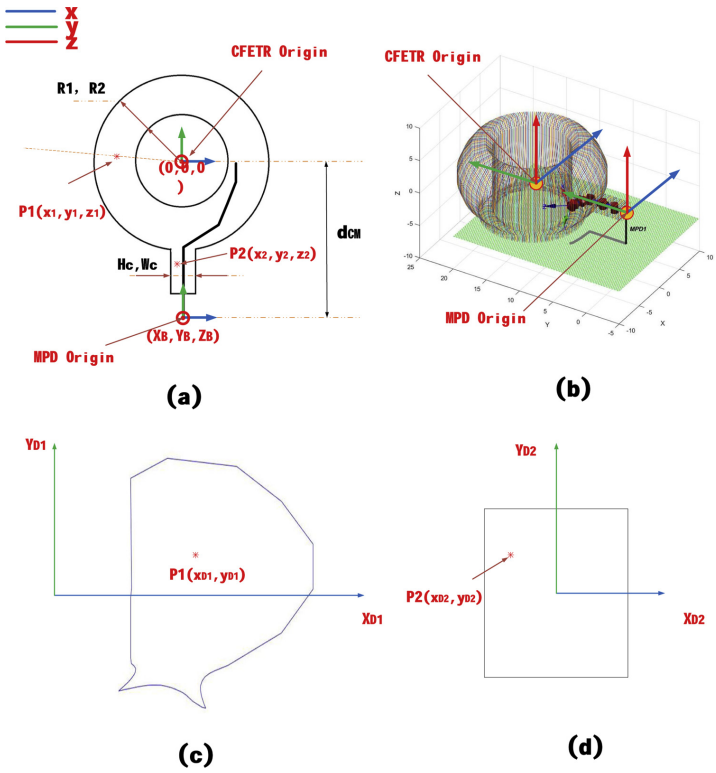

Fig. 4. Mathematic model of the CFETR.
a: relationship between the CFETR and the MPD in top view, b: 3D reconstruction of the CFETR by mathematical modeling, c: main body sectional view of the CFETR, d: tunnel's (cask's) sectional view of the CFETR.

value [26]. The RRT is a time-consuming method. When the interval of exploring is not small enough, it would miss some solutions [27,28]. According to these investigations, this paper uses an ACO method, which can search global optimum and has faster solving speed in the calculation. The specific procedure of the ACO of IK will be introduced in the next section.

This paper adopts a geometric & algebra method to analyze this problem. According to the MPD structure, the whole robot is divided intotwo parts: the first part from joint 0 to joint 7, and the rest joints as the second part, such that the kinematics solutions for the joints in each part can be calculated easily. Meanwhile, there is a good geometric feature that the origin of coordination 6 and coordination 7 is coincident as shown in Fig. 3. The forward kinematic relationship in the two parts is listed in Eq. 12.

$$\begin{cases} T_{END} = T_{MPD}^{CFETR} \cdot T_{11}^{0} \\ T_{11}^{0} = T_{7}^{0} \cdot T_{11}^{7} \\ T_{11}^{7} = T_{8}^{7} \cdot T_{9}^{8} \cdot T_{10}^{9} \cdot T_{11}^{10} \\ T_{7}^{0} = T_{1}^{0} \cdot T_{2}^{1} \cdot T_{3}^{2} \cdot T_{4}^{3} \cdot T_{5}^{4} \cdot T_{6}^{5} \cdot T_{7}^{6} \\ T_{6}^{0} = T_{1}^{0} \cdot T_{2}^{1} \cdot T_{3}^{2} \cdot T_{4}^{3} \cdot T_{5}^{4} \cdot T_{6}^{5} \end{cases} \tag{12}$$

An iteration procedure is in Fig. 6. Through setting different target matrices for two parts, the DAACO, which is an intelligent ant colony optimization algorithm, is applied to analyze each part respectively. After calculating the results of joints, the collision check algorithm is committed to ensure collision-free. When every requirement of IK is met, the output solutions are achieved.

The target matrix T_{END} includes the target orientation matrix R_{END} and the target position vector P_{END} which are the input of the flowchart of MPD's inverse kinematics.

$$T_{END} = \begin{bmatrix} R_{END} & P_{END} \\ 0 & 1 \end{bmatrix} \tag{13}$$

where R_{END} is $[X_{END} \quad Y_{END} \quad Z_{END}]$ and P_{END} is $\begin{bmatrix} p_x \\ p_y \\ p_z \end{bmatrix}$.

To demand the geometric restriction of the algorithm, a point P_7 is generated in the inner space of CFETR randomly, and the y-axis of position $P_{7,y}$ should be smaller than the target position p_y in the y-axis direction.

The transformation from coordination 0 to coordination 7 can be deduced as Eq. 14 and 15 shown.

$${}_{7}^{0}\mathrm{T} = \begin{bmatrix} {}_{7}^{0}R & {}_{7}^{0}P \\ 0 & 1 \end{bmatrix} \tag{14}$$

where ${}_{7}^{0}R$ is the rotation matrix between coordination B to coordination 7. ${}_{7}^{0}P$ is the position vector between coordination B to coordination 7.

Furthermore, the position of P_7 is only related to joints 1–5

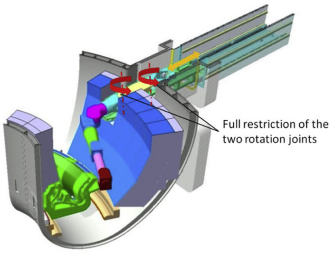

a Full restriction of the two rotation joints (Case 1)

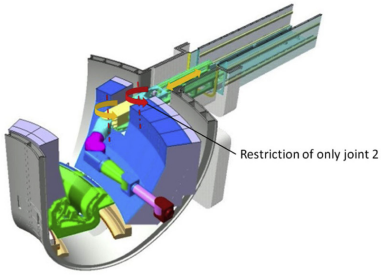

b Restriction of only joint 2 (Case 2)

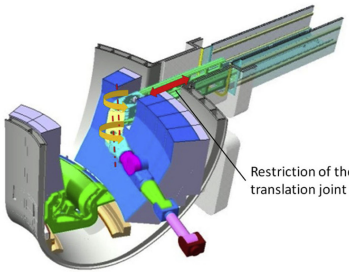

c Restriction of the translation joint (Case 3)

Fig. 5. a) Full restriction of the two rotation joints (Case 1).
b)Restriction of only joint 2 (Case 2).
c)Restriction of the translation joint (Case 3).

according to Eq. 15. Eq. 15a is the universal position matrix. Substituting Table 1 into Eqs. 15a, 15b, 15c and 15d are deduced which represent case 1, case 2 and case 3 respectively.

$$ {}^{0}_{7}P = \begin{bmatrix} 2000(c_{23}c_4s_5 - s_{23}c_5) + 1965s_{23} + 1750c_2 \\ 2000(s_{23}c_4s_5 + c_{23}c_5) - 1965c_{23} + 1750s_2 + d_1 \\ 2000s_4s_5 \end{bmatrix} \tag{15a} $$

$$ {}^{0}_{7}P = \begin{bmatrix} -2000c_4s_5 \\ -2000c_5 + 3715 + d_1 \\ 2000s_4s_5 \end{bmatrix} \tag{15b} $$

$$ {}^{0}_{7}P = \begin{bmatrix} -2000(s_3c_4s_5 + c_3c_5) + 1965c_3 \\ 2000(c_3c_4s_5 - s_3c_5) + 1965s_3 + 1750 + d_1 \\ 2000s_4s_5 \end{bmatrix} \tag{15c} $$

$$ {}^{0}_{7}P = \begin{bmatrix} 2000(c_{23}c_4s_5 - s_{23}c_5) + 1965s_{23} + 1750c_2 \\ 2000(s_{23}c_4s_5 + c_{23}c_5) - 1965c_{23} + 1750s_2 + 4455 \\ 2000s_4s_5 \end{bmatrix} \tag{15d} $$

Combining Eq. 15 and Eq. 12, the DAACO can find the IK solution for joint 1–5. The next step is to calculate the rest of the joints. According to the DH method, the ${}^{6}_{11}T$ can be represented by Eq. 16. The algorithm of DAACO for inverse kinematics is shown in Table 2.

$$ {}^{6}_{11}T = {}^{0}_{6}T^{-1} \cdot {}^{0}_{11}T \tag{16} $$

At the same time, ${}^{6}_{11}T$ can also be represented in the forward kinematics mode as Eq. 17, and it is a cost function of joint 6-9. Combining Eq. 12, 15, and 16, the DAACO can find the rest of the joints.

$$ {}^{6}_{11}\mathrm{T} = \begin{bmatrix} {}^{6}_{11}R & {}^{6}_{11}P \\ 0 & 1 \end{bmatrix} \tag{17} $$

Because of the geometric restriction of the CFETR and the MPD, the solution for some desired orientations and positions are not always existed. In the workspace of the CFETR, some points' positions can be determined independently. Thus, lots of end effectors of MPD are designed for completing high accuracy maintenance furtherly.

4.3. Collision check with surroundings

A collision check is necessary for obtaining a reasonable solution. Every segment of the MPD can be enveloped with a cylinder. The robot's collision problem can be regarded as a cylinder collision problem. However, the CFETR has a complicated geometric model and there is no hook face to fit its inner 3D surface with an explicit formula. Due to this reason, a collision check can be transferred into a 2D problem that is circle collision checking with a section plane, and the circle is the section plane of the MPD. Computer graphics would be very useful for solving this problem. Every picture of a section plane can be transferred into a greyscale image. For better understanding and reading, colorful pictures are shown in this paper instead of greyscale images. However, the greyscale images are used in the calculation for the DAACO. In Fig. 8 a^{th} column shows an initial state of the sectional view. After rendering, in b^{th} column the light blue one also shows an initial state of sectional view for a better view. Because of the picture's scale's problem, the dark blue circle looks like an oval which represents MPD's section plane in c^{th} column. After rendering the CFETR's section again, d^{th} column can be obtained to represent the collision state. The difference between a^{th} and d^{th} column in gray-scale type is then used for the collision check. When the difference matrix of grayscale images has been solved, the Boolean matrix corresponding to the difference matrix can be obtained. A threshold value can be decided according to the rendering gray value. The rows 1, 2, 3 and 4 represent four states: the MPD colliding free with the main body of the CFETR, the MPD colliding with the main body of the CFETR, the MPD colliding free with the tunnel of the CFETR, and the MPD colliding with the tunnel of the CFETR respectively.

4.4. Self-collision of MPD

When all joint values have been gained, the self-collision checking algorithm will be appliedThe radius of the enveloped cylinder which is mentioned in Section 4.3 will be used for checking. The self-collision checking process is shown in Table 4. After this procedure, the output will give whether there is a collision-free solution.

5. Results and conclusion

The 100 samples have been tested by using the DAACOIK algorithm and the results are shown in Table 5. From the results, only 87 samples can obtain a meaningful solution. Furthermore, the results of position accuracy in 87 samples and the results of orientation accuracy in 15

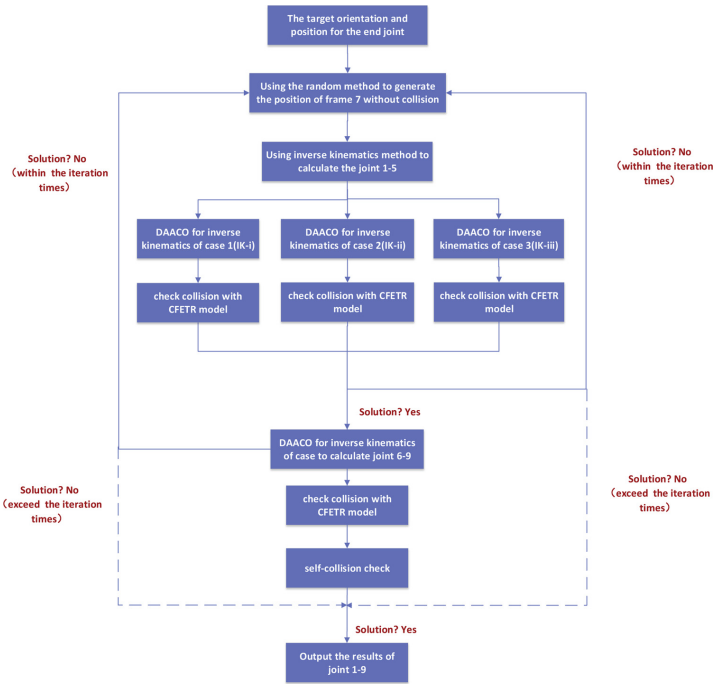

Fig. 6. Flowchart of MPD's inverse kinematics.

samples are shown in Fig. 9. Some indexes of absolute error are shown in Table 6, and the results are reasonable enough for the long and redundant robot.

The results of the DAACOIK are verified by the simulation. The DAACOIK is very useful for the off-line control of the MPD. In the future, the hardware coding of the algorithm would be tested for measuring its calculation time. Meanwhile, online control would be tested. Furthermore, the GPU accelerating algorithm will be studied because of the computer graphics based collision-free procedures.

Declaration of Competing Interest

The authors declare that they have no known competing financial interests or personal relationships that could have appeared to influence the work reported in this paper.

CRediT author statement

Zhang Tao: conceptualization, methodology, writing-original draft preparation
Yong Cheng: mechanical modeling of robot
Huapeng Wu: supervision, revising
Yuntao Song: supervision, revising
Sheng Yan: visualization, investigation, DH modeling of robot
Heikki Handroos: supervision
Lei Zheng: mechanical modeling of robot, visualization
Haibiao Ji: mechanical modeling of robot, visualization
Hongtao Pan: mechanical modeling of robot

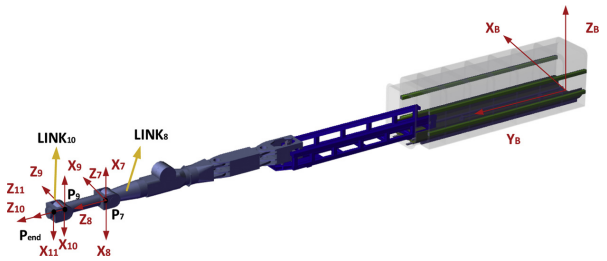

Fig. 7. Geometric model of joint 7-10.

Table 2
the DAACO's principle of IK.

Input: the target matrix T_{end}, the range limitation of joints, the accuracy of the algorithm (AA)
While $II < = IN$ **do**
Initialize all parameters: Xi, τ_0
Update τ, p
Calculate the cost function G, η
If $G < AA^* exp\ (IN - II)$
If $IT - II = 0$
Output ⟵ Desired joint value j_d
Else
using Xi which belongs to top 5 in G's value to generate new Xi by inheritance, variation and hybridization for the next iteration
End if
End if
End while

Note: $AA^* exp\ (IN - II)$ is dynamic accuracy of DAACO.

Table 3
Restriction of parameters among joints 1-3.

Case index	$d_1(mm)$	θ_2(deg)	θ_3(deg)
1	[-1965,2705)	90	90
2	[2705,4455)	90	[-90,90]
3	4455	[90,270]	[-90,90]

Table 4
Algorithm of self-collision.

Input: spatial line segment SL_i, cylinder's radius CR_i corresponding to SL_i
For i = 1:8
For j = i + 1:9
If j-i = 1
A bool B_{ij} to check whether only one crossing point of SL_i, SL_j
Else
A bool B_{ij} to check the distance of SL_i, SL_j > CR_i + CR_j
End
End
End
$\prod B_{ij} = 1$?
Yes, no self-collision
No, self-collision

Table 5
100 samples' result for DAACOIK.

solution number	orientation	position
15	√	√
72	×	√
13	×	×

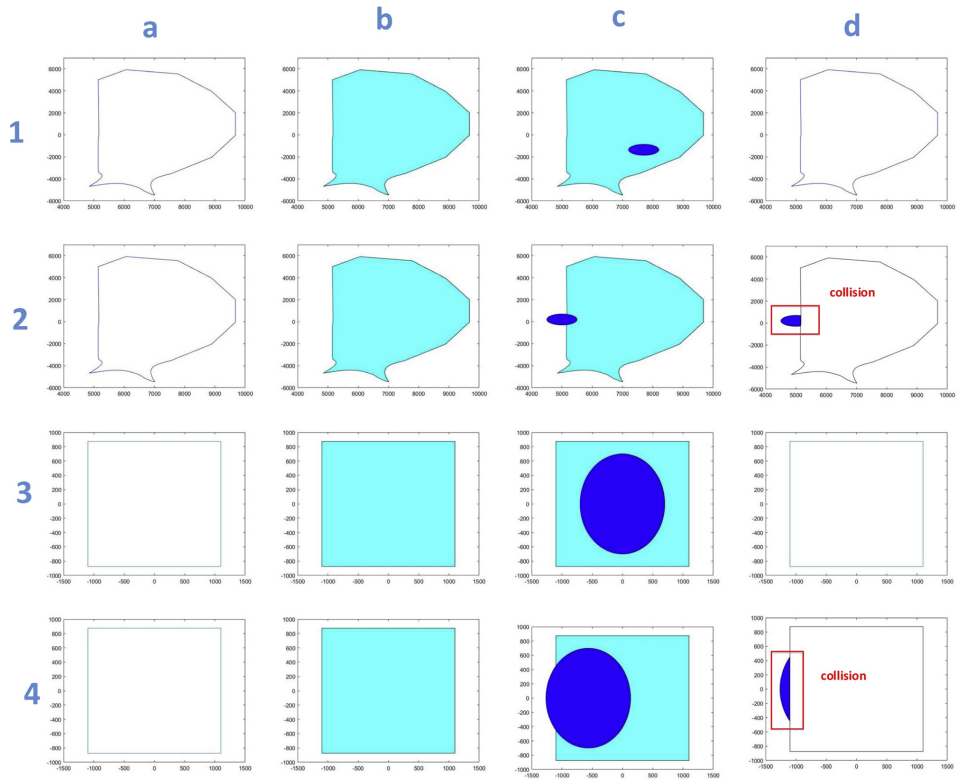

Fig. 8. Four different states for collision check between MPD and CFETR.

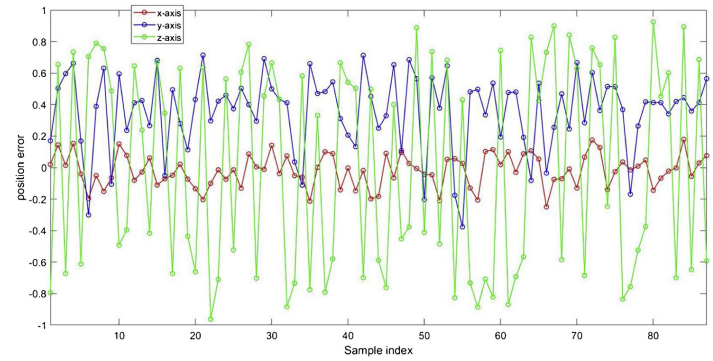

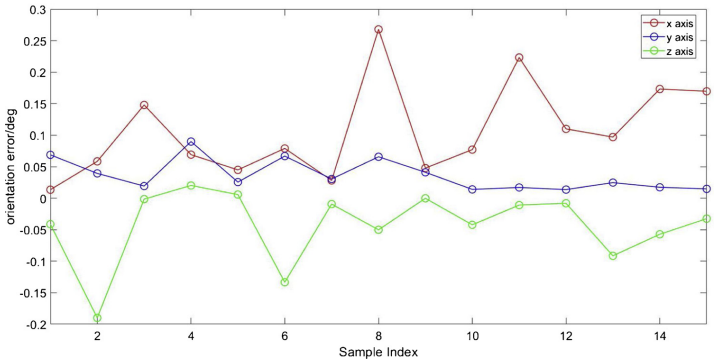

Fig. 9. Position an orientation accuracy of DAACOIK.

Table 6
Some analysis indexes of DAACO's IK.

	Position/mm			Orientation/deg		
	x axis	y axis	z axis	x axis	y axis	z axis
mean	0.0830	0.3953	0.6381	0.1071	0.0365	0.0463
Standard deviation	0.0610	0.1772	0.1648	0.0743	0.0247	0.0542

Acknowledgements

Thanks to the ASIPP and LUT's work fellow for the inspiration about this geometric algorithm. This project is funded by the Comprehensive Research Facilities in Support of CFETR (2017YFE0300503).

Appendix A. Supplementary data

Supplementary material related to this article can be found, in the online version, at doi:https://doi.org/10.1016/j.fusengdes.2020.111522.

References

[1] Y. Song, S. Wu, Y. Wan, et al., Concept design on RH maintenance of CFETR Tokamak reactor[J], Fusion Eng. Des. 89 (9–10) (2014) 2331–2335.
[2] S.K. Saha, Introduction to Robotics, Chinese Machine Press, 2009.
[3] T. Zhang, et al., Deformation modeling of remote handling EAMA robot by recurrent neural networks, Ind. Rob. 46 (2) (2019) 300–310.
[4] M.S. Manuelraj, P. Dutta, K.K. Gotewal, et al., Structural analysis of ITER multipurpose deployer[J], Fusion Eng. Des. 109–111 (2016) 1296–1301.
[5] H. Pan, K. He, Y. Cheng, Y. Song, Y. Yang, E. Villedieu, et al., Conceptual design of east multi-purpose maintenance deployer system, Fusion Eng. Des. 118 (2017) 25–33.
[6] C.H. Choi, A. Tesini, R. Subramanian, et al., Multi-purpose deployer for ITER in-vessel maintenance[J], Fusion Eng. Des. 98–99 (2015) 1448–1452.
[7] Kelsey P. Hawkins. Analytic Inverse Kinematics for the Universal Robots UR-5/UR-10 Arms.
[8] C.S.G. Lee, M. Ziegler, Geometric approach in solving inverse kinematics of puma robots. IEEE Transactions on Aerospace and Electronic Systems, AES 20 (6) (1984) 695–706.
[9] A. Liegeois, Automatic supervisory control of configuration and behavior of multibody mechanisms, IEEE Trans. Syst. Man Cybern. 7 (12) (1977) 868–871.
[10] C.A. Klein, C.H. Huang, Review of pseudoinverse control for use with kinematically redundant manipulators. IEEE Transactions on Systems, Man, and Cybernetics, SMC 13 (2) (1983) 245–250.
[11] D.E. Orin, W.W. Schrader, Efficient computation of the Jacobian for robot manipulators, Int. J. Rob. Res. 3 (4) (1984) 66–75.
[12] Y. Nakamura, H. Hanafusa, Inverse kinematic solutions with singularity robustness for robot manipulator control, J. Dyn. Syst. Meas. Control 108 (3) (1986) 163–171.
[13] S. Momani, Z.S. Abo-Hammour, O.M.K. Alsmadi, Solution of inverse kinematics problem using genetic algorithms, Appl. Math. Inf. Sci. 10 (1) (2016) 225.
[14] R. Koker, A genetic algorithm approach to a neural-network-based inverse kinematics solution of robotic manipulators based on error minimization, Inf. Sci. (2013).
[15] P. Beeson, B. Ames, IEEE 2015 IEEE-RAS 15th International Conference on

Humanoid Robots (Humanoids) - Seoul, South Korea (2015.11.3-2015.11.5)] 2015 IEEE-RAS 15th International Conference on Humanoid Robots (Humanoids) - TRAC-IK: an Open-source Library for Improved Solving of Generic Inverse Kinematics, IEEE-RAS International Conference on Humanoid Robots (pp.928-935), IEEE, 2015.
[16] A.R.J. Almusawi, D.L. Canan, K. Sadettin, A new artificial neural network approach in solving inverse kinematics of robotic arm (denso vp6242), Comput. Intell. Neurosci. 2016 (2016) 1–10.
[17] S. Starke, N. Hendrich, S. Magg, J. Zhang, An efficient hybridization of Genetic Algorithms and Particle Swarm Optimization for inverse kinematics, IEEE International Conference on Robotics & Biomimetics, IEEE, 2017.
[18] H.C. Huang, C.P. Chen, P.R. Wang, Particle swarm optimization for solving the inverse kinematics of 7-DOF robotic manipulators, IEEE International Conference on Systems, IEEE, 2012.
[19] J. Denavit, A kinematic notation for lower-pair mechanisms based on matrices, J. Appl. Mech. 22 (1955) 215–221.
[20] H. Ji, Y. Gu, J. Wu, Z. Liu, X. Fan, J. Ma, et al., Reverse engineering of cfetr vacuum vessel mockup, IEEE Trans. Plasma Sci. (2018) 1–5.
[21] M. Dorigo, C. Blum, Ant colony optimization theory: a survey, Theor. Comput. Sci. 344 (2–3) (2005) 243–278.
[22] Z. Cui, X. Cai, Using social cognitive optimization algorithm to solve nonlinear equations, IEEE International Conference on Cognitive Informatics, IEEE, 2010.
[23] B. Siciliano, Kinematic control of redundant robot manipulators: a tutorial, J. Intelligent Robotic Syst.: Theory Appl. 3 (3) (1990) 201–212.
[24] S. Abbasbandy, B. Asady, Newton"s method for solving fuzzy nonlinear equations, Appl. Math. Comput. 159 (2) (2004) 349–356.
[25] W.U. Xinyuan, Improved muller method and bisection method with global and asymptotic superlinear convergence of both point and interval for solving nonlinear equations, Appl. Math. Comput. 166 (2) (2005) 299–311.
[26] C. Kanzow, N. Yamashita, M. Fukushima, Erratum to "levenberg–marquardt methods with strong local convergence properties for solving nonlinear equations with convex constraints" ☆: [j. Comput. Appl. Math. 173 (2005) 321–343], J. Comput. Appl. Math. 177 (2) (2005) 241.
[27] A.P. Bry, Rapidly-exploring Random Belief Trees for Motion Planning Under Uncertainty. IEEE International Conference on Robotics & Automation, (2011).
[28] K. Wang, et al., Inverse kinematics research using obstacle avoidance geometry method for EAST Articulated Maintenance Arm (EAMA), Fusion Eng. Des. (2017) 1–11.

Publication II

Zhang, T., Song, Y., Wu, H. and Wang, Q.
A novel method to identify DH parameters of the rigid serial-link robot based on a geometry model

Reprinted with permission from
Industrial Robot
Vol. 48 No. 1, pp. 157-167, 2020

A novel method to identify DH parameters of the rigid serial-link robot based on a geometry model

Tao Zhang
Institute of Plasma Physics Chinese Academy of Sciences (ASIPP), Chinese Academy of Sciences, Beijing, China; University of Science and Technology of China, Hefei, China and Lappeenranta University of Technology (LUT), Lappenranta, Finland

Yuntao Song
Institute of Plasma Physics Chinese Academy of Sciences (ASIPP), Chinese Academy of Sciences, Beijing, China

Huapeng Wu
Lappeenranta University of Technology (LUT), Lappenranta, Finland, and

Qi Wang
Institute of Plasma Physics Chinese Academy of Sciences (ASIPP), Chinese Academy of Sciences, Beijing, China and Huainan New Energy Research Center, Anhui Provincial Key Laboratory of Special Welding, Hefei, China

Abstract

Purpose – Every geometric model corresponding to a unique feature whose errors of parameters uncorrelated, so the linearization technique can be successfully applied. The solution of a linear least square problem can be applied straightforwardly. This method has advantages especially in calibrate the redundant robot because it's relatively small. The parameters of kinematics are unique and determined by this algorithm.

Design/methodology/approach – In this paper, a geometric identification method has been studied to estimate the parameters in the Denavit–Hartenberg (DH) model of the robot. Through studying the robot's geometric features, specific trajectories are designed for calibrating the DH parameters. On the basis of these geometric features, several fitting methods have been deduced so that the important geometric parameters of robots, such as the actual rotation centers and rotate axes, can be found.

Findings – By measuring the corresponding motion trajectory at the end-effector, the trajectory feature can be identified by using curve fitting methods, and the trajectory feature will reflect back to the actual value of the DH parameters.

Originality/value – This method is especially suitable for rigid serial-link robots especially for redundant robots because of its specific calibration trajectory and geometric features. Besides, this method uses geometric features to calibrate the robot which is relatively small especially for the redundant robot comparing to the numerical algorithm.

Keywords Curve fitting, Lagrange, Robot calibration, Robot kinematic

Paper type Research paper

1. Introduction

Fusion energy is future energy, and lots of test reactor tokamaks have been or are going to be built in the world, such as the China Fusion Engineering Test Reactor (CFETR) (Song *et al.*, 2013), ITER (Janeschitz, 2001), Japanese J-Demo (Tanaka and Takatsu, 2008.), k-Demo in Korea (Kim *et al.*, 2013) and the European DEMO (Maisonnier, 2008). The reactor needs regular maintenance with remote handling (RH) robot systems. Because of radiation, RH robots are developed for different tasks in the reactors. Because of high accuracy requirements, the geometric parameters of the robot need to be identified after the robot built up.

Industrial robots are highly flexible, repeatable and effective for numbers of manufacturing tasks (Taylor, 1986). Kinematic calibration is a hot research topic, and the achieved methods can be classified into three groups: open-loop, closed-loop and screw-axis measurement methods (Hollerbach and Wampler, 1996; Chang *et al.*, 2018). The open-loop measurement method needs extra measuring tools, such as calibrating cameras or laser trackers. Nubiola and Bonev (2013) and Nubiola *et al.* (2013) have introduced two approaches to

The current issue and full text archive of this journal is available on Emerald Insight at: **https://www.emerald.com/insight/0143-991X.htm**

Industrial Robot: the international journal of robotics research and application
 [ISSN 0143-991X]
[DOI 10.1108/IR-05-2020-0103]

Thanks to the ASIPP and LUT's work fellow for the inspiration about this geometric algorithm, especially a senior fellow apprentice Kun Wang. This project is funded by the Comprehensive Research Facilities in Support of CFETR (2017YFE0300503).

Received 22 May 2020
Revised 30 June 2020
15 July 2020
Accepted 16 July 2020

calibrate parameters with a laser tracker, and they are common for calibrating robots in manufacture industrial. The closed-loop measurement method does not need external measurement devices (Bennett and Hollerbach, 1991), while a manipulator is formed by a mobile closed kinematic chain and the joint angles will be read from the joint sensors to help identify the kinematic parameter. In screw-axis measurement methods (Santolaria *et al.*, 2014; Santolaria *et al.*, 2012), the circle point analysis calibrates the robot by determining the actual transformation relationship between consecutive joints. In these methods, geometric algorithms (Ikits and Hollerbach, 1997) or intelligent algorithms have been used in the calibration process. Intelligent algorithms use artificial intelligent search methods to find the parameters of robot. Those methods include the particle swarm optimization method (Wang *et al.*, 2018), the genetic algorithm (Zhuang *et al.*, 1997), the simulated annealing algorithm (Zhuang *et al.*, 1994) and the tabu search algorithm (Daney *et al.*, 2005). Intelligent algorithms generally have more complex calculations and complicated coding. Geometric methods have been studied for certain specified configuration robots (Ikits and Hollerbach, 1997). However, using certain specified geometric features will limit the applications, as an industrial robot always has more geometric features. In this article, a geometric algorithm that can be applied for general robots has been studied, and it integrates the three geometric fitting methods, i.e. the spatial plane fitting, the spatial circle fitting and the feet of a common normal fitting. After fitting these features, all the parameters defined in the Denavit–Hartenberg (DH) model can be found. This method uses a specific trajectory to find corresponding geometric features. Lots of calibration methods focus on the numerical algorithm, such as gradient search, heuristic search and the others which are difficult to tune a large number of parameters especially for redundant robots. However, the errors of parameters in the geometric calibration are relatively small (Wu *et al.*, 2015). Every geometric model corresponding to a unique feature whose errors of parameters uncorrelated, so the linearization technique can be successfully applied. The solution of a linear least square problem can be applied straightforwardly. This method has advantages especially in calibrate the redundant robot because it's relatively small. The parameters of kinematics are unique and determined by this algorithm.

This article includes five sections. The introduction in Section 1 illustrates the background of robots and related works. Section 2 introduces the mathematical method. Section 3 reveals a specific procedure of a geometric algorithm and uses a six-DOF robot to test and validate the method. Section 4 shows the experiment results and discussions. Section 5 contains a summary and comments on this work.

2. Preliminary

A six-DOF robot is used as shown in Figure 1 to explain the principle of the calibration method. Each of the joints will independently move one by one from their initial positions. The motion from each joint causes a corresponding motion at the end-effector. By measuring the corresponding motion trajectory at the end-effector, the trajectory feature can be identified by using curve fitting methods, and the trajectory feature will reflect back to the actual value of the DH parameters. For example, one rotation axis is the normal vector through the center of the circle formed at the end effector. By the center and normal vector's fitting, the actual center normal vector can be estimated. In the designed trajectories, the rotation centers are the point of intersection of two different axes, such as the 1st joint's origin is the intersect point of Axis 1 and Axis 2. But in an actual case, there may be no cross-point. By fitting the feet of common normal between two joint axes, the error of intersection point can be identified. For example, points M and N are the feet of common normal between Axis 1 and Axis 2 in Figure 2. The origin of the frame is always on the corresponding rotation axis, which is Axis 1 for Frame 1. So the foot of common normal, which is point M in Axis 1, is the origin of the 1st frame. This algorithm integrates three fitting geometric models, i.e. the spatial plane fitting, the spatial circle

Figure 1 Geometric features of trajectory

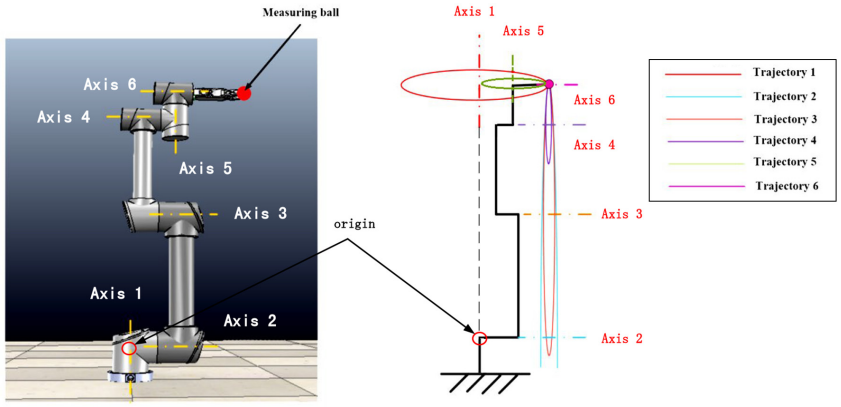

Figure 2 Geometric features between different axes (using the frame 1 as example)

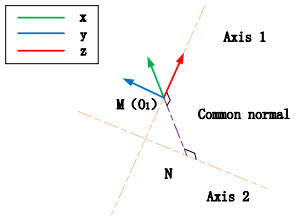

fitting and the feet of the common normal fitting, to ensure all the parameters in the DH can be calculated. After origins and rotation axes estimated, the twist angles and link lengths can be calculated accordingly.

In the modeling, three steps are taken as follows: first, the spatial plane fitting to find the normal vectors of circle planes, which are the direction of the rotation axe; the second step is to perform the spatial circle fitting to find rotation centers; the third step is to estimate actual origin by using the feet of the common normal fitting.

2.1 The spatial plane fitting

The first step is the spatial plane fitting. A spatial plane's normal vectors are the axes of the robot DH model. A common plane (Π) formula can be written as the equation (1). Through the transformation of formula (1). The formula of equation (1) can be written as the equation (2), which is more geometric meaningful:

$$A_\Pi x + B_\Pi y + C_\Pi z = D_\Pi \tag{1}$$

where $\overrightarrow{n_\Pi}$ is the normal vector of plane (Π), $\overrightarrow{n_\Pi} = (A_\Pi, B_\Pi, C_\Pi)$ and D_Π is a constant coefficient of plane (Π):

$$A^*_\Pi x + B^*_\Pi y + C^*_\Pi z = D^*_\Pi \tag{2}$$

where $\overrightarrow{n^*_\Pi}$ is the unit normal vector of the plane (Π), and $n^*_\Pi = (A^*_\Pi, B^*_\Pi, C^*_\Pi)$, D^*_Π is the distance between Cartesian coordination origin (0,0,0) to plane (Π).

The distance $d_{i,\Pi}$ from an arbitrary point i to plane Π can be expressed in equation (3):

$$d_{i,\Pi} = |A^*_\Pi x_i + B^*_\Pi y_i + C^*_\Pi z_i - D^*_\Pi| \tag{3}$$

An error estimator defined by the Euclidean distance is a sum of n points' distance to the desired plane Π:

$$E_\Pi = \sum d_{i,\Pi}{}^2 \tag{4}$$

To solve the least error for the designed plane, the method of Lagrange multiplier can be adopted, and the Lagrangian function is given in equation (5):

$$f_\Pi = E_\Pi - \lambda_\Pi \cdot \left(A^*_\Pi{}^2 + B^*_\Pi{}^2 + C^*_\Pi{}^2 - 1\right) \quad \lambda_\Pi \epsilon R \tag{5}$$

where λ_Π is Lagrange multiplier.

Instead of solving the minimum error of E_Π, we solve the Lagrangian function's minimum value. The minimum solution is obtained when the first partial derivatives of the function equal to zero. By calculating the $\frac{\partial f_\Pi}{\partial D_\Pi} = 0$, equation (6) is deduced:

$$D^*_\Pi = A^*_\Pi \bar{x} + B^*_\Pi \bar{y} + C^*_\Pi \bar{z} \tag{6}$$

where $\bar{x} = \frac{\sum_{i=1}^{n} x_i}{n}, \bar{y} = \frac{\sum_{i=1}^{n} y_i}{n}$, and $\bar{z} = \frac{\sum_{i=1}^{n} z_i}{n}$.

Substituting equation (6) to partial derivative functions ($\frac{\partial f_\Pi}{\partial A^*} = 0$, $\frac{\partial f_\Pi}{\partial B^*} = 0$, $\frac{\partial f_\Pi}{\partial C^*} = 0$), equation (7) can be deduced as a matrix form:

$$M_\Pi \cdot \overrightarrow{n^*_\Pi}^T = \lambda_\pi \cdot \overrightarrow{n^*_\Pi}^T \tag{7}$$

where:

$$M_\Pi = \begin{bmatrix} \sum \Delta x_i \cdot \Delta x_i & \sum \Delta x_i \cdot \Delta y_i & \sum \Delta x_i \cdot \Delta z_i \\ \sum \Delta x_i \cdot \Delta y_i & \sum \Delta y_i \cdot \Delta y_i & \sum \Delta y_i \cdot \Delta z_i \\ \sum \Delta x_i \cdot \Delta z_i & \sum \Delta y_i \cdot \Delta z_i & \sum \Delta z_i \cdot \Delta z_i \end{bmatrix},$$

$\Delta x_i = x_i - \bar{x}$, $\Delta y_i = y_i - \bar{y}$, and $\Delta z_i = z_i - \bar{z}$.

The eigenvalue of equation (7) can be calculated from equation (8):

$$|M_\Pi - \lambda_\Pi \cdot \leq I| = 0 \tag{8}$$

The most suitable solution of plane normal vector $n^*_\Pi = (A^*_\Pi, B^*_\Pi, C^*_\Pi)^T$ is a column vector or eigenvector corresponding to $\lambda_{\Pi\min}$ which is the eigenvalue of M_Π.

2.2 The spatial circle fitting

The second step is the spatial circle fitting to seek the centers of these circles. These centers can help determine frames in the DH model from the previous study. The designed trajectories of the robot are spatial circles. A spatial circle can be regarded as a crossing curve between a spatial sphere S and a plane Π as Figure 3 shown. A common spatial sphere equation can be written in equation (9):

$$(x - x_S)^2 + (x - y_S)^2 + (x - z_S)^2 = R_S{}^2 \tag{9}$$

As for plane Π which points lie on, the method in Section 2.1 can be referred to calculate its plane normal vector. These points lie around the circle as shown in Figure 3(a). The n points can form $n - 1$ line segments that are end to end, and those line segment bisectors are vertical with plane normal vector. According to this feature, every line segment bisector's formula can be deduced:

$$\Delta x_i \cdot x_S + \Delta y_i \cdot y_S + \Delta z_i \cdot z_S - l_{S,i} = 0 \quad (i = 1, 2, \ldots, n-1) \tag{10}$$

where: $\Delta x_i = x_{i+1} - x_i, \Delta y_i = y_{i+1} - y_i, \Delta z_i = z_{i+1} - z_i$, and $l_{S,i} = \frac{x_{i+1}{}^2 + y_{i+1}{}^2 + z_{i+1}{}^2 - x_i{}^2 - y_i{}^2 - z_i{}^2}{2}$.

However, actual line segment bisectors may have some joint errors with normal vector; therefore, a joint error estimator is designed for every line segment bisector in equation (11). At

Figure 3 A spatial circle and its geometric feature

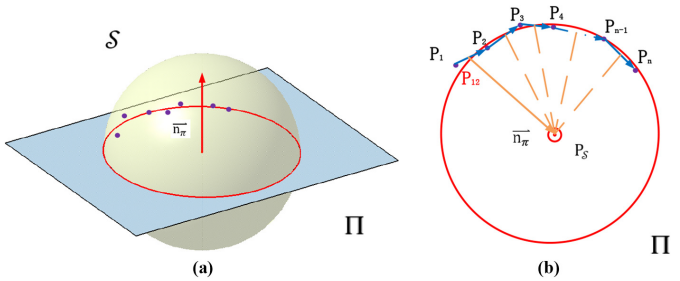

the same time, a total joint error estimator is deduced as equation (12):

$$e_{S,i} = \Delta x_i \cdot \mathrm{x}_S + \Delta y_i \cdot \mathrm{y}_S + \Delta z_i \cdot \mathrm{z}_S - l_{S,i} \tag{11}$$

$$\boldsymbol{E}_S = M_S \cdot \boldsymbol{X}_S - \boldsymbol{L}_S \tag{12}$$

where: $\boldsymbol{E}_S = \left[e_{S0C1}, e_{S0C2} \cdots e_{S-1}\right]^T$, $M_S = \begin{bmatrix} \Delta x_1 & \Delta y_1 & \Delta z_1 \\ \Delta x_2 & \Delta y_2 & \Delta z_2 \\ \cdots & \cdots & \cdots \\ \Delta x_{n-1} & \Delta y_{n-1} & \Delta z_{n-1} \end{bmatrix}$, $\boldsymbol{X_S} = [x_S, y_S, z_S]^T$ and $\boldsymbol{L_S} = [l_{S,1}, l_{S,2}, \ldots, l_{S,n-1}]$.

To obtain the minimum error, the least square method is used. The normal equation of equation (13) is built as equation (14) (Huang, 2003):

$$M_S{}^T \cdot I \cdot M_S \cdot \boldsymbol{X}_S - M_S{}^T \cdot I \cdot \boldsymbol{L}_S = 0 \tag{13}$$

where I is the identity matrix, and its size is as same as the row size of M_S.

As seen from Figure 3, the center of circle also belongs to plane Π and its geometric restriction is defined as equation (14):

$$\mathbf{n}_\Pi^\star \cdot \mathbf{X}_S - D_\Pi^* = 0 \tag{14}$$

By combining equations (13) and (14), a fitting relation of the circle is achieved as equation (15) and its solution as equation (16):

$$M_{S,\Pi} \cdot \mathbf{X}_S = D_{S,\Pi} \tag{15}$$

where $M_{(S,\Pi)} = \begin{bmatrix} MS^T \cdot I \cdot M_S \\ \mathbf{n}_\Pi^* \end{bmatrix}$ and $D_{S,\Pi} = \begin{bmatrix} MS^T \cdot I \cdot \boldsymbol{L_S} \\ D_\Pi^* \end{bmatrix}$.

$$\mathbf{X}_S = K_{S,\Pi}{}^{-1} \cdot B_{S,\Pi} \tag{16}$$

where $K_{S,\Pi} = M_{S,\Pi}{}^{-1T} Is^2 M_{S,\Pi}{}^{s^2}$ and $B_{S,\Pi} = M_{S,\Pi}{}^T Is^2 D_{S,\Pi}$.

As the spatial circle is a crossing curve of a spatial sphere S and a plane Π, the radius of spatial sphere S can be substituted to equation (17). After fitting, the centers X_S of circles are calculated and used in Section 2.3 for further modeling:

$$\mathrm{R}_S = \frac{\sum |\mathrm{X}_i - \mathrm{X}_S|}{n} \tag{17}$$

where $\mathbf{X}_i = (x_i, y_i, z_i)$.

2.3 The feet of common normal fitting of two spatial line

The robot's axes and origins are relative with the previous normal vectors and centers of circles, while the robot motions following the designed trajectory. The rotation centers are the intersections of two different axes. In actual fitting, the feet of common normal between two different axes, having no intersection, will be regarded as the origin in the DH model, for example, Axis 1 and Axis 2 in Figure 2. So point M, which is the foot of common normal, will replace the theoretical intersection as the origin of the first frame. Supposing there are two spatial lines l_1 and l_2 with two points $o_{l1}(x_{l1}, y_{l1}, z_{l1})$, and $o_{l2}(x_{l2}, y_{l2}, z_{l2})$ lying on the each line, the directional vectors of two lines are notated as $\overrightarrow{\boldsymbol{n}_{l1}} = (A_{l1}, B_{l1}, C_{l1})$, and $\overrightarrow{\boldsymbol{n}_{l2}} = (A_{l2}, B_{l2}, C_{l2})$ respectively. Generally, the o_{l1}, o_{l2} and $\overrightarrow{n_{l1}}$, $\overrightarrow{n_{l2}}$ are the centers of circles and normal vectors, respectively. Using these parameters, the common normal can be decided uniquely. The two spatial lines must have a common normal, and its two feet of common normal P_M (x_M, y_M, z_M) and P_N (x_M, y_M, z_M) are the intersection points of common normal with line l_1 and line l_2, respectively.

The common normal vector $\overrightarrow{\boldsymbol{P_M P_N}}$ can be written as $(x_N - x_M, y_N - y_M, z_N - z_M)$.

2.3.1 Geometric method of solving feet of a common normal

The geometric relation of two spatial lines is shown in Figure 4, and the equations are given as equation (18):

$$\begin{cases} (x_N - x_M) \cdot A_{l1} + (y_N - y_M) \cdot B_{l1} + (z_N - z_M) \cdot C_{l1} = 0, & (18a) \\ (x_N - x_M) \cdot A_{l2} + (y_N - y_M) \cdot B_{l2} + (z_N - z_M) \cdot C_{l2} = 0, & (18b) \\ \dfrac{x_M - x_{l1}}{A_{l1}} = \dfrac{y_M - y_{l1}}{B_{l1}} = \dfrac{z_M - z_{l1}}{C_{l1}}, & (18c) \\ \dfrac{x_N - x_{l2}}{A_{l2}} = \dfrac{y_N - y_{l2}}{B_{l2}} = \dfrac{z_N - z_{l2}}{C_{l2}}. & (18d) \end{cases}$$

Equation (19) is obtained when $Cl_1\, s^2\, Cl_2 \neq 0$.

$$\begin{cases} x_M = x_{l1} + \dfrac{A_{l1}}{C_{l1}}\ (z_M - z_{l1}), & (19a) \\ y_M = y_{l1} + \dfrac{B_{l1}}{C_{l1}}\ (z_M - z_{l1}), & (19b) \\ x_N = x_{l2} + \dfrac{A_{l2}}{C_{l2}}\ (z_N - z_{l1}), & (19c) \\ y_N = y_{l2} + \dfrac{B_{l2}}{C_{l2}}\ (z_N - z_{l1}). & (19d) \end{cases}$$

Equation (20) can be deduced from equation (18a), (18b) and (19).

$$K_l \cdot \begin{bmatrix} z_M \\ z_N \end{bmatrix} = B_l \tag{20}$$

where: $K_l = \begin{bmatrix} \dfrac{A_{l1}}{C_{l1}} \cdot A_{l1} + \dfrac{B_{l1}}{C_{l1}} \cdot B_{l1} + C_{l1} & -\left(\dfrac{A_{l2}}{C_{l2}} \cdot A_{l1} + \dfrac{B_{l2}}{C_{l2}} \cdot B_{l1} + C_{l1}\right) \\ \dfrac{A_{l1}}{C_{l1}} \cdot A_{l2} + \dfrac{B_{l1}}{C_{l1}} \cdot B_{l2} + C_{l2} & -\left(\dfrac{A_{l2}}{C_{l2}} \cdot A_{l2} + \dfrac{B_{l2}}{C_{l2}} \cdot B_{l2} + C_{l2}\right) \end{bmatrix}$,

$$B_l = \begin{bmatrix} \left[(x_{l2} - x_{l1}) - \left(\dfrac{A_{l2}}{C_{l2}} \cdot z_{l2} - \dfrac{A_{l1}}{C_{l1}} \cdot z_{l1}\right)\right] \cdot A_{l1} + \left[(y_{l2} - y_{l1}) - \left(\dfrac{B_{l2}}{C_{l2}} \cdot z_{l2} - \dfrac{B_{l1}}{C_{l1}} \cdot z_{l1}\right)\right] \cdot B_{l1} \\ \left[(x_{l2} - x_{l1}) - \left(\dfrac{A_{l2}}{C_{l2}} \cdot z_{l2} - \dfrac{A_{l1}}{C_{l1}} \cdot z_{l1}\right)\right] \cdot A_{l2} + \left[(y_{l2} - y_{l1}) - \left(\dfrac{B_{l2}}{C_{l2}} \cdot z_{l2} - \dfrac{B_{l1}}{C_{l1}} \cdot z_{l1}\right)\right] \cdot B_{l2} \end{bmatrix}.$$

The direction vector of line cannot be zero vector, and the rank of K_l can be 1 or 2. The z_M and z_N are calculated by equation (21) and other parameters can be calculated by equation (19):

$$\begin{cases} \begin{bmatrix} z_M \\ z_N \end{bmatrix} = K_l^{-1} \cdot B_l, & \text{if } rank(K_l) = 2 & (21a) \\ z_M = z_N = \left[\left(\dfrac{A_{l1}}{C_{l1}} \cdot z_{l1} - \dfrac{A_{l2}}{C_{l2}} \cdot \le z_{l2}\right) + (x_{l2} - x_{l1})\right] / \left(\dfrac{A_{l1}}{C_{l1}} - \dfrac{A_{l2}}{C_{l2}}\right), & \text{if } rank(K_l) = 1 \& \cap A_{l1} \cdot C_{l2} \neq A_{l1} \cdot C_{l2} & (21b) \\ z_M = z_N = z_{l1}. & \text{otherwise} & (21c) \end{cases}$$

2.3.2 Parametric equation method of solving feet of a common normal

The parametric equation is a useful way to find the spatial line. It needs adding new parameters t_{l1} and t_{l2}. While the parametric equation method is adopted to get a high accuracy numerical solution, the general parametric equations of two spatial line l_1 and l_2 can be written as equation (22).

Figure 4 Geometric model of two spatial lines

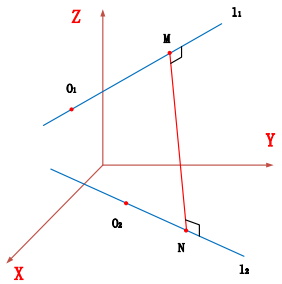

$$\begin{cases} \dfrac{x_M - x_{l1}}{A_{l1}} = \dfrac{y_M - y_{l1}}{B_{l1}} = \dfrac{z_M - z_{l1}}{C_{l1}} = t_{l1} & (22a) \\ \dfrac{x_N - x_{l2}}{A_{l2}} = \dfrac{y_N - y_{l2}}{B_{l2}} = \dfrac{z_N - z_{l2}}{C_{l2}} = t_{l2} & (22b) \end{cases}$$

The solution of t_{l1} and t_{l2} is:

$$\begin{bmatrix} t_{l1} \\ t_{l2} \end{bmatrix} = M_l^{-1} \cdot \begin{bmatrix} \overrightarrow{\boldsymbol{n}_{l1}}^{\,T} \cdot (\boldsymbol{X}_{l1} - \boldsymbol{X}_{l2}) \\ \overrightarrow{\boldsymbol{n}_{l2}}^{\,T} \cdot (\boldsymbol{X}_{l1} - \boldsymbol{X}_{l2}) \end{bmatrix} \tag{23}$$

where $\boldsymbol{X}_{l1} = (x_{l1}, y_{l1}, z_{l1})^T$, $\boldsymbol{X}_{l2} = (x_{l2}, y_{l2}, z_{l2})^T$ and $M_l = \begin{bmatrix} \overrightarrow{\boldsymbol{n}_{l1}}^{\,2} & -\overrightarrow{\boldsymbol{n}_{l1}} \cdot \overrightarrow{\boldsymbol{n}_{l2}}^{\,T} \\ \overrightarrow{\boldsymbol{n}_{l2}} \cdot \overrightarrow{\boldsymbol{n}_{l1}}^{\,T} & -\overrightarrow{\boldsymbol{n}_{l2}}^{\,2} \end{bmatrix}$.

In this method, there are two exceptional cases that should be discussed in detail. The first exceptional case is the singularity of the coefficient matrix of M_l. When the rank of M_l is equal to 1, it means that the two lines are parallel or coincided with each other, and the o_{l1} is regarded as the foot of common normal. The second exceptional case is that some elements of common normal or directional vectors $\overrightarrow{\boldsymbol{n}_{l1}}$ and $\overrightarrow{\boldsymbol{n}_{l2}}$ are equal to zero, and this leads to meaningless equation (23), as the corresponding denominators are equal to zero. In this case, the line is parallel to one axis of coordination. Thus, the solution of the corresponding nominator of that equation should be equal to zero. For example, when B_{l1} is zero, the corresponding nominator demands the equation $y_M - y_{l1} = 0$.

Considering the calculation efficiency of the algorithm, the methods should be dynamically selected by the following principle:

$$\begin{cases} Geometric\ method & C_{l1} \cdot C_{l2} \neq 0 \\ Parametric\ equation\ method\ others, (\ if\ C_{l1},\ z_M - z_{l1} = 0; if\ C_{l2},\ z_N - z_{l2} = 0) \end{cases}$$

By dynamically selecting the two methods, the effect of the algorithm can be promoted.

3. Methodology of building geometric robot model

For better performance of the algorithm, a six-revolute-joint robot was used to test the procedure of calibration. The algorithm is shown as the flowchart (Figure 5). It mainly has six steps that are:

1 rotate each revolute joint individually;
2 measure the fitting points of end-effectors;
3 fit circles;
4 evaluate the result of the fitting;
5 build up a geometric model; and
6 calculate DH parameters.

The camera-based method and the laser-based method are common means for measuring positions of end effector (Newman *et al.*, 2000; Palmieri *et al.*, 2018). The former one is more complex because the camera requires calibration, and the accuracy of calibration is influenced by the position of the camera, the camera resolution, light and so on. The second way is more effective and accurate but expensive.

Figure 5 Algorithm of geometric method

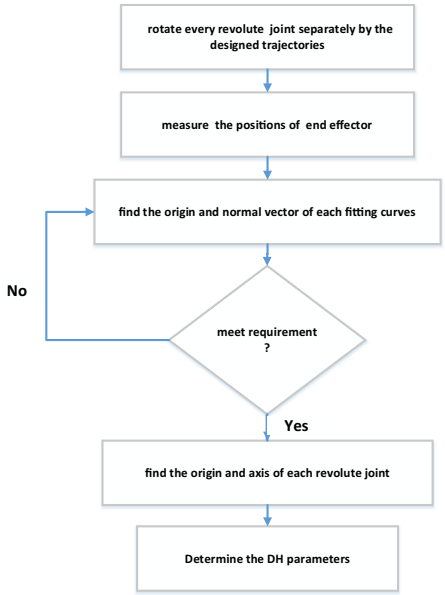

The mechanic model of the robot is shown in Figure 6. Based on the DH modeling convention, the ideal DH frames of the robot are set up and the DH parameters are shown in Table 1. In Table 1, there is a d_6' which represents the distance between ball's origin and o_6 or o_7. The frame of the o_7' is the mean value of the last group of measuring data.

3.1 Finding fitting circle by geometric method

Every revolute joint of the robot moves separately, six groups of data are recorded in Figure 7(a). The normal vectors of the fitting plane and the circles' centers shown in Figure 7(b) are calculated. More details are shown in Figure 7(c). However, for point group 6 in Figure 7(a), it looks like a point other than a circle due to the sixth joint's motion nearly won't change the position of the end effector. The calibration accuracy is

Figure 6 DH model of industrial robot Luban

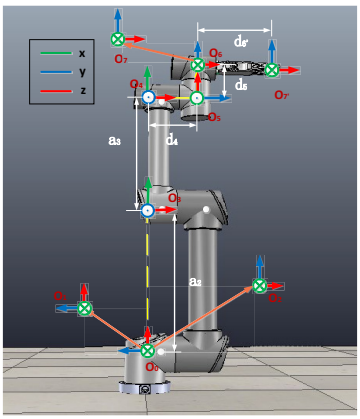

Table 1 DH parameter of industrial robot Luban

	α/rad	a/mm	d/mm	θ/rad
0	0	0	0	0
1	$\pi/2$	0	0	θ_1
2	0	a_2	0	θ_2
3	0	a_3	0	θ_3
4	$\pi/2$	0	d_4	θ_4
5	$\pi/2$	0	d_5	θ_5
6	0	0	d_6'	θ_6

Figure 7 Geometric modeling procedure for normal vectors and origin vectors

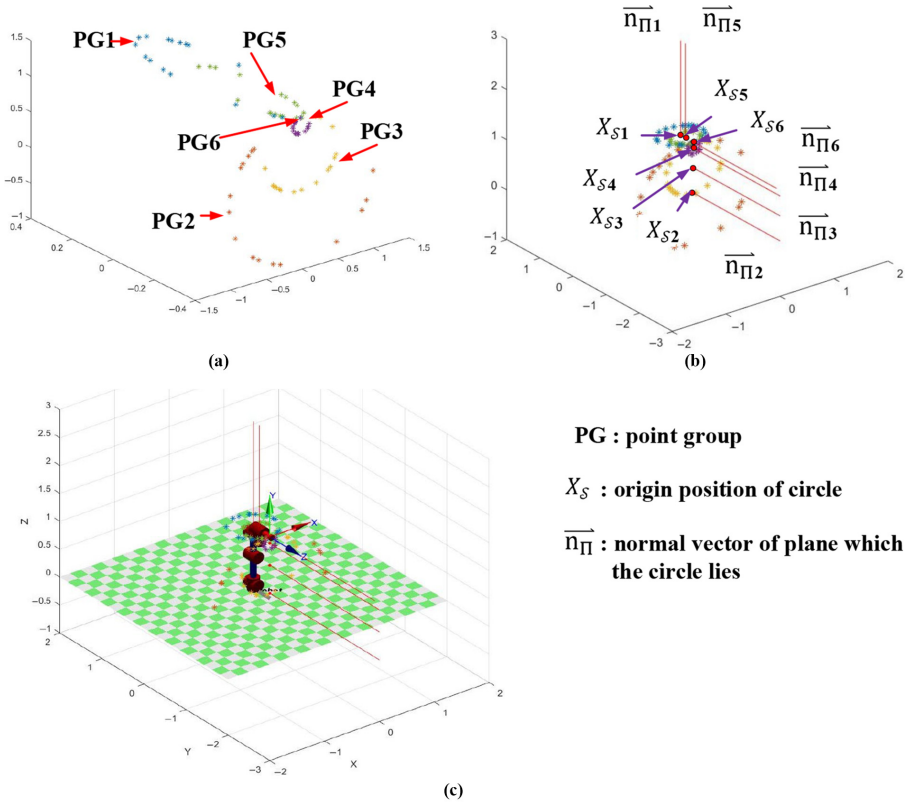

Notes: (a) Group data cloud of robot; (b) fitting normal vectors and origins; (c) fitting normal vectors origins and robot model by MATLAB

influenced by the number of points in groups, thus at least ten points should be measured for every joint and the step size should be over 10 degrees to ensure effectiveness. To get rid of the white noise, a filter is designed.

3.2 Filtering data with empirical rules

The empirical rule, i.e. a probabilistic method can be used to evaluate the performance (En.wikipedia.org. 2020). One effective geometric evaluation method is to calculate the shape error by distance and radius. The standard deviations for distance and radius are σ_π and σ_S, respectively:

$$\sigma_\pi = \sqrt{\frac{\left(\mathrm{d}_{i,\Pi} - \overline{\mathrm{d}_{i,\Pi}}\right)^T \cdot \leq \left(\mathrm{d}_{i,\Pi} - \overline{\mathrm{d}_{i,\Pi}}\right)}{n-1}} \tag{24}$$

$$\sigma_S = \sqrt{\frac{\left(\mathrm{R}_{i,S} - \overline{\mathrm{R}_{i,S}}\right)^T \cdot \left(\mathrm{R}_{i,S} - \overline{\mathrm{R}_{i,S}}\right)}{n-1}} \tag{25}$$

where $\overline{\mathrm{d}_{i,\Pi}}$ is the mean of $d_{i,\Pi}$ and $\overline{\mathrm{R}_{i,S}}$ is the mean of $\mathrm{R}_{i,S}$.

The empirical rule is shown in Figure 8, where there are confidence levels. As seen from Figure 8, 99.7% of values fall within the three standard derivations of the mean. The filter is designed by the 3σ rule.

Algorithm for the 3σ rule:

- use point data to fit geometric features;
- calculate $d_{i,\Pi}$, $\mathrm{R}_{i,S}$ and mean $\overline{\mathrm{d}_{i,\Pi}}$, $\overline{\mathrm{R}_{i,S}}$; and
- filter data.

Figure 8 Empirical rule and confidence levels

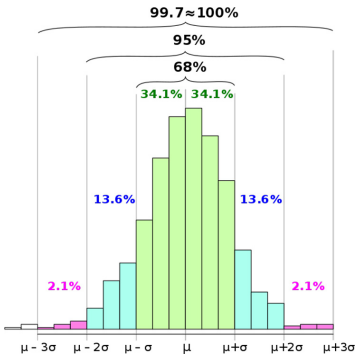

3.3 Building up frames according to the definition of Denavit–Hartenberg model

The normal vectors and corresponding centers of circles are used to form spatial lines. In the DH model, axes are the spatial lines or common normals, and origins are the intersection points of those lines with corresponding common normals. Following the definition of the DH modeling, an experimental robot model is built. For example, $\overrightarrow{\boldsymbol{n_{\Pi,1}}}$, $\boldsymbol{X_{S1}}$, $\overrightarrow{\boldsymbol{n_{\Pi,2}}}$, $\boldsymbol{X_{S2}}$ are used to find the crossing point o_0, z-axis $\left(\overrightarrow{\boldsymbol{n_{\Pi,1}}}\right)$ and y-axis $\left(\overrightarrow{\boldsymbol{n_{\Pi,2}}}\right)$ of $0th$ frame. Then the right-hand method is used to find the x axis of $0th$ frame. The rest of axes and origins are built accordingly as shown in Figure 9(a). The robot frame in Figure 9(b) is the fitting model which is built by this rule.

3.4 Calculating Denavit–Hartenberg parameters following definition

The parameters of a robot are deduced according to the definition of the DH method. Here are some definitions of the DH parameters:

- Joint angle θ_i: the angle of rotation from the Axis $\mathbf{X_{i-1}}$ to the Axis $\boldsymbol{X_i}$ about the Axis $\boldsymbol{Z_{i-1}}$. It is the joint variable if joint i is rotary.
- Joint distance d_i: the distance from the origin of the $(i-1)th$ coordinate system to the intersection of the Axis $\boldsymbol{Z_{i-1}}$ and the Axis $\boldsymbol{X_i}$ along the Axis $\boldsymbol{Z_{i-1}}$. It is the joint variable if joint i is prismatic.
- Link length a_i: the distance from the intersection of the Axis $\boldsymbol{Z_{i-1}}$ and the Axis $\boldsymbol{X_i}$ to the origin of the ith coordinate system along the Axis $\boldsymbol{X_i}$.
- Link twist angle α_i: the angle of rotation from the Axis $\boldsymbol{Z_{i-1}}$ to the Axis $\boldsymbol{Z_i}$ about the Axis $\boldsymbol{X_i}$

According to the DH convention, the θ_i and α_i can be regarded as twist angels between vector's projections $\boldsymbol{X_{i,XY}}$, $\boldsymbol{Z_{i,YZ}}$ and target vectors $\boldsymbol{X_i}$, $\boldsymbol{Z_{i-1}}$ respectively as shown in equations (26) and (27):

$$\begin{cases} Y = \boldsymbol{Z_{i-1}} \times \boldsymbol{X_{i-1}} \\ \boldsymbol{X_i} = a_{i,\theta}\boldsymbol{X_{i-1}} + b_{i,\theta}\boldsymbol{Y} + c_{i,\theta}\boldsymbol{Z_{i-1}} \\ \boldsymbol{X_{i,XY}} = a_{i,\theta}\boldsymbol{X_{i-1}} + b_{i,\theta}\boldsymbol{Y} \\ \theta_i = \arccos\left(\dfrac{\boldsymbol{X_{i,XY}} \cdot \boldsymbol{X_i}}{|\boldsymbol{X_{i,XY}}| \cdot |\boldsymbol{X_i}|}\right) \end{cases} \tag{26}$$

$$\begin{cases} Y = \boldsymbol{Z_{i-1}} \times \boldsymbol{X_i} \\ \boldsymbol{Z_i} = a_{i,\alpha}\boldsymbol{X_i} + b_{i,\alpha}\boldsymbol{Y} + c_{i,\alpha}\boldsymbol{Z_{i-1}} \\ \boldsymbol{Z_{i,YZ}} = b_{i,\alpha}\boldsymbol{Y} + c_{i,\alpha}\boldsymbol{Z_{i-1}} \\ \alpha_i = \arccos\left(\dfrac{\boldsymbol{Z_{i,YZ}} \cdot \boldsymbol{Z_{i-1}}}{|\boldsymbol{Z_{i,YZ}}| \cdot |\boldsymbol{Z_{i-1}}|}\right) \end{cases} \tag{27}$$

Four parameters o_{i-1}, $\boldsymbol{Z_{i-1}}$, o_i and $\boldsymbol{X_i}$ are used to calculate the joint distance and the link length. These parameters define two lines and the corresponding two feet of common normal M_i and N_i. The distance from the origin of the $(i-1)th$ coordinate system to the intersection of the $\boldsymbol{Z_{i-1}}$ axis and the $\boldsymbol{X_i}$ axis can be denoted as $\mathbf{L}_{i,d}$. And the distance from the intersection of the $\boldsymbol{Z_{i-1}}$ axis and the $\boldsymbol{X_i}$ axis to the origin of the ith coordinate

Figure 9 (a) Mathematic model of robot; (b) fitting model of robot

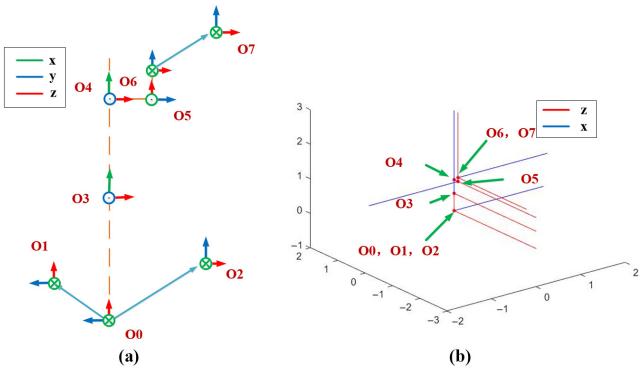

system can be denoted as $\mathbf{L}_{i,a}$. According to the DH convention, the equations can be deduced as follow:

$$\begin{cases} \mathbf{L}_{i,d} = N_i - o_{i-1} \\ \mathrm{d}_i = \dfrac{\mathbf{L}_{i,d} \cdot \boldsymbol{Z}_{i-1}}{|\boldsymbol{Z}_{i-1}|} \end{cases} \tag{28}$$

$$\begin{cases} \mathbf{L}_{i,a} = o_i - M_i \\ \mathrm{a}_i = \dfrac{\mathbf{L}_{i,a} \cdot \boldsymbol{X}_i}{|\boldsymbol{X}_i|} \end{cases} \tag{29}$$

4. Case study and results

4.1 Experimental setup

To obtain accurate results, a laser measuring method to obtain the end effector's position is adopted. The laser tracker is Leica AT960, whose accuracy is $15\,\mu\mathrm{m} + 6\,\mu\mathrm{m/m}$ (Hexagon Manufacturing Intelligence. 2020). The calibration system includes the laser tracker, robot and a laser measuring ball, as Figure 10 shows. The laser measuring ball is linked at the end tip. For each measurement, the joint values $\mathrm{J}({\theta_1}^m, {\theta_2}^m, {\theta_3}^m, {\theta_4}^m, {\theta_5}^m, {\theta_6}^m)$ are recorded, and the end effector positions P_{ee} $({x_{ee}}^m, {y_{ee}}^m, {z_{ee}}^m)$ are measured by the laser tracker. Every joint moves individually and points can be recorded.

4.2 Experiments with robot and results

The physical experiments with robot Luban were committed to verify the algorithm. By this algorithm, the DH parameters of Luban are calculated in Table 2 and indices of robot Luban are shown in Table 3. Position error plots are shown in Figure 11.

Figure 10 (a) Schematic diagram of experiment; (b) laboratory experiment in lab

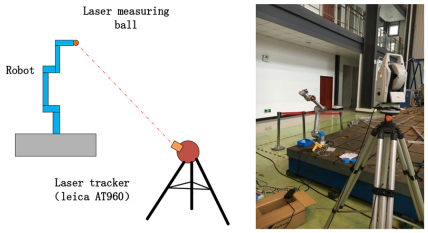

(a) (b)

The maximum position error is $5.6048 \times 10^{-4}\,mm$. The standard deviation of the results shows the algorithm results are stable. In the fusion application, the motion accuracy of the robot is around 0.001 mm which demands the design of the fusion application and it is the universal industrial standard. Comparing to the stereo vision algorithm based autonomous robot calibration (Zhang *et al.*, 2017), the calibration accuracy is improved greatly because the model is unique with the restriction of LSM. Comparing with Guanbin's results (Gao *et al.*, 2018), this method is better than Guanbin's method in time-consuming. The time spent in the calculation is 2.568 and 1.7123 *s* with and without building 3 D view in Matlab (The computer configuration: Intel(R) Core(TM) i7-5500U CPU @2.40 GHz, RAM 8 G, Win10 64 bit). The reason is that the Jacobian matrix, which is 3 by 24, needs to be calculated in Guanbin's method for every sample's iterations. What's more, the Guanbin's Jacobian matrix uses the singular value decomposition to do the dimension reduction analysis, which also complicates the solving procedure. According to the analysis, the space complexity of the algorithm of Guanbin is larger than the geometric method which need not iteration.

5. Conclusions and future work

In this article, a DH parameter identification method based on the geometric model was proposed. The experimental results have shown the geometric method is a very useful and simple way, being based on the DH parameter definition and the least square method, to reduce complex calculations. The main idea of this algorithm is finding the least error in every fitting procedure of the DH model and its advantages are as following:

- Compared to other methods that need to calculate the Jacobian matrix, the geometric method can determine a model uniquely and especially reduce the computational cost.
- Most intelligent algorithms can also solve the calibration problems and find the parameters. However, the intelligent algorithms are mostly based on great data for training, testing and validation, the process will cause overfitting and lower efficiency. And for those cases out of training data, the accuracy will become low. Besides, most intelligent algorithms cannot identify the parameters which may have co-relation with others (except Markov Monte Carlo algorithms); therefore, they cannot handle calibration problem precisely for the robots which have redundant degrees of freedom. For the geometric method, however, it can find uniquely answer for any kind of serial robots.

Table 2 The experimental DH parameters of Luban

	α/°	a/mm	d/mm	θ/°
1	0	0	0	–
2	89.997628	0	0	0
3	9.7387692e−04	499.920830	6.0062018e−05	89.999925
4	0.007442900	396.05868	0	0
5	89.9940462	2.7755575e−17	142.493238	90.001137
6	89.999608	2.2204460e−16	112.522514	179.993626
7	0	0	250.013002	–

Table 3 The indices of robot Luban

	Maximum (mm)	Standard deviation (mm)	Average (mm)	Absolute average (mm)
Position error	5.604842e–04	8.8200705e–05	3.1343745e–04	3.134374e–04
***x*-axis position error**	−3.695606e−04	1.028226e−04	−1.250163e−04	1.328032e−04
***y*-axis position error**	−4.024017e−04	8.873898e−05	−1.945386e−04	1.945386e−04
***z*-axis position error**	−3.701478e−04	9.757018e−05	−1.571290e−04	1.621207e−04

Figure 11 Position error of physical experiment

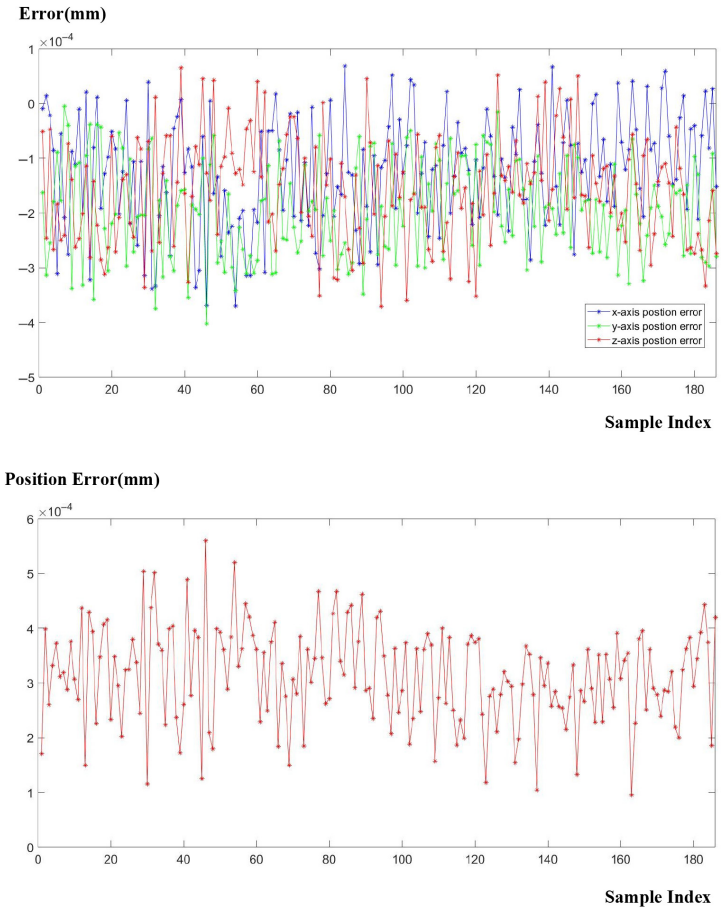

- The method proposed in the paper can find any kind of joint parameters, like revolute joints or prismatic joints. It is a good universal method for industrial applications.

In the future, we will study the methods integrate geometric method with intelligent methods, such that the new method can be widely applied to any kind of robots in industrial with high efficiency and accuracy.

References

Bennett, D. and Hollerbach, J. (1991), "Autonomous calibration of single-loop closed kinematic chains formed by manipulators with passive endpoint constraints", *IEEE Transactions on Robotics and Automation*, Vol. 7 No. 5, pp. 597-606.

Chang, C., Liu, J., Ni, Z. and Qi, R. (2018), "An improved kinematic calibration method for serial manipulators based on POE formula", *Robotica*, Vol. 36 No. 8, pp. 1244-1262.

Daney, D., Papegay, Y. and Madeline, B. (2005), "Choosing measurement poses for robot calibration with the local convergence method and Tabu search", *The International Journal of Robotics Research*, Vol. 24 No. 6, pp. 501-518.

En.wikipedia.org (2020), "68–95–99.7 Rule", available at: https://en.wikipedia.org/wiki/68%E2%80%9395%E2%80%9399.7_rule (Accessed 15 July 2020).

Gao, G., Sun, G., Na, J., Guo, Y. and Wu, X. (2018), "Structural parameter identification for 6 DOF industrial robots", *Mechanical Systems and Signal Processing*, Vol. 113, pp. 145-155.

Hexagon Manufacturing Intelligence (2020), "Leica absolute tracker AT960", available at: www.hexagonmi.com/products/laser-tracker-systems/leica-absolute-tracker-at960 (accessed 15 July 2020).

Hollerbach, J. and Wampler, C. (1996), "The calibration index and taxonomy for robot kinematic calibration methods", *The International Journal of Robotics Research*, Vol. 15 No. 6, pp. 573-591.

Huang, J. (2003), "Least-squares solution of the matrix equation $[a_1 xb_1, a_2 xb_2]= [c,d]$", *Journal of Sichuan Normal University*, Vol. 26 No. 4, pp. 370-372.

Ikits, M. and Hollerbach, J. (1997), "Kinematic calibration using a plane constraint", *Proceedings of International Conference on Robotics and Automation*.

Janeschitz, G. (2001), "Plasma–wall interaction issues in ITER", *Journal of Nuclear Materials*, Vols 290/293, pp. 1-11.

Kim, K., Oh, S., Baek, S., Titus, P., Brown, T., Kessel, C. and Zhai, Y. (2013), "A preliminary conceptual design study for Korean fusion demo reactor magnets", *2013 IEEE 25th Symposium on Fusion Engineering (SOFE)*.

Maisonnier, D. (2008), "European DEMO design and maintenance strategy", *Fusion Engineering and Design*, Vol. 83 Nos 7/9, pp. 858-864.

Newman, W., Birkhimer, C., Horning, R. and Wilkey, A. (2000), "Calibration of a Motoman P8 robot based on laser tracking", *Proceedings 2000 ICRA. Millennium Conference. IEEE International Conference on Robotics and Automation. Symposia Proceedings (Cat. No.00CH37065)*.

Nubiola, A. and Bonev, I. (2013), "Absolute calibration of an ABB IRB 1600 robot using a laser tracker", *Robotics and Computer-Integrated Manufacturing*, Vol. 29 No. 1, pp. 236-245.

Nubiola, A., Slamani, M. and Bonev, I. (2013), "A new method for measuring a large set of poses with a single telescoping ballbar", *Precision Engineering*, Vol. 37 No. 2, pp. 451-460.

Palmieri, G., Palpacelli, M., Carbonari, L. and Callegari, M. (2018), "Vision-based kinematic calibration of a small-scale spherical parallel kinematic machine", *Robotics and Computer-Integrated Manufacturing*, Vol. 49, pp. 162-169.

Santolaria, J., Conte, J. and Ginés, M. (2012), "Laser tracker-based kinematic parameter calibration of industrial robots by improved CPA method and active retroreflector", *The International Journal of Advanced Manufacturing Technology*, Vol. 66 Nos 9/12, pp. 2087-2106.

Santolaria, J., Conte, J., Pueo, M. and Javierre, C. (2014), "Rotation error modeling and identification for robot kinematic calibration by circle point method", *Metrology and Measurement Systems*, Vol. 21 No. 1, pp. 85-98.

Song, Y., Wu, S., Li, J., Wan, B., Wan, Y., Fu, P., Ye, M., Liu, S. and Gao, X. (2013), "Concept design of CFETR Tokamak machine", *2013 IEEE 25th Symposium on Fusion Engineering (SOFE)*.

Tanaka, S. and Takatsu, H. (2008), "Japanese perspective of fusion nuclear technology from ITER to DEMO", *Fusion Engineering and Design*, Vol. 83 Nos 7/9, pp. 865-869.

Taylor, W. (1986), "Robotics in practice by J. F. Engelberger Kogan page, London, 1980(£10.C)", *Robotica*, Vol. 4 No. 4, pp. 286-286.

Wang, W., Song, H., Yan, Z., Sun, L. and Du, Z. (2018), "A universal index and an improved PSO algorithm for optimal pose selection in kinematic calibration of a novel surgical robot", *Robotics and Computer-Integrated Manufacturing*, Vol. 50, pp. 90-101.

Wu, Y., Klimchik, A., Caro, S., Furet, B. and Pashkevich, A. (2015), "Geometric calibration of industrial robots using enhanced partial pose measurements and design of experiments", *Robotics and Computer-Integrated Manufacturing*, Vol. 35, pp. 151-168.

Zhang, X., Song, Y., Yang, Y. and Pan, H. (2017), "Stereo vision based autonomous robot calibration", *Robotics and Autonomous Systems*, Vol. 93, pp. 43-51.

Zhuang, H., Wang, K. and Roth, Z. (1994), "Optimal selection of measurement configurations for robot calibration using simulated annealing", *Proceedings of the 1994 IEEE International Conference on Robotics and Automation*.

Zhuang, H., Wu, J. and Huang, W. (1997), "Optimal planning of robot calibration experiments by genetic algorithms", *Proceedings of IEEE International Conference on Robotics and Automation*.

Corresponding author

Qi Wang can be contacted at: 807073429@qq.com

Publication III

Tao, Z., Song, Y., Wu, H., Zheng, L., Cheng, Y., Handroos, H., Zhang, X., and Ji, H.
Hybrid collision detection perceptron of the robot in the fusion application

Reprinted with permission from
Fusion Engineering and Design
Vol.160: 111800, 2020

Fusion Engineering and Design 160 (2020) 111800

Contents lists available at ScienceDirect

Fusion Engineering and Design

journal homepage: www.elsevier.com/locate/fusengdes

Hybrid collision detection perceptron of the robot in the fusion application

Zhang Tao[a,b,c], Yuntao Song[a], Huapeng Wu[c], Lei Zheng[a,*], Yong Cheng[a,d], Heikki Handroos[c], Xuanchen Zhang[a,b], Haibiao Ji[a,c]

[a] Institute of Plasma Physics Chinese Academy of Sciences (ASIPP), Chinese Academy of Sciences, He'fei, 230000, China
[b] University of Science and Technology of China, He'fei, 230000, China
[c] Lappeenranta University of Technology (LUT), Lappeenranta, Finland
[d] Huainan New Energy Research Center, Anhui Provincial Key Laboratory of Special Welding, Huai'nan, 232000, China

ARTICLE INFO

Keywords:
Hybrid perceptron
Collision detection
Fusion robot

ABSTRACT

In a complicated fusion device, the robot is at risk of colliding with its surroundings when it moves. In this article, a hybrid collision detection perceptron is studied to ensure the safety for both the fusion device and the robot. Primary component analysis is adopted as a preprocessor for extracting the features of the data. The stochastic gradient descent, Adam and Adagrad are used as classifiers with different learning rate methods. From the simulation results, it proves that this hybrid perceptron is more valid than the traditional detection method based on the dynamic model, and it reduces the complexity of robot modeling.

1. Introduction

Fusion devices have lots of complicated mechanisms, such as China Fusion Engineering Test Reactor (CFETR) [1], ITER [2], the Japanese J-Demo [3], k-Demo in Korea [4] and the European DEMO [5]. Remote handling is a universal way to maintain these devices. As of today, many studies have been made about inspection, such as the EAST Articulated Maintenance Arm (EAMA) [6], Articulated Inspection Arm (AIA) [7], and so on. At the same time, more and more researchers tend to study the developed maintenance works such as screwing, renewal of components, welding, and so on. These operations need more delicate maintenance algorithms such as path planning, force and position control, and collision detection. Multi-Purpose Deployer (MPD) is a remote handling system that is inspired by AIA, EAMA, and other fusion robot designs [8]. It includes two parts: the body and dual arm effectors. In fact, the main body robot is a heavy and long chain robot that only concentrates on rough positioning for the dual arm effector on the fusion device. The dual arm effectors mainly focuses on delicate work, such as the renewal of tiny components. The workspace for effectors is smaller and more irregular than the body arm in Fig. 1. They might collide with fusion devices, which would affect the safety of both the robots and the reactors, so collision detection for the dual arm effectors is important. However, the traditional method builds the dynamic model to detect collision [9], which is inefficient and complex in modeling because the end effectors for MPD would require increasingly different mechanisms and demand different maintenance in the future. A universal and intelligent method is more important to meet these requirements. This article introduces a hybrid collision detection perceptron for MPD end effectors, and the simulation proves its validity.

This article comprises four chapters. The first chapter introduces some background and presents the necessity of the algorithm. The preliminary algorithm is illustrated in a step-by-step way in section 2. The third section shows the simulation and the results of the perceptron, while the fourth section summarizes and comments on this work.

2. Hybrid collision detection perceptron

A robot must always be calibrated on kinematics and dynamics parameters before it is put into use to ensure the accuracy of the robot's motion. The normal method of collision detection is to calculate the error between the nominal generated force and the actual generated force which can be calculated by dynamic model and be simulated or measured by simulator or sensor respectively to detect collision. For example, for a real robot, the nominal current and actual current are indexes to show the nominal and actual forces' value which can be estimated by the dynamic model and measured by sensor respectively. The difference between these indexes can be used for judging the collision. Hence, it is necessary to build up a dynamic model for the robot and calibrate all of the physical parameters basing on this method. However, building a robot dynamic model is complicated. As for the dynamic model of a serial robot, a minimum set of physical parameters would exist that should be calibrated for dynamic equation based on the

* Corresponding author.
E-mail address: 1395532235@qq.com (L. Zheng).

https://doi.org/10.1016/j.fusengdes.2020.111800
Received 18 February 2020; Received in revised form 26 April 2020; Accepted 28 May 2020

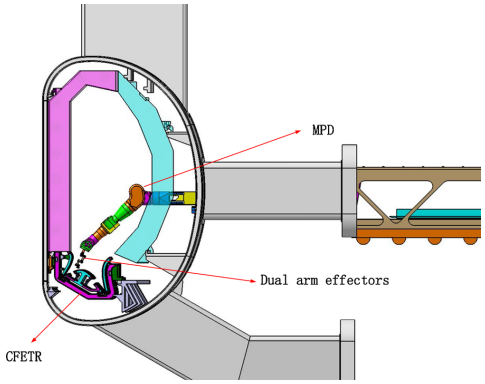

Fig. 1. MPD with dual arm effectors.

minimum set of inertial parameters method [10]. Swevers has shown in [11] that those physical parameters were calibrated by excitation trajectory and maximum likelihood estimation (MLE). For example, there are 21 parameters for robot KUKA IR 361. The backward of the algorithm is that modeling of dynamic equations based on the Euler-Lagrange equation is complicated. Meanwhile, the results from the estimation of torque would include Gaussian noise. However, the machine learning method does not need to develop a complicated physical model. Collision detection can be regarded as a binary classification. Using the Principal Component Analysis (PCA), data on robot motion can be recorded, and the data's dimensions can be reduced so that the more significant information will be observed in the primary components' figures. Furthermore, the processed data can be easily classified by perceptron. The hybrid collision detection perceptron is organized in four parts: the robot's PCA model, Logistic Regression (LR), optimization, and hybrid perceptron. The relationship between them is that PCA is the pro-processor, the LR is a classifier, and optimization is an optimizer in the perceptron. Comparing to the other perceptron, this hybrid perceptron combines two parts which are statistics to reduce the dimension of data and machine learning algorithm to train the classifier. The modeling of the perceptron is introduced in this part.

2.1. PCA model

In all robot systems, data on position, speed, and acceleration can be obtained at every step. These signals would be processed or used directly to control a robot manipulator. Meanwhile, this data can train a collision detection perceptron. As for a 7 DOF, there is n× 21 matrix of data, where n is the sample number. Through 100 simulation experiments, 5000 groups of data are recorded forming the two data sheets of the robot system, which are signal matrix (SM) and collision vector (CV). The CV has the information on collision, the elements of which are 1 or -1. However, the SM together with CV cannot be classified directly by perceptron as the accuracy is too low. PCA is a statistical procedure that uses an orthogonal transformation to convert a set of observations of possibly correlated variables into a set of values of linearly uncorrelated variables called principal components (PCs). PCs that have different possible variance could form a series of new coordinates to map the original data into a new PC space. The PCA would always use the singular value decomposition (SVD) method [12]. The SM can be factorized by SVD as shown in Eq. (1):

$$\Psi = U\Sigma V^{T} \tag{1}$$

where Ψ is a datasheet, which is also SM in this algorithm, and Ψ is n× p matrix (n > p). p represents the features of the data. Σ denotes an n× p rectangular diagonal matrix of positive numbers (singular values) σ_k of Ψ. U is an n× n matrix, the columns of which are orthogonal unit vectors of length n called the left singular vectors of Ψ ; and V is a p-by-p whose columns are orthogonal unit vectors of length p and are the right singular vectors of Ψ.

The projection of original data in the PC space can be given in the matrix T, which are the scores that can be used for machine learning instead of the original data.

$$T = U\Sigma \tag{2}$$

In [13], I.T. Jolliffe described the relationship between the rectangular diagonal matrix Σ, the left singular U and the right singular matrix V, which is arbitrary data. Ψ can use the product of new matrixes that are composed by the first of several column vectors of a diagonal and singular matrix to denote its features approximately. This procedure is called dimension reduction (DR). Other key points are that is a rectangular diagonal matrix of positive numbers (singular values) σ_k, which indicates the amplitude of variation of the original data's projection in corresponding PCs, and its singular values would reduce rapidly as the index of k becomes larger.

2.2. Logistic regression

Collision detection can be regarded as a binary classification. The SM is data that is distributed in a high dimension space. A perceptron that is a hyperplane usually behaves badly in classification without preprocessing. The main reasons for this are that coefficients of the regression plane are hard to train because of the original data lacks features. All the data can be projected into PCs and its value is the row vector of U. Supposing k PCs are used for the analysis of collision, the input and output spaces are $\chi \subseteq \mathscr{R}^k$ and $\mathscr{Y} = \{y_1 = +1, y_2 = -1\}$ respectively (+ 1 means safe and − 1 means collision), where k is the number of the data's features. The input vector x∈ χ denotes a sample that can be classified by a perceptron. The hyperplane $\omega^{T} \cdot x + b = 0$ is a separating hyperplane that can classify the high dimension space into two parts: a collision space and a safe space. The ω and b are weights and an intercept respectively. Fig. 2 shows a physical model in two dimensions of the perceptron. The weight vector ω, which is also a normal vector of the hyperplane, can form a border between the collision space and the safe space. The norm of $\frac{b}{\|\omega\|}$ shows the Euclidean distance between the original point and hyperplane. The size of the weight vector ω and input vector x are both k dimensions. In a perceptron, a weight vector ω may not be unique because there might be lots of separating hyperplanes (e.g. the imaginary line in Fig. 2). However, uncertainty regarding the weight vector ω will not influence accuracy if the data is separable. The weight vector ω can be trained by the machine learning algorithm.

The hyperplane can be solved efficiently by LR. LR is a classical

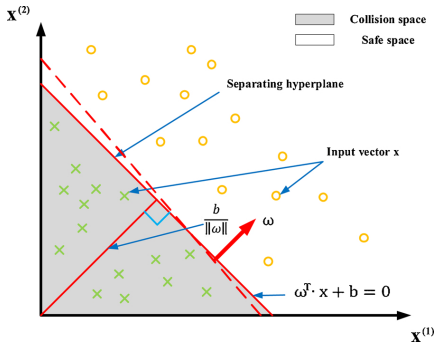

Fig. 2. Perceptron of collision detection.

classification method that has been used widely in many applications including document classification, computer vision, natural language processing, and bioinformatics [14]. In this paper, LR is shown in Eq. (3), which is effective in binary classification.

$$f_i(\omega, b) = \log(1 + e^{-y_i \cdot (\omega^T \cdot x_i + b)}) = sigmod(y_i \cdot (\omega^T \cdot x_i + b)) \tag{3}$$

The condition probability of label $\mathscr{Y}$ is given by Eq. (4). $\omega^T \cdot$ x+ b= 0 defines the hyperplane on the feature space, of which Prob(yx) = 0.5. The condition probability Prob(yx) is larger than 0.5 if the $\omega^T \cdot$ x+ b has the same sign as y= +1, and less than 0.5 otherwise.

$$Prob(y_i x_i) = \frac{1}{1 + e^{-y_i \cdot (\omega^T \cdot x_i + b)}} \tag{4}$$

The logistic loss is the mean of the samples' LR in Eq. (5). The task of the classifier is finding reasonable weights and an intercept using intelligent machine learning, which can be interpreted as $\min_{\omega,b} f(\omega, b)$. When adding the ℓ_1 -norm regularization to $f(\omega, b)$, the ℓ_1 -norm regularized LR problem is denoted in Eq. (6).

$$f(\omega, b) = \frac{1}{n}\sum_{i=1}^{n} f_i(\omega, b) = \frac{1}{n}\sum_{i=1}^{n} \log(1 + e^{-y_i \cdot (\omega^T \cdot x_i + b)}) = -\frac{1}{n} log \prod_{i=1}^{n} Prob(y_i x_i) \tag{5}$$

$$\min_{\omega,b} f(\omega, b) + \lambda \|\omega\|_1 \tag{6}$$

where $\lambda > 0$ is a regularization parameter.

The next section introduces different algorithms such as the stochastic gradient descent (SGD) algorithm, and the Adam and Adagrad solving parameters of perceptron by iteration.

2.3. Optimization

2.3.1. Optimizer

There are lots of optimizers of intelligent control. Compared to other algorithms such as convolutional neural network, ant colony optimization, and particle swarm optimization, the SGD [9], Adam [15], and Adagrad [16] have lower complexities of algorithms so they can be applied in real time control for industrial applications. The gradient updating of the ℓ_1 -norm regularized LR problem can be simplified with Eq. (5), which is deduced in Eq. (7). These procedures are the key to optimizing.

$$\begin{cases} \nabla_b f(\omega, b) = -\frac{1}{n}\Gamma^T(1 - \mathbf{P}) \\ \nabla_\omega f(\omega, b) = -\frac{1}{n}\Psi^T(1 - \mathbf{P}) \end{cases} \tag{7}$$

where $\Gamma = y_1, y_2, \ldots\ldots, y_n{}^T$, $\Psi = y_1 \cdot x_1, y_2 \cdot x_2, \ldots\ldots, y_n \cdot x_n{}^T$, 1 is a n× 1 vector of all, and $\mathbf{P} = \mathbf{sig}(\omega^T \cdot x_1 + b), \mathbf{sig}(\omega^T \cdot x_2 + b), \ldots\ldots, \mathbf{sig}(\omega^T \cdot x_n + b)$.

More generally, the intercept can be regarded as a weight. Correspondingly, the input matrix should be expanded as $\chi \subseteq \mathscr{R}^{k+1}$ where 1 represents adding another first column. Eq. (7) can be simplified by Eq. (8) and the new weights are $\theta = \omega, b^T$. The $\overline{\mathbf{P}}$, $\bar{\Psi}$ are corresponding matrixes based on the expanded input data.

$$\nabla_\theta f = \frac{1}{n}\bar{\Psi}^T(1 - \overline{\mathbf{P}}) \tag{8}$$

The weight updating of SGD, Adam and Adagrad are generalized in Algorithm 1, Algorithm 2, and Algorithm 3 respectively, which can speed up convergence [17].

Algorithm 1 The weight updating of SGD

- Updating the weights:

$$\theta \leftarrow \theta - \alpha \cdot \nabla_\theta f$$

(α: learning rate)

Algorithm 2 The weight updating of Adam

- Updating biased first moment estimate $\mathbf{s_1}$:

$$\mathbf{s_1} \leftarrow \rho_1 \cdot \mathbf{s_1} + (1 - \rho_1) \cdot \nabla_\theta f$$

- Updating biased second moment estimate $\mathbf{s_2}$:

$$\mathbf{s_2} \leftarrow \rho_2 \cdot \mathbf{s_2} + (1 - \rho_2) \cdot \nabla_\theta f^T \cdot \nabla_\theta f$$

- Updating time step:

$$t = t + 1$$

- Correcting bias in first moment $\hat{\mathbf{s}}_1$:

$$\hat{\mathbf{s}}_1 \leftarrow \frac{\mathbf{s_1}}{1 - \rho_1{}^t}$$

- Correcting bias in first moment $\hat{\mathbf{s}}_2$:

$$\hat{\mathbf{s}}_2 \leftarrow \frac{\mathbf{s_2}}{1 - \rho_2{}^t}$$

- Updating the weights:

$$\theta \leftarrow \theta - \alpha \cdot \frac{\hat{\mathbf{s}}_1}{\sqrt{\hat{\mathbf{s}}_2} + \delta}$$

(ρ_1, ρ_2: exponential decay rates for moment estimates, which are in 0,1), suggested defaults: 0.9 and 0.999 respectively; t: time step whose initial value is 0; δ: small constant, perhaps 10^{-8})

Algorithm 3 The weight updating of Adagrad

- Accumulate squared gradient $\mathbf{r}$:

$$\mathbf{r} \leftarrow \mathbf{r} + \nabla_\theta f^T \cdot \nabla_\theta f$$

- Updating the weights:

$$\theta \leftarrow \theta - \frac{\alpha}{\delta + \sqrt{\mathbf{r}}} \cdot \nabla_\theta f$$

(δ: small constant, perhaps 10^{-7}, the initial value of $\mathbf{r}$ is zero)

2.3.2. Learning rate

The algorithms that are based on the gradient descent method updates or tunes weights by learning rates α. There are four classical methods: fixed, decay 1 (denominator decay), decay 2 (exponential decay), and decay 3 (root decay) listed in Table 1. By combining different algorithms with different learning rate updates, the behaviors of the algorithm of collision detection can be analyzed.

2.4. Hybrid perceptron algorithm

Basing on the previous fundament, the flowchart of the hybrid perceptron is shown in Fig. 3. The input is the training data of the robot's information such as the joint angle, velocity and force/current. The output of the perceptron is the predicted collision binary labels. The main body of perceptron includes two parts, which are PCA and classifier. The PCA can be regarded as a preprocessor as with other preprocessors, such as mean centering [18], uniform transformation, and so on. The classifier includes three parts which are the problem, optimizer, and learning rate. In this hybrid perceptron, they refer to ℓ_1 -norm regularized LR, SGD/Adam/Adagrad, and fixed/decay1/decay2/decay3 respectively. After training the model, the perceptron can estimate the collision according to the customer input. Algorithm 4 is showed as follows:

Algorithm 4 The algorithm of Hybrid perceptron

Input: data, batch size, time step $t = 0$, termination t_{end}

Using PCA to preprocess data

Dividing data into mini batches according to the batch size

While $t < t_{end}$

Updating the weights according to the selected algorithm with some batch;

Calculating the cost function of all data;

Updating time step:

$$t \leftarrow t + 1$$

End

Output: weights/perceptron

More generally, this hybrid perceptron should add a threshold to enhance the robustness and safety of the robot because it would be too late if the perceptron to detect the collision. When the hybrid perceptron was determined, the hyperplane would be solved uniquely. The Euclidean distance in Eq. (9) can be solved as a potential parameter for avoiding the risk of collision.

$$d = \frac{|\omega^T \bullet x_1 + b|}{\|\omega^T\|} \tag{9}$$

When the output of perceptron is -1 which means safe, the Euclidean distance would be calculated. The principle with complete safety or potential risk is decided by a designed threshold d_{thre}. Although it would influence some efficient for remote handling, it ensures the safety for both the robot and fusion devices.

3. Simulation and results

3.1. Simulation

For a robot, current, speed, and position messages of the robot's joint can be measured by the sensor at every step. These messages combine with the kinematic model, dynamic model, and independent parameters, which are total mass, independent entries of the inertia tensor and the center of mass [10], which can represent a dynamic rigid robot model in any state. There are lots of simulators of the dynamic model, including Gazebo, Adams, Vrep, and so on. However, Vrep, with CoppeliaSim for the robot, is a special platform that is integrated development environment based on a distributed control architecture: each object/model can be individually controlled via an embedded script, a plugin, an ROS or BlueZero node, a remote API client, or a custom solution. This makes CoppeliaSim very versatile and ideal for multi-robot applications. Controllers can be written in C/C++, Python, Java, Lua, Matlab, or Octave. A urdf file is a robot property file

Table 1
Tuning learning rate method of algorithm.

Method	Rules
Fixed	$\alpha = \alpha_0$
Decay1	$\alpha = \frac{1}{1+\eta_{decay} * N_{epoch}} * \alpha_0$
Decay2	$\alpha = 0.95^{N_{epoch}} * \alpha_0$
Decay3	$\alpha = \frac{k_{decay}}{\sqrt{N_{epoch}}} * \alpha_0$

(α_0: initial value of learning rate; η_{decay}: decay rate; N_{epoch}: epoch number, which is also time step in Algorithm 2; k_{decay}: positive constant).

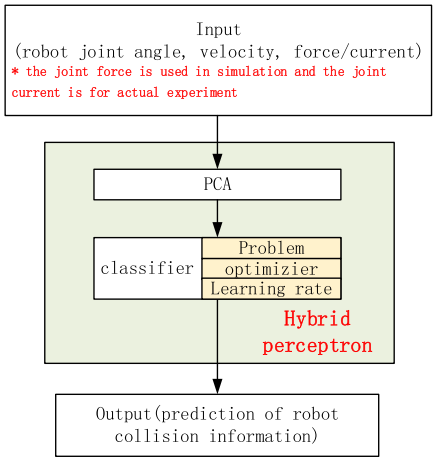

Fig. 3. Flowchart of hybrid collision detection perceptron algorithm.

that defines geometric model, joint type, and independent parameters. When the urdf file is loaded in Matlab and Vrep respectively, a simultaneous model is built up where the model in Matlab is a sensor and controller that can read joint messages and send a control message, and the model in Vrep is a physical prototype that can move as a real robot. In this part, a simulation of KUKA LBR iiwa is tested by Vrep and the architecture is designed as shown in Fig. 4. The KUKA LBR iiwa is one of the dual arm effectors of MPD. In Vrep, there are five parts that are mainly used in the simulation, including a physical dynamic model, physical kinematics model, collision model, physical engine and sensor. The first three are generated automatically when a urdf file is loaded and the last two should be customized based on the application. The physical dynamic model is a 3D model that includes the geometric shape, the physical parameters such as mass, inertia tensor and the center of mass. The physical kinematics model defines the geometric size, joint type and kinematic relationship between different segments of the robot. The collision model refers to a geometric model with grid processing which is only for the collision. Usually, this is also a universal method for checking the interference as same as Catia and Solidworks. Basing on this mechanism of Vrep, it's convenient to obtain the collision message (y= ±1) from the simulation by the collision model. The Matlab model includes a robot mathematic model, a hybrid perceptron, a controller, and data storage. The robot mathematical model contains kinematics and dynamics equations so that the states of the robot, such as the position of the end effector and the generalized force of joint, can be calculated synchronously based on real-time data. A hybrid perceptron can judge a collision based on the supervised machine learning model. The data storage can update the current data and hybrid perceptron model.

Bi-plot is a universal analytical tool for PCA which uses different PCs as the axis to show the status of data [19]. The values of point in bi-plot is the original data's scores corresponding to some PC. For analyzing data sheets with PCA, the different bi-plots can be drawn by combining different PCs. The blue lines are other PCs which are converted into some PCs' bi-plot. Fig. 5 shows two states that are collision and safety, respectively. For example, there is an obvious border between collision and safety by PC1&PC2 bi-plot in Fig. 5a. However, PC1 &PC5 bi-plot cannot classify collision and safety.

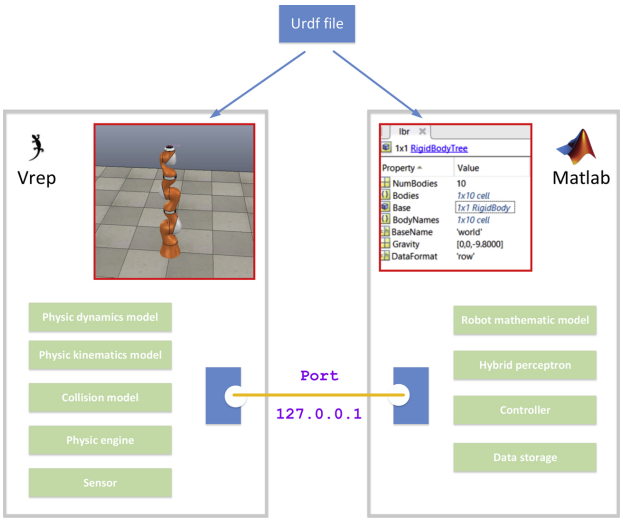

Fig. 4. Simulation diagram between Vrep and Matlab.

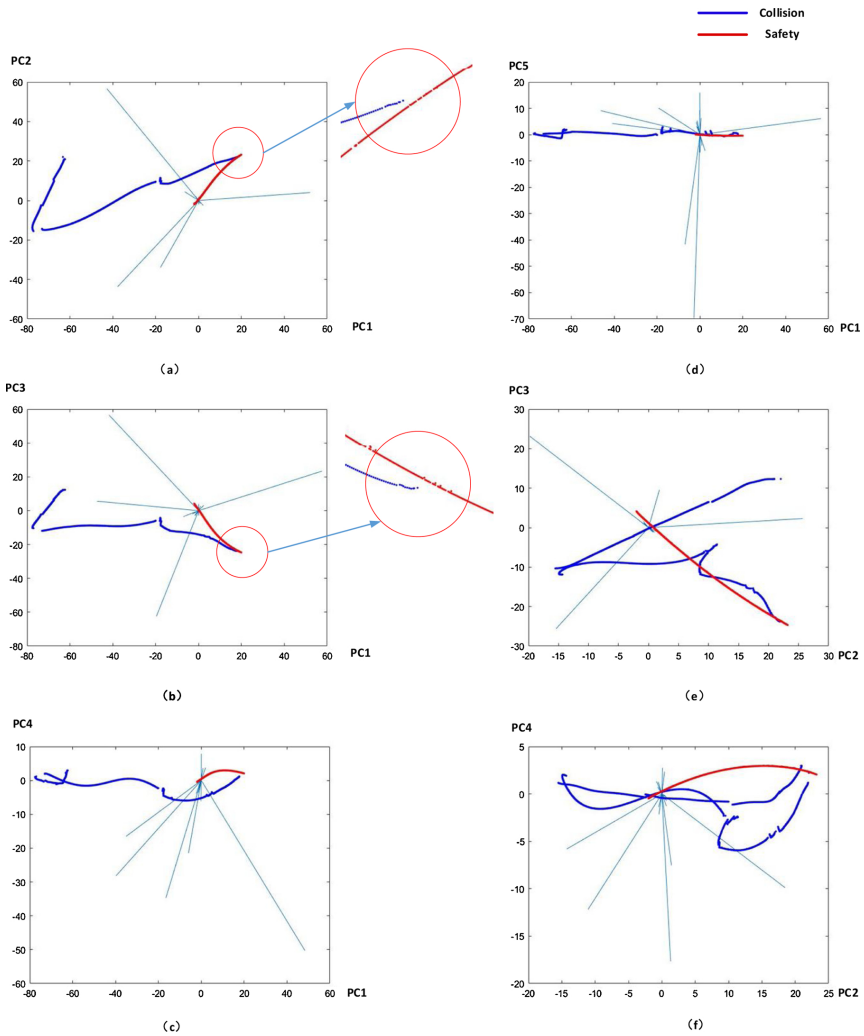

Fig. 5. Biplots of principal component analysis.

3.2. Results

Collision detection can be analyzed using PCA analysis. Fig. 5 shows the biplots of data. From the figures a, b, and c, there is a specific border between the collision and safety space, which shows the flexibility of PCA for preprocessing. As we knew, the optimizers are sensitive to the initial value of the learning rate. The experiments are committed by α= 0.1,1 with a step size of 0.01, with the batch size equal to 10 in Fig. 6. Modeling with the 4000 training sets and 1000 testing sets, as shown in Table 2, the maximum accuracy is 0.9880 in testing sets by the SGD-fixed algorithm with α= 0.94. The maximum mean accuracy is 0.8857 by SGD- decay2. However, the Adagrad has two invalid combinations, which are Adagrad-fixed and Adagrad-decay3. The perceptron's maximum, minimum and mean of them are same, whose N/A means inoperative in Table 2. Overall, the SGD algorithm has better properties than the others. The experiment results of cost and accuracy are shown in Figs. 7 and 8 with α= 0.94. Although the SGD with the fixed learning rate did not converge, the accuracy is higher than other

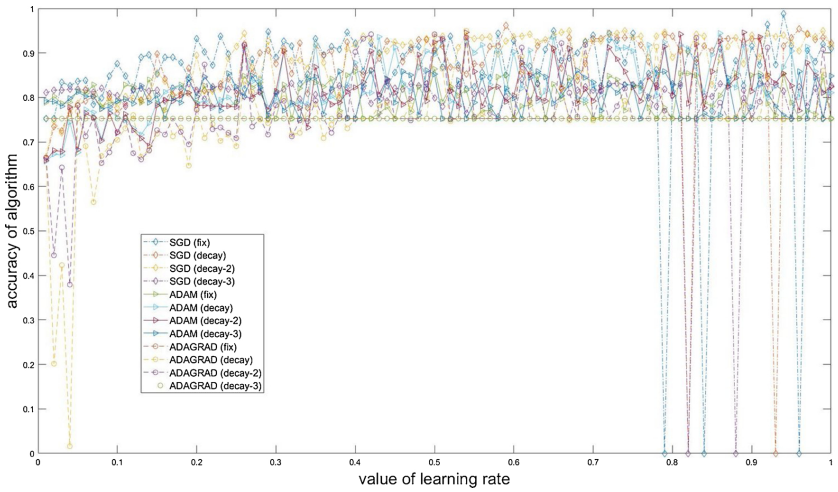

Fig. 6. Accuracy of algorithm with different initial learning rates.

Table 2
Some indexes of algorithm with different learning rates.

Accuracy	maximum	minimum	mean	variance
SGD-fixed	0.9880	0	0.8507	0.0249
SGD-decay1	0.9621	0	0.8584	0.0187
SGD-decay2	0.9501	0.6667	0.8857	0.0038
SGD-decay3	0.8403	0	0.7903	0.0135
Adam-fixed	0.8643	0.7525	0.8015	0.0012
Adam-decay1	0.9461	0.6567	0.8300	0.0045
Adam-decay2	0.9461	0.6587	0.8160	0.0040
Adam-decay3	0.8603	0.7525	0.8028	0.0014
Adagrad-fixed	0.7525	0.7525	0.7525	N/A
Adagrad-decay1	0.9501	0.0160	0.7429	0.0129
Adagrad-decay2	0.9421	0.3792	0.7658	0.0073
Adagrad-decay3	0.7525	0.7525	0.7525	N/A

combinations. From Fig. 7, the misclassification is mainly centralized between − 1, −2 of x_2 for SGD, and between − 2,0.5 of x_1 for Adam. The classifier for Adagrad is invalid. Besides, Fig. 7 shows that convergence has little relation to the accuracy of the classifier.

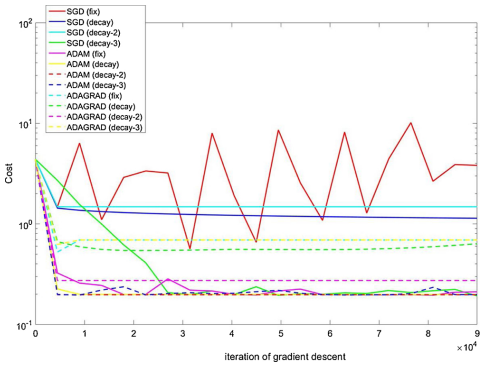

Fig. 7. Cost of algorithm with.α= 0.94

4. Conclusions and future work

The results of the hybrid perceptron for collision detection are flexible. This algorithm will be tested in the physical fusion robot in the future. It indicates the flexibility of the dynamic model free method of fusion robot and can reduce the complexity of dynamic modeling, especially for heavy and large-scale fusion robots. However, the accuracy cannot reach 100 %, which might be sensitive to the initial value's precision or the calculating precision of the algorithm. The Kalman predicted or other predicted algorithms can be studied further to prevent the collision, together with a hybrid perceptron to promote accuracy. Meanwhile, the definition of actual robot's collision would be defined basing on the current criterion or other methods. Furthermore, this algorithm will be tested in the physical prototype of dual arm effectors. The real-time performance will be studied to help optimize the algorithm.

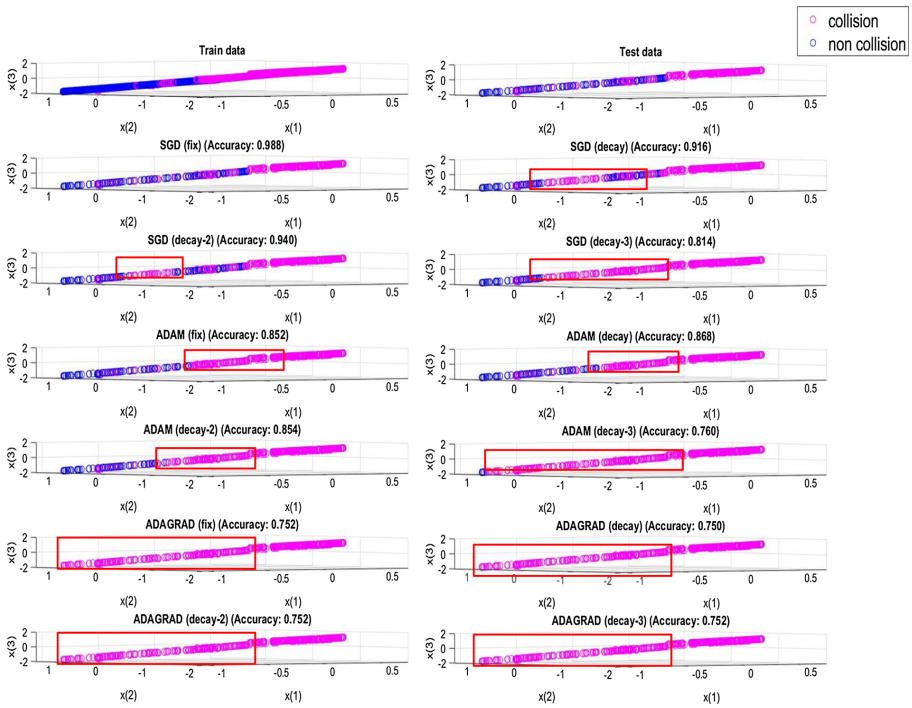

Fig. 8. Accuracy of algorithm with.α= 0.94

CRediT authorship contribution statement

Zhang Tao: Conceptualization, Methodology, Writing - original draft. **Yuntao Song:** Supervision. **Huapeng Wu:** Supervision. **Lei Zheng:** Visualization. **Yong Cheng:** . **Heikki Handroos:** Supervision. **Xuanchen Zhang:** . **Haibiao Ji:** Visualization.

Declaration of Competing Interest

The authors declare that they have no known competing financial interests or personal relationships that could have appeared to influence the work reported in this paper.

Acknowledgments

This project is funded by Engineering Design in support of CFETR 2017YFE0300503. Thanks to the ASIPP and LUT colleagues for the inspiration about this geometric algorithm.

Appendix A. Supplementary data

Supplementary material related to this article can be found, in the online version, at doi:https://doi.org/10.1016/j.fusengdes.2020.111800.

References

[1] Y.T. Song, S.T. Wu, J.G. Li, B.N. Wan, Y.X. Wan, P. Fu, et al., Concept design of cfetr tokamak machine, IEEE Trans. Plasma Sci. 42 (3) (2014) 503–509.
[2] JANESCHITZ, Plasma-wall interaction issues in iter, J. Nucl. Mater. 290 (73) (2001) 1–11.
[3] S. Tanaka, H. Takatsu, Japanese perspective of fusion nuclear technology from iter to demo, Fusion Eng. Des. 83 (7-9) (2008) 865–869.
[4] K. Kim, S. Oh, S.H. Baek, P. Titus, Y. Zhai, A preliminary conceptual design study for Korean fusion Demo Reactor magnets, Fusion Engineering (SOFE), 2013 IEEE 25th Symposium on. IEEE (2013).
[5] D. Maisonnier, European demo design and maintenance strategy, Fusion Eng. Des. 83 (7-9) (2008) 858–864.
[6] Tao Zhang, et al., Deformation modeling of remote handling EAMA robot by recurrent neural networks, Ind. Rob. 46 (2) (2019) 300–310.
[7] Y. Perrot, J.J. Cordier, J.P. Friconneau, L. Gargiulo, E. Martin, J.D. Palmer, et al., Iter articulated inspection arm (aia): R&D progress on vacuum and temperature technology for remote handling, Fusion Eng. Des. 75-79 (2005) 537–541 (none).
[8] H. Pan, K. He, Y. Cheng, Y. Song, Y. Yang, E. Villedieu, et al., Conceptual design of east multi-purpose maintenance deployer system, Fusion Eng. Des. 118 (2017) 25–33.
[9] Peter C. Müller, Robot dynamics and control: Mark W. Spong and M. Vidyasagar, Automatica 28 (3) (1992) 655–656.
[10] M. Gautier, W. Khalil, Direct calculation of minimum set of inertial parameters of serial robots, IEEE Trans. Robot. Autom. 6 (3) (1990) 368–373.
[11] J. Swevers, C. Ganseman, D. Tukel, J.D. Schutter, H.V. Brussel, Optimal robot excitation and identification, IEEE Trans. Robot. Autom. 13 (5) (1997) 730–740.
[12] D. Kalman, A singularly valuable decomposition: the svd of a matrix, Coll. Math. J. (0) (2020), https://doi.org/10.1080/07468342.1996.11973744.
[13] I. Jolliffe, Principal component analysis, International Encyclopedia of Statistical Science, (2011), pp. 1094–1096.
[14] H. Robbins, S. Monro, A stochastic approximation method, Herbert Robbins Selected Papers, (1985), pp. 102–109.
[15] D. Kingma, J. Ba, Adam: a method for stochastic optimization, Computer Science, (2014).
[16] J. Duchi, E. Hazan, Y. Singer, Adaptive subgradient methods for online learning and stochastic optimization, J. Mach. Learn. Res. 12 (7) (2011) 257–269.
[17] I. Goodfellow, Y. Bengio, A. Courville, Deep Learning, The MIT Press, Cambridge, MA, 2017.
[18] J.D. Kromrey, L. Foster-Johnson, Mean centering in moderated multiple regression: much ado about nothing, Educ. Psychol. Meas. 58 (1) (1998) 42–67.
[19] Christina Lyra, T. Halme, A. Torsti, T. Tenkanen, Kaarina Sivonen, Site-specific restriction endonucleases in cyanobacteria, J. Appl. Microbiol. 89 (2001) 979–991, https://doi.org/10.1046/j.1365-2672.2000.01206.x.

Publication IV

Zhang, T., Song, Y., Wu, H., Handroos, H., Cheng, Y., and Zhang, X.
Deformation modeling of remote handling EAMA robot by recurrent neural networks

Reprinted with permission from
Industrial Robot
Vol.46, No.2. pp300-310, 2019

Deformation modeling of remote handling EAMA robot by recurrent neural networks

Tao Zhang
Institute of Plasma Physics Chinese Academy of Sciences (ASIPP), Chinese Academy of Sciences, Hefei, China and University of Science and Technology of China, Hefei, China and School of Energy Systems, Lappeenranta University of Technology (LUT), Lappenranta, Finland
Yuntao Song
Institute of Plasma Physics Chinese Academy of Sciences (ASIPP), Chinese Academy of Sciences, Hefei, China
Huapeng Wu and Heikki Handroos
Department of Mechanical Engineering, School of Energy Systems, Lappeenranta University of Technology, Lappeenranta, Finland
Yong Cheng
Huainan New Energy Research Center, Anhui Provincial Key Laboratory of Special Welding, Hefei, China, and
Xuanchen Zhang
Institute of Plasma Physics Chinese Academy of Sciences, Hefei, Anhui, China

Abstract

Purpose – Remote handling (RH) manipulators have been widely studied for maintenance tasks in fusion reactors. Those tasks always require heavy load, high accuracy and large work space for manipulators. Traditionally, the maintenance of fusion devices always depends on manual RH. With the development of calculating ability, the intelligent automatic maintenance makes it possible for a fusion device instead of the previous manual operation. As the flexibility of arm and the deformation of manipulator will cause problems, which are mainly inaccuracy and lower efficiency. This paper aims to study an effective way to promote the arm behavior to solve these problems.

Design/methodology/approach – By making use of the experimental advanced superconducting tokamak articulated maintenance arm as a platform, a series of experiments is designed to measure errors of kinematics and to collect the database of the flexible arm. Through studying the data and the arm structure, recurrent neural network (RNN) method was adopted to estimate the deformation of flexible arm and eventually compensate deformation in robot control to achieve higher accuracy.

Findings – By means of delicate RNN modeling, errors of kinematics have been reduced to a smaller order than the RH mode. This intelligent maintenance method will also reduce complexity of operations in maintenance.

Originality/value – This paper presents the use of an artificial intelligent algorithm to solve a nonlinear deformation problem of the flexible arm. The results demonstrate that it is efficient in dealing with this problem in fusion application. The RNN's successful application has also shown that intelligent algorithms can be widely applied in fusion maintenance.

Keywords Deformation estimation, EAMA, Flexible robot, Recurrent neural network

Paper type Case study

1. Introduction

A fusion device is a complicated, high-radiant and hyper thermal reactor (Li, 2015). To meet the demands of reactor's effective use, the advanced remote handling (RH) technology is inevitably required for assembly and maintenance of components under radiation condition (Tada *et al.*, 1995). Long and flexible arms have big workspace so that they can complete a large-size reactor's maintenance. However, the long length and flexibility of arms make it difficult to control the robot in the deployment. Due to the complicated operation atmosphere in fusion application, flexible arms are always deployed slowly so that their deformation is nearly regarded as a static problem in an actual operation (Shi *et al.*, 2017). There are two dominant trends in fusion maintenance, which are RH and intelligent maintenance. RH is a manual operation which is equipped with sensors such as cameras in atmosphere and cameras in hand to monitor and control robot motion by workers. In contrast to RH, intelligent maintenance focuses on automatic motion to commit some task, as the complicated surrounding cannot ensure camera's delicate work, and thus in RH mode, a well-experienced operator is always needed. Currently, many

The current issue and full text archive of this journal is available on Emerald Insight at: **www.emeraldinsight.com/0143-991X.htm**

Industrial Robot: the international journal of robotics research and application
46/2 (2019) 300–310
 [ISSN 0143-991X]
[DOI 10.1108/IR-08-2018-0171]

Received 19 August 2018
Revised 11 October 2018
6 November 2018
Accepted 8 November 2018

works have been done in manual RH, while intelligent maintenance research will attract more attention in future.

Technology in RH has been studied a lot in Europe since the beginning of this century. The "Tile Carrier Transfer Facility" and Octant 1 boom for RH system, a heavy-weighted robot system to aid the manipulator to travel up in the vessel with an extended boom comprising five new links totaling 9.4 m in length, have been developed by the Joint European Torus (Loving *et al.*, 2012). The articulated inspection arm (AIA) (Cordier *et al.*, 2003; Perrot *et al.*, 2005) in France and EAST articulated maintenance arm (EAMA; EAST: experimental advanced superconducting tokamak) (Shi *et al.*, 2016) in China are both articulated flexible arms, which are equipped with a gripper or a camera and adopt flexible cable connections. The AIA is an 8-m-long multi-link carrier with five identical modules of diameter of 160 mm. The EAMA is a long multi-link carrier with length of 9.9 m and weight of 98.88 kg. The multi-purpose deployer (MPD) (Manuelraj *et al.*, 2016) is an RH maintenance robot, which uses joint connection in ITER. The whole arm of MPD is more than 28 ton in weight and is 18 m in length. A hybrid kinematic manipulator (Keep *et al.*, 2017), which weighs 80 ton, is being designed at Remote Applications in Challenging Environments of UK Atomic Energy Authority to handle large breeder blanket segments for demonstration fusion power reactor. All in all, each robot, mentioned above, adopts the RH maintenance. Furthermore, a long length and heavy weight of a robot will cause a big deflection error in the RH of fusion application, and the error needs to be estimated and compensated to improve performance during maintenance processes. In traditional RH, the sag of robot is manually adjusted by operators, but it is also time-consuming and less effective in error compensation. Self-compensation is absolutely necessary in intelligent automatic maintenance.

Recently, more and more researchers have paid attention on the problem and have come up with intelligent maintenance methods to solve it. Li *et al.* (2018) adopted deterministic and Bayesian artificial neural networks (NNs) to analyze the flexible joint's deformation by using simulation results to train network without actual tests. Shi *et al.* (2017) adopted the back propagation NN in solving static errors about the EAMA segment, concerned about three-dimensional errors. Flexible arms always have six-dimensional errors, which include three positional errors and three orientational errors. Mou (1997) has done some work on structural, kinematic and thermal-induced errors in 1997 with the help of NNs. He found that errors between a rigid model and an actual model have some differences, which would influence the robot accuracy. Through the NN and the inverse kinematics simulation, machine tools' accuracy has been promoted. Frik and Kleutges (1997) used the feed forward network to predict the elastic deformation of arms, and more than 90 per cent predictions are useful for sag estimation. Johnson *et al.* (1990) came up with an adaptive model-based NN controller through neural network payload estimation; he succeeded in estimating error to enhance tracking accuracy in variable payload. As the error models of robots are nonlinear in different positions, artificial intelligence algorithms offer better solutions than traditional compensation methods.

This paper is concerned about the long and heavy-weighted flexible arm's deformation compensation by adopting a supervised method, i.e. the recurrent neural network (RNN). The RNN was first deduced by Williams and Zipser (1989) in 1989. The algorithm does not require a precisely defined training interval and has some memory functions that consider all previous results' influence during iteration.

This paper first introduces an RNN modeling method for estimating the deflection of EAMA robot and then describes the compensation method. The paper is organized as follows: in Section 2, the deformation kinematics model, compensational network structure and compensation algorithm (CA) of EAMA are presented; in Section 3, the mathematic model of the EAMA's segment IV, as an important segment model, is built. According to the mathematic model, a relevant experiment was set up and results have been shown and discussed in detail. Future work and conclusions are given in Section 4.

2. Deformation kinematics modeling of robot experimental advanced superconducting tokamak

The EAST (internal designation HT-7U), shown in Figure 1, is an experimental superconducting tokamak magnetic fusion energy reactor in Hefei, China. It is the first tokamak to use superconducting toroidal and poloidal magnets. Due to rigorous atmosphere restriction of fusion application, the EAMA's design parameters are extreme as shown in Table I. Through several iterated designs for EAMA, the ASIPP designed an arm as Figure 2 shows, which is a long flexible arm equipped with a 3-DOF gripper. To achieve enough operating space and load capacity of the arm, the cable driven and clevis structure has been adopted. However, this type of long and flexible mechanism also brings problem of big error due to its flexibility and heavy weight. It is vital to eliminate the error and compensate error to ensure the arm can deploy better.

Figure 1 EAST

Table I D-H parameters of the EAMA's segment

Temperature	Running: 80°C; baking: 120°C
DOFs	1 (shuttle) + 7 (arm) + 3 (gripper)
Operating conditions	EASTVV, R: 1920 mm, r: 550 mm
Docking port	EAST P port, ϕ250 mm
Workspace	Inspection: 100%, maintenance: ~90%
Port and CASK dimension	Diameter: ~160 mm, CASK length: ~10 m
Payload	25 kg for arm, 2 kg for gripper
Repeatable Accuracy	~20 mm

2.1 Deformation kinematics with joints and payload variants

In the design of EAMA system (Shi *et al.*, 2016), the actuators are placed inside robot tubes with cables to drive arm. In addition, through horizontal rods, the parallelogram structure can ensure that the axis of rotation joint is always vertical. However, because of the flexible cables and the coupling of parallelogram structure, the deformation of arm is nonlinear and not unique, e.g. a vertical force on the center of the arm end may cause both vertical deformation and twist deformation about the arm axis. The structure's nonlinearity will lead to the deformation's irregularity, and the segment of arm's sag cannot be regarded as a beam's deformation easily (Verl *et al.*, 2006), and thus, we need find a way to predict the error instead of traditional manual compensation methods.

Actually, when a robot is deployed to commit a mission, it is always equipped with tools and payload, and robot's self-flexibility and external payload will also influence its accuracy. Furthermore, different poses of robots (different joint values) with the same external payload lead to different deflection.

When we use the end of arm frame as a study object, robot error mainly includes two parts: position and orientation errors, which represent the gap between the theoretical frame and real frame, are described by pose errors and denoted as a vector with six components: δ_x, δ_y, δ_z, $\delta\theta_x$, $\delta\theta_y$ and $\delta\theta_z$:

$$\delta = \begin{bmatrix} \delta_x & \delta_y & \delta_z & \delta\theta_x & \delta\theta_y & \delta\theta_z \end{bmatrix}^T \tag{1}$$

where δ_x, δ_y and δ_z are the displacement errors between the real and theoretical frame and $\delta\theta_x$, $\delta\theta_y$ and $\delta\theta_z$ are the angle errors between the real and theoretical frame, which are also regarded as errors in pitch, yaw and roll.

The aim of this study is to find a modeling method to estimate the errors and finally eliminate the errors of flexible arm. Figure 3 shows two different arm states.

2.2 Recurrent neural network modeling of deformation kinematics

The NN is an efficient estimating method for a nonlinear system, and it has been widely used in many circumstances, such as autonomous navigation and error estimation. It has been developed in several decades and made some progress in many fields, especially in artificial intelligent control. Considering the repeatability problem of robot (Figure 12), we

Figure 2 Mechanical structure of EAMA

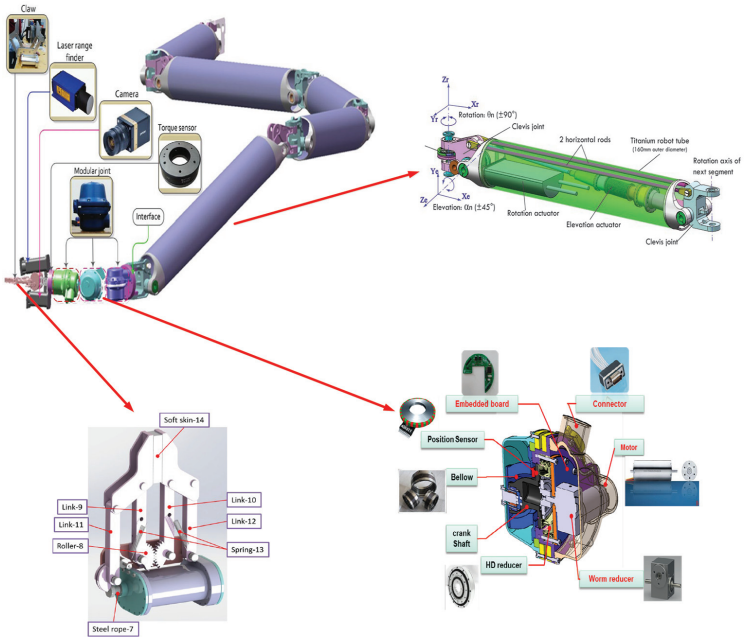

Figure 3 Position relations between the real frame and theoretical frame

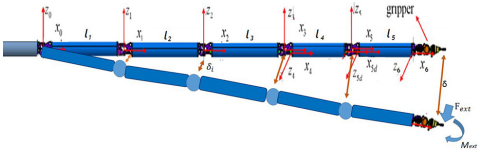

find that the position of some states cannot been uniquely determined with current payload and joint state. The position of measure points also is relevant with the previous position, and the memory function for estimating error is suitable in EAMA application. Compared with other methods, the RNN methods do not require a precisely defined training interval and have some memory functions that consider all previous results' influence during iteration. Therefore, we choose the RNN method to estimate deformation, and it showed excellent performance.

There are two ways to solve this problem, as shown in Figure 4. In the figure, both the serial network structure and the whole network structure can build up the network to estimate error. The serial network structure has five sub-networks, and the whole network structure only has one network. For the second structure, only single segment experiment should be tested, and it would be easier than the first structure that deploys the EAMA in the big space. As we know, the EAMA is a huge-scale and low-speed robot. If we want to collect enough data to build up a network, it would be a time-consuming process. In this paper, the serial network structure is studied and the specific procedures are introduced as follows.

Figure 4 Two different network structures for EAMA

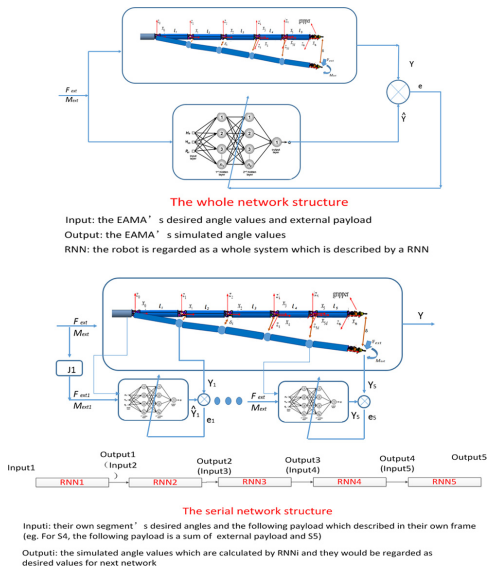

The RNN is a nonlinear and memory-based network (Zhang *et al.*, 2007). We assume that a multivariable plant is an i-inputs and j-outputs system and can be described as follows:

$$X(p+1) = W(p)x(p) + V(p)\mathrm{h}(p) + \theta \tag{2}$$

$$h(p) = S(X(p)) = \frac{1}{1+e^{-X(p)}} \tag{3}$$

where:

p = the time step;
$X(p)$ = the input vector of neural neuron;
θ = the threshold applied to neuron;
$h(p)$ = the output vector of neural neuron;
$W(p)$ = the weight vector of previous layer output;
$V(p)$ = the weight vector of current layer for recurrent/memory; and
$S(\cdot)$ = the logistic squashing function of neural node (the sigmoid function is adopted).

According to the rule, the RNN (Botvinick and Plaut, 2006) can be established as shown in Figure 5. This network adopts dynamic back propagation algorithm to train all weights. Some notations in Figure 5 can be described as follows:

I = The input vector for network, equaling to $[i_1\ i_2 \ldots i_{i-1}\ i_i]^T$ and i-dimension vector
O = The output vector for network, equaling to $[o_1\ o_2 \ldots o_{j-1}\ o_j]^T$ and j-dimension vector
$X_{l,m}$ = The input vector for neural neuron, which represents the $m-th$ input of the $l-th$. hidden layer
$H_{l,m}$ = The output vector for neural neuron, which represents the $m-th$ output of the $l-th$ hidden layer
$w_{l,m,j}$ = The connective weight between the $m-th$ output from the $l-th$ layer and the $j-th$ input from the $(l+1)-th$ layer (the input layer's l is equal to 0)$v_{l,m}$ = The $m-th$ node's self-current weight at the $l-th$ hidden layer.

To minimize the error of output, a cost function/equation is designed as equation (4). The error is a six-dimensional vector that are the differences between designed position and

Figure 5 Diagram of RNN

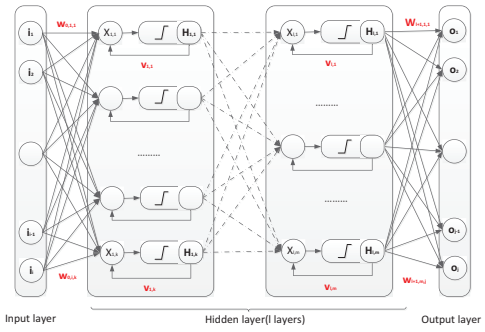

orientation values and actual position and orientation values. The network input consists of the desired segment joint values, external force and external moment, while the network output consists of the predicted joint values that would be used in control for promoting the arm's behavior:

$$E(p) = \frac{1}{2}\sum e_i(p)^2 \tag{4}$$

where:

$$e_i(p) = y_{i,d}(p) - y_i(p) \tag{5}$$

Here, $y_{i,d}(p)$ and $y_i(p)$ are the designed value and the actual value of output layer for ith sample.

Weight updating adopts the back propagation gradient rules. Through gradient descent, tendency will reach optimal values. Weights updating rule is given as:

$$\mathrm{w(p+1)} = \mathrm{w(p)} + \Delta\mathrm{w(p)} \tag{6}$$

$$\mathrm{v(p+1)} = \mathrm{v(p)} + \Delta\mathrm{v(p)} \tag{7}$$

where:

$$\Delta\mathrm{w(p)} = -\alpha\frac{\partial E}{\partial w} = \alpha\cdot\mathrm{x(p)}\cdot\varepsilon\mathrm{(p)} \tag{8}$$

$$\Delta\mathrm{v(p)} = -\alpha'\frac{\partial E}{\partial v} = \alpha'\cdot\mathrm{x(p)}\cdot\varepsilon\mathrm{(p)} \tag{9}$$

Δw, Δv = the differential of weights;
α, α' = the learning rates, being positive constant and less than 1;
x = the neural node's input; and
ε = the error gradient at neuron.

Output prediction is obtained by using iterative method, and detailed steps of the calculation are described as follows:

The EAMA is a large-scaled robot with length over 9.9 m. It is not efficient to build the whole arm model as a full network, because a big arm experiment process is very slow and complicated. So our proposed method is to build a segment network and deduce it to the whole arm forming a serial network, which is combination of a series of single segment network. Segment's error can be easily estimated using RNN with the above study and to generalize universal condition; we built up the mathematic model as shown in Figure 6, which is a j-segment robot arm. By using the base frame as the global frame, the D-H transformation from joint center $Node_i$ to the base frame can be written as equation (10), where the gravity center of Link i in base frame is expressed by ${}^{i}_{B}P_G$:

Figure 6 Universal fusion robot mathematic model

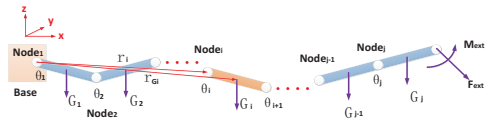

$$ {}^{i}_{B}T = \begin{bmatrix} {}^{i}_{B}R & {}^{i}_{B}P \\ 0 & 1 \end{bmatrix} \tag{10}$$

where:

${}^{i}_{B}T$ = is the D-H transformation from joint center $Node_i$ in base frame;
${}^{i}_{B}R$ = is the D-H rotation transformation from joint center $Node_i$ in base frame; and
${}^{i}_{B}P$ = is the position of joint center $Node_i$ in base frame.

For $Node_i$, the following segments can be regarded as external force and moment. For Segment i, force and moment that are described in base frame and its own frame can be written as equations (11)-(14):

$$ {}^{i}_{B}\mathrm{F} = \sum_{k=i+1}^{k=j} G_k + \mathrm{F}_{ext} \tag{11}$$

$$ {}^{i}_{B}M = \sum_{k=i+1}^{k=j} (r_{G_k} - r_i)\times G_k + M_{ext} + (r_{j+1} - r_i)\times \mathrm{F}_{ext} \tag{12}$$

where:

G_i = the gravity of link i described in the base frame;
${}^{i}_{B}\mathrm{F}$ ${}^{i}_{B}M$ = the whole external force and moment in the ith segment that are described in the base frame respectively;
F_{ext}, M_{ext} = the extern force and moment that are applied in the arm respectively;
r_{G_i}, r_i = the position of the ith segment barycenter and joint center that are described in the base frame respectively.

The whole force and moment in the ith segment that are described in their own frames can be stated as equations (13) and (14), respectively:

$$ {}^{i}_{i}\mathrm{F} = {}^{i}_{B}R^{T}\,{}^{i}_{B}F \tag{13}$$

$$ {}^{i}_{i}M = {}^{i}_{B}R^{T}\,{}^{i}_{B}M \tag{14}$$

Here, θ_i, ${}^{i}_{i}F$ and ${}^{i}_{i}M$ are external inputs for RNN. For each RNN, every segment deformation δ_i can be calculated using the above method, and deformation can be divided into two parts: orientation error $\delta_{o,i}$ and position error $\delta_{p,i}$. The total deformation for the fusion robot is given as:

$$\delta_{o,tol} = \sum \delta_{o,i} = \sum (RNN)_{o,i} \tag{15}$$

$$\begin{aligned}\delta_{p,tol} &= \sum \delta_{p,i}\cdot {}^{i}_{B}R + \delta_{o,i}\times {}^{end}_{i}r \\ &= \sum (RNN)_{p,i}\cdot {}^{i}_{B}R + (RNN)_{o,i}\times {}^{end}_{i}r\end{aligned} \tag{16}$$

where:

RNN_i = the ith segment's RNN; and
${}^{end}_{i}r$ = the end frame described in the ist frame.

2.3 Compensation algorithm for error

The first, second and third segments of EAMA each have only one rotation joint. However, both fourth and fifth segments

have an elevation and a rotation joint. As EAMA arm has only pitch and roll joints, it is possible to compensate the position errors (along X, Y, Z direction) but not able to compensate the orientation errors. So we use a gripper, which has extended rotations about X, Y, Z direction, to compensate its orientation errors. For the position errors, we can make a value function, equation (17), which indicates square error of position accuracy:

$$\Omega(F_{ext}, M_{ext}, \Theta) = \left(FK(\Theta) + \delta_{p,tol}(F_{ext}, M_{ext}, \Theta) - \tilde{P}\right)^2 \tag{17}$$

where:

$\Omega(F_{ext}, M_{ext}, \Theta)$ = is the value function that indicates square error of position accuracy;
$FK(\Theta)$ = is the forward kinematics function based on rigid hypothesis;
$\tilde{P}$ = is the desired position; and
Θ = is the vector of joint values.

To minimize error, we can differentiate equation (18) to find the most suitable joint values:

$$\frac{d\,\Omega}{d\,\Theta} = \left(FK(\Theta) + \delta_{p,tol}(F_{ext}, M_{ext}, \Theta) - \tilde{P}\right) \times \left(\frac{dFK}{d\,\Theta} + \sum \frac{d\left((RNN)_{p,i} \cdot {}^{i}_{B}R + (RNN)_{o,i} \times {}^{end}_{i}r\right)}{d\,\Theta}\right) \tag{18}$$

To simplify expression of equation (18), we introduce equation (19):

$$RNN_i = (RNN)_{p,i} \cdot {}^{i}_{B}R + (RNN)_{o,i} \times {}^{end}_{i}r \tag{19}$$

In equation (18), $\frac{dFK}{d\,\Theta}$ is the Jacobian Matrix of the arm, where:

$$\frac{dRNN_i}{d\,\Theta} = \frac{\partial RNN_i}{\partial^i_i F} \cdot \frac{\partial^i_i F}{\partial\,\Theta} + \frac{\partial RNN_i}{\partial^i_i M} \cdot \frac{\partial^i_i M}{\partial\,\Theta} + \frac{\partial RNN_i}{\partial\,\Theta} \tag{20}$$

Furthermore, RNN is a supervised NN, and it is faster to use numerical derivative than mathematic derivative. So, equation (18) can be rewritten in another way as equation (21):

$$\frac{dRNN_i}{d\,\Theta} = \frac{RNN_i(\Theta + \Delta\,\Theta) - RNN_i(\Theta)}{\Delta\,\Theta} \tag{21}$$

Now we use stochastic gradient descent (SGD) method to update new joint angles to seek optimal values. The SGD method is a drastic simplification for a large-scale machine learning problem compared to gradient descent (Bottou, 2010). We built up SGD as equation (22):

$$\Theta(\mathrm{n}+1) = \Theta(\mathrm{n}) - \gamma_n \cdot \nabla RNN \tag{22}$$

where:

∇RNN = the collection of $\frac{dRNN_i}{d\,\Theta}$ that can be calculated by equation (20); and
y_n = the gain of the SGD in the nth step.

In this system, we use equation (23) to update y_n:

$$\gamma_n = \gamma_0(1 + \lambda \cdot \gamma_0 \cdot n)^{-1} \tag{23}$$

The specific compensation procedure is shown in Figure 7. We input the angles and payload information into a system to calculate compensational values for position in Cartesian space. Through monitoring position error, we can decide whether it is necessary to iterate joint angle values. While they meet the demand, the iteration process will stop, and compensational joint angle values are transmitted to the controller.

3. Case study

3.1 Deformation kinematics of segment IV

The way to solve deformation of a flexible arm is by studying some segment and deducing its network to form a bigger network. The EAMA's structure is shown in Figure 2. Being compared to other segments, Segments 4 and 5 are more complex, and both have two revolute joints and cables to control the arm motion. Moreover, the sag of EAMA is mainly caused by these two segments. It is important to do some dedicated work about deformation compensation to improve the arm performance. The Denavit–Hartenberg (D-H) is the most important method for robot's kinematics. Accordingly, the relationship in adjacent frames (coordinate frame i and frame i-1) can be given by a homogenous transformation matrix A_i and

$$A_i = \begin{bmatrix} \cos\theta_i & -\sin\theta_i\cos\alpha_i & \sin\theta_i\sin\alpha_i & a_i\cos\theta_i \\ \sin\theta_i & \cos\theta_i\cos\alpha_i & -\cos\theta_i\sin\alpha_i & a_i\sin\theta_i \\ 0 & \sin\alpha_i & \cos\alpha_i & d_i \\ 0 & 0 & 0 & 1 \end{bmatrix} \tag{24}$$

where θ_i, a_{i-1}, d_i and α_{i-1} are link parameters of joint i.

Figure 7 CA procedure of EAMA

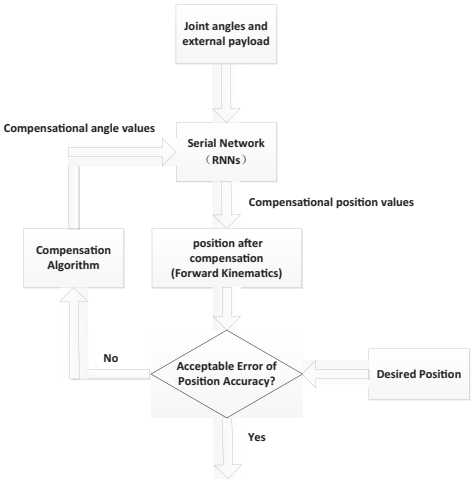

Figure 8 shows the mathematic model of the prototype. Four frames (F_b, F_1, F_2, F_3) in parallelogram structure as the schematic diagram are shown at the bottom of Figure 8. Frame 4 coincides with the measuring point. Because of the parallelogram, there is a passive joint in F_2. Using the D-H method to analyze the whole structure, the parameters can be obtained, and these are listed in Table II. Total transformation for this segment can be calculated by using equation (25):

$$\mathrm{T} = \mathrm{A}_1 \cdot \mathrm{A}_2 \cdot \mathrm{A}_3 \cdot \mathrm{A}_4 \tag{25}$$

Through this theoretical modeling, we can build the mathematical model of Segment 4 and obtain its theoretical position and orientation messages that will be compared with experimental results.

After substituting all D-H parameters into equation (2), the transformation matrix is:

$$\mathrm{T} = \begin{bmatrix} \cos\theta_0 & -\sin\theta_0 & 0 & l_1 \cdot \cos\theta_0 + l_2 \cdot \cos\theta_0 \cdot \cos\theta_1 + l_3 \cdot \cos\theta_0 \\ \sin\theta_0 & \cos\theta_0 & 0 & l_1 \cdot \sin\theta_0 + l_2 \cdot \sin\theta_0 \cdot \cos\theta_1 + l_3 \cdot \sin\theta_0 \\ 0 & 0 & 1 & l_2 \cdot \sin\theta_1 + l_4 \\ 0 & 0 & 0 & 1 \end{bmatrix} \tag{26}$$

3.2 Experimental setup

Many researchers have done relevant work about measuring error. Jiří Volech measured the target center points with the help of laser to design its own error compensation controller and made some progress in improving arm behaviors (Volech *et al.*, 2014). According to previous studies, a testing platform is designed (Figures 9 and 10). There are three measuring points in an L-shape bar, and they can be used to calculate the real frame of a segment. Through applying force and torque to simulate some future task, flexible deformation can be measured using the laser tracker (Leica AT401). Gravity-orientated load and torque load can be tested as shown in Figures 9 and 10, respectively. With the help of a laser tracker, the measure points' information can be indirectly recorded.

Figure 8 Mathematics model of prototype

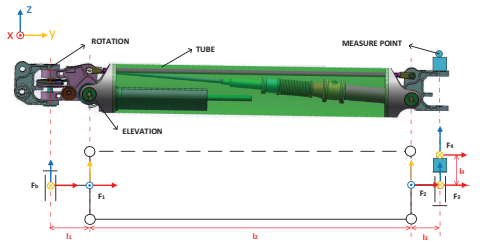

Table II D-H parameters of the EAMA's segment

Index	α_i	a_i	d_i	θ_i
1	90°	l_1	0	θ_0
2	–90°	l_2	0	θ_1
3	0	0	l_3	$-\theta_1$
4	0	0	l_4	0

Figure 9 Gravity-orientated loads for the segment

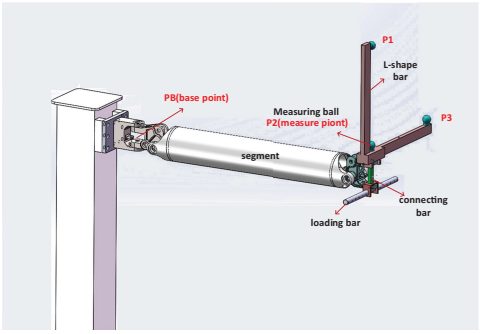

Figure 10 Torque loads for the segment

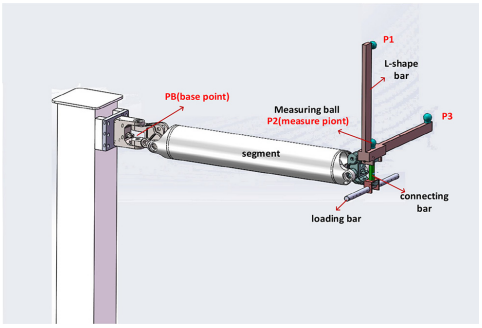

We use P to represent weight (Figure 9), which is a weight loading on the segment. The torque bar (Figure 10) can rotate along with the rotation axis, and its rotation angle is θ_{Bar}. According to the parallelogram law, we use τ_0 and τ_{90} to represent torque, which are components of external torque at the y-axis and x-axis, respectively. Following the mechanics principle, the external force vector is:

$$\Psi = \begin{bmatrix} P \\ \tau_0 \\ \tau_{90} \end{bmatrix} = \begin{bmatrix} P \\ P_0 \cdot l \cdot \cos\theta_{Bar} \\ P_{90} \cdot l \cdot \sin\theta_{Bar} \end{bmatrix} \tag{27}$$

where

l = the distance from force point to the center of mass;
θ_{Bar} = the angle with respect to the y-axis; and
Ψ = the external force, applied at the end of the segment; the input of RNN.

Figure 11 shows specific testing procedures in the RH lab. The Leica AT401 can track measuring balls and record data

Figure 11 Accuracy measuring testing in RH lab

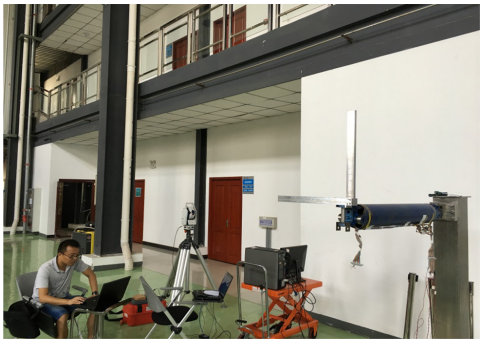

automatically. Through this platform, we can collect input data, the desired joint values and external payload and output data, which can be calculated by values of the measuring balls.

3.3 Recurrent neural network modeling of one segment and results

We can find that deformation estimation between tensile and compressive state is different by means of studying the data of the measuring balls. Through applying different payloads ranging from 0 to 24 kg and then from 24 kg to 0 (the interval is 4 kg) for the same joint setting value, there are 13 points in each of the measure points. Figure 12 shows the positions of four main measure points in different payloads. From Figure 12, it can be inferred that repeatability is not good with same payloads when the segment is in certain state that load is added or reduced to the same value. Because the deformation of tensile and compressive state is different in cables and can cause bad repeatability, a state flag that shows the segment's state (tensile or compressive state) should be added into the network to give better predictions. As the current state (payload and joint values) can only determine uniquely the position and this position is also relative with the previous state, we should use some memorable algorithm to solve this case. The RNN has a memorable function and can address this problem perfectly.

Through selecting different payload that is equipped at the end of the segment, the behavior of the arm accuracy can be tested using the laser tracker. This is a slow-motion process so that the arm's problem can be regarded as statics. In the experiment, 124 groups of data have been collected. We used 103 sets of data for training the RNN and 21 sets for verification. Figures 13 and 14 reveal position errors and orientation errors of the segment, respectively. Through 10,000 iterations, error tendency comes to convergence. The oscillation ranges of Position errors and angle errors are no more than 0.1 mm and 0.015°, respectively. In addition, position errors mainly range from 0.03 to 0.83 (mm) and orientation errors from 0.021 to 0.035 (degree). From Figure 13, we can learn that x-axis error has a bigger gap than the y-axis and z-axis error. The reason is that the segment's

Figure 12 Positions of four main measure points in different payloads of some pose

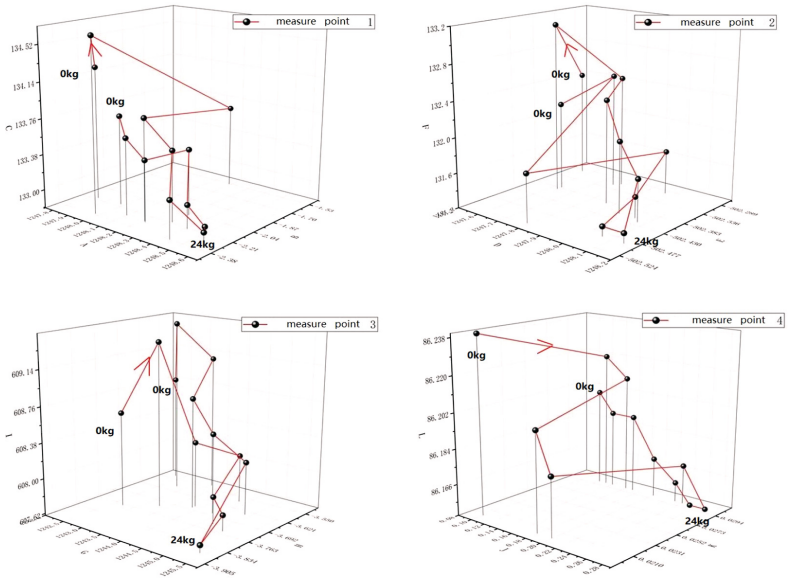

Note: Measured by measuring balls in Figure 9

Figure 13 position error's estimation of segment in 10,000 iterations

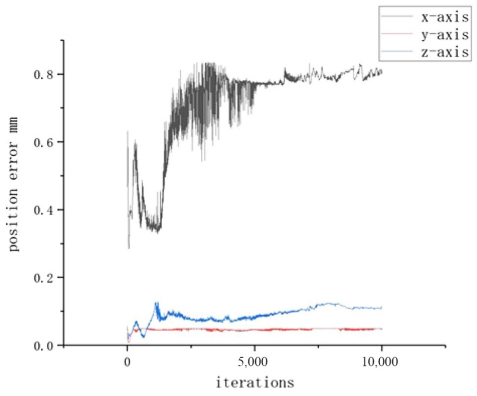

Figure 14 Orientation error's estimation of segment in 10,000 iterations

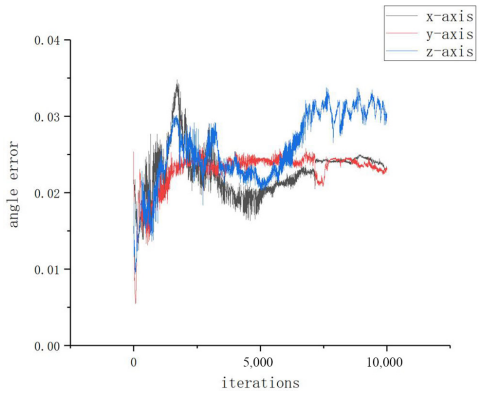

mechanism only has the y-z plane's parallelogram structure. At the same time, the rotation joint is driven by cables, and the deformation of cables will influence the accuracy along the *x*-axis; thus, the predictions along the *x*-axis have bigger error over other axes.

The percentage refers to the ratio of error relative to actual values. Figure 15 shows that the *y*-axis and *z*-axis position error percentages range from 0 to 0.030 and the *x*-axis position error percentage ranges from 0.035 to 0.540 with a larger magnitude over the other counterparts. However, the *x*-axis position error is no more than 0.8 mm such that this a little big percentage error will not influence position accuracy. Figure 16 shows the angle error percentages of the segment and indicates that the majority of the percentages are in the range of 0.00-0.20. As the magnitude of orientation errors is less than 0.035 degree, the orientation errors in different directions are acceptable.

Figure 15 Position error percentages of the 21 sets of verification data

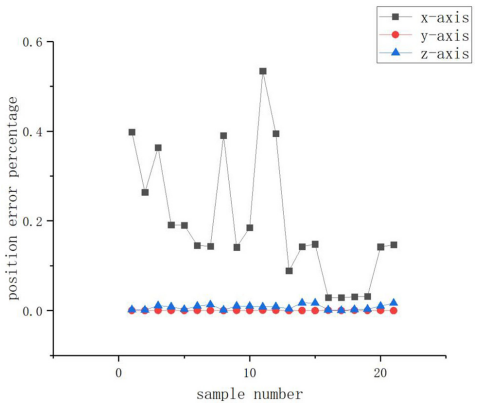

Figure 16 Orientation error percentages of the 21 sets of verification data

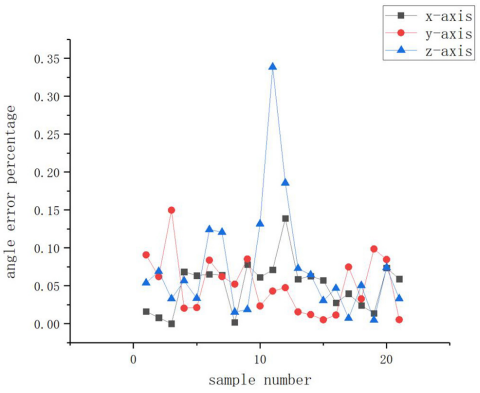

3.4 Full robot deformation estimation and compensation results

Through above study, we can gain a network for every single segment. Then we can similarly build up network for the whole arm, which was mentioned in Sections 2.2 and 2.3. We use the RNN to train each segment to gain weights in network and use the CA to calculate results; the designed and compensational joint values are deduced and listed in Table III. This adequately turns out the feasibility of the RNN and CA. From Table I, we can find that the repeatable accuracy is 20 mm before the compensation in the RH mode. In the experiment, the external force and moment are F_{ext} = 19.6 N and $M_{x,ext}$ = 19.6 N·m and $M_{y,ext}$ = 0 N·m respectively. We selected γ_0 = 0.52 and λ = 1.2 in SGD. The desired joint values and compensational joint values after 353 iterations are listed in Table III, and the position errors with CA iterations are

Table III Desired and compensational joint values of EAMA

Joint	S1	S2	S3	S4a	S4b	S5a	S5b
Desired joint value (degree)	10.00	5.00	−10.00	5.00	20.00	−15.00	10.00
compensational joint value (degree)	9.74	4.65	−10.17	5.32	20.22	−14.35	10.21

Notes: S is abbreviation of segment (S1 means the joint of Segment 1); a means rotation joint (S4a means the rotation joint of Segment 4); and b means elevation joint (S4b means the elevation joint of Segment 4)

shown in Figure 17. When iteration ends, the whole arm position accuracy in *x*-, *y*- and *z*-axes are 1.74276, 4.29624 and 1.77928 mm, respectively, and the total position error $\delta_{p,tol}$ is 4.96596 mm in Cartesian space.

4. Conclusion and future work

RH manipulators have been widely studied for maintenance tasks in fusion reactors. Those tasks always require heavy load, high accuracy and large work space for manipulators. Traditionally, the maintenance for fusion device always depends on manual RH. With the development of calculating ability, the intelligent automatic maintenance makes it possible for a fusion device instead of the previous manual operation, as the flexibility of arm and the deformation of manipulator will cause problems, which are mainly inaccuracy and lower efficiency. This paper introduces a long-beam-redundant degree robot arm (EAMA) for fusion application. As the structure of robot is highly nonlinear, the deflection is also highly nonlinear with respect to the payload. To estimate and compensate the deflection, this paper introduces a nonlinear RNN method to estimate deformation of each segment of robot. Meanwhile, a compensation method for the redundant robot deformation by means of CA has been studied. The reasonable result has been mentioned in the paper. As this paper only considers the effect of statics on the deformation of segments, ignoring dynamics of the robot system, real-time CAs need to be studied in near future to ensure that the robot fulfills the intelligent automatic maintenance operation.

Figure 17 Position error of the whole arm by CA in Cartesian space

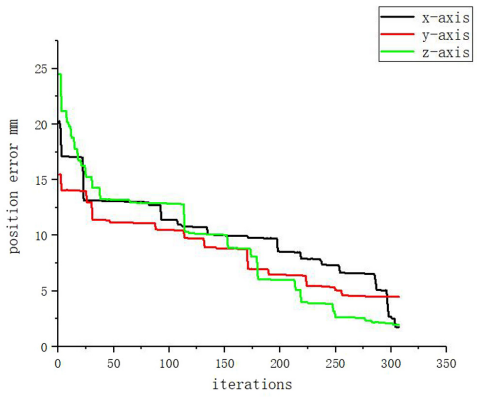

References

Bottou, L. (2010), *Large-Scale Machine Learning with Stochastic Gradient Descent*, Physica-Verlag HD, Heidelberg, 177-186.

Botvinick, M. and Plaut, D. (2006), "Short-term memory for serial order: a recurrent neural network model", *Psychological Review*, Vol. 113 No. 2, pp. 201-233.

Cordier, J., Friconneau, J.P., Gargiulo, L., Grisolia, C., Palmer, J.D., Perrot, Y. and Samaille, F. (2003), "Articulated inspection arm for ITER, a demonstration in the tore supra tokamak", *20th IEEE/NPSS Symposium on Fusion Engineering, Proceedings*, pp. 197-200.

Frik, M. and Kleutges, M. (1997), "Approximation of elastic deformations of robot arms using neural networks", Zamm Journal of Applied Mathematics & Mechanics Zeitschrift Für Angewandte Mathematik Und Mechanik, S91-S92.

Johnson, M.E., Leahy, M.B., Jr. and Rogers, S.K. (1990), "Payload-invariant servo control using artificial neural networks", *Proceedings of SPIE - The International Society for Optical Engineering*, p.1294.

Keep, J., Wood, S. and Gupta, N. (2017), "Remote handling of DEMO breeder blanket segments: blanket transporter conceptual studies", *Fusion Engineering & Design*, Vol. 124, pp. 420-425.

Li, J. (2015), "The status and progress of tokamak research", *Physics*, Vol. 45 No. 2, pp. 88-97.

Li, M., Wu, H. and Handroos, H. (2018), "Comparison of deformation models of flexible manipulator joints for use in DEMO", *IEEE Transactions on Plasma Science*, Vol. 46 No. 5, pp. 1198 -1204.

Loving, A., Allan, P., Sykes, N., Collins, S. and Murcutt, P. (2012), "Development and application of high volume remote handling systems in support of JET and ITER", *Fusion Engineering and Design*, Vol. 87 Nos 5/6, pp. 880-884.

Manuelraj, M.S., Dutta, P., Gotewal, K.K., Rastogi, N., Tesini, A. and Choi, C.H. (2016), "Structural analysis of ITER multi-purpose deployer", *Fusion Engineering and Design*, Vol. 109, pp. 1296-1301.

Mou, J. (1997), "A method of using neural networks and inverse kinematics for machine tools error estimation and correction", *Journal of Manufacturing Science and Engineering*, Vol. 119 No. 2, p. 247.

Perrot, Y., Cordier, J.J., Friconneau, J.P., Gargiulo, L., Martin, E., Palmer, J.D. and Tesini, A. (2005), "ITER articulated inspection arm (AIA): R&d progress on vacuum and temperature technology for remote handling", *Fusion Engineering and Design*, Vols 75/79, pp. 537-541.

Shi, S.S., Wu, H.P., Song, Y.T. and Handroos, H. (2017), "Mechanical design and error prediction of a flexible manipulator system applied in nuclear fusion environment", *Industrial Robot: An International Journal*, Vol. 44 No. 6, pp. 711-719.

Shi, S.S., Song, Y.T., Cheng, Y., Villedieu, E., Bruno, V., Feng, H.S., Wu, H.P., Wang, P., Hao, Z.W., Li, Y., Wang, K. and Pan, H.T. (2016), "Conceptual design main progress of EAST articulated maintenance arm (EAMA) system", *Fusion Engineering and Design*, Vol. 104, pp. 40-45.

Tada, E., Maisonnier, D. and Herndon, J. (1995), "Remote handling technology development for fusion experimental reactors", *Fusion Engineering and Design*, Vol. 29, pp. 249-261.

Williams, R. and Zipser, D. (1989), "A learning algorithm for continually running fully recurrent neural networks", *Neural Computation*, Vol. 1 No. 2, pp. 270-280.

Verl, A., Croon, N., Kramer, C., Garber, T. and Pritschow, G. (2006), "Force free add-on position measurement device for the TCP of parallel kinematic manipulators", *CIRP Annals*, Vol. 55 No. 1, pp. 407-410.

Volech, J., Mráz, L., Šika, Z. and Valášek, M. (2014), "Model of flexible robot with deformation detection", *Procedia Engineering*, Vol. 96, pp. 510-516.

Zhang, Y., Wang, F., Song, Y., Chen, Z. and Yuan, Z. (2007), "Recurrent neural networks-based multivariable system PID predictive control", *Frontiers of Electrical and Electronic Engineering in China*, Vol. 2 No. 2, pp. 197-201.

Further reading

Storn, R. and Price, K. (1997), "Differential evolution - a simple and efficient heuristic for global optimization over continuous spaces", *Journal of Global Optimization*, Vol. 11 No. 4, pp. 341-359, doi: 10.1023/A:1008202821328.

Corresponding author

Tao Zhang can be contacted at: zhangtao@ipp.ac.cn

ACTA UNIVERSITATIS LAPPEENRANTAENSIS

927. FARFAN OROZCO, FRANCISCO JAVIER. In-depth analysis of the global power infrastructure - Opportunities for sustainable evolution of the power sector. 2020. Diss.

928. KRAINOV, IGOR. Properties of exchange interactions in magnetic semiconductors. 2020. Diss.

929. KARPPANEN, JANNE. Assessing the applicability of low voltage direct current in electricity distribution - Key factors and design aspects. 2020. Diss.

930. NIEMINEN, HARRI. Power-to-methanol via membrane contactor-based CO2 capture and low-temperature chemical synthesis. 2020. Diss.

931. CALDERA, UPEKSHA. The role of renewable energy based seawater reverse osmosis (SWRO) in meeting the global water challenges in the decades to come. 2020. Diss.

932. KIVISTÖ, TIMO. Processes and tools to promote community benefits in public procurement. 2020. Diss.

933. NAQVI, BILAL. Towards aligning security and usability during the system development lifecycle. 2020. Diss.

934. XIN, YAN. Knowledge sharing and reuse in product-service systems with a product lifecycle perspective. 2020. Diss.

935. PALACIN SILVA, VICTORIA. Participation in digital citizen science. 2020. Diss.

936. PUOLAKKA, TIINA. Managing operations in professional organisations – interplay between professionals and managers in court workflow control. 2020. Diss.

937. AHOLA, ANTTI. Stress components and local effects in the fatigue strength assessment of fillet weld joints made of ultra-high-strength steels. 2020. Diss.

938. METSOLA, JAAKKO. Good for wealth or bad for health? Socioemotional wealth in the internationalisation process of family SMEs from a network perspective. 2020. Diss.

939. VELT, HANNES. Entrepreneurial ecosystems and born global start-ups. 2020. Diss.

940. JI, HAIBIAO. Study of key techniques in the vacuum vessel assembly for the future fusion reactor. 2020. Diss.

941. KAZARNIKOV, ALEXEY. Statistical parameter identification of reaction-diffusion systems by Turing patterns. 2020. Diss.

942. SORMUNEN, PETRI. Ecodesign of construction and demolition waste-derived thermoplastic composites. 2020. Diss.

943. MANKONEN, ALEKSI. Fluidized bed combustion and humidified gas turbines as thermal energy conversion processes of the future. 2020. Diss.

944. KIANI OSHTORJANI, MEHRAN. Real-time efficient computational approaches for hydraulic components and particulate energy systems. 2020. Diss.

945. PEKKANEN, TIIA-LOTTA. What constrains the sustainability of our day-to-day consumption? A multi-epistemological inquiry into culture and institutions. 2021. Diss.

946. NASIRI, MINA. Performance management in digital transformation: a sustainability performance approach. 2021. Diss.

947. BRESOLIN, BIANCA MARIA. Synthesis and performance of metal halide perovskites as new visible light photocatalysts. 2021. Diss.

948. PÖYHÖNEN, SANTERI. Variable-speed-drive-based monitoring and diagnostic methods for pump, compressor, and fan systems. 2021. Diss.

949. ZENG, HUABIN. Continuous electrochemical activation of peroxydisulfate mediated by single-electron shuttle. 2021. Diss.

950. SPRINGER, SEBASTIAN. Bayesian inference by informative Gaussian features of the data. 2021. Diss.

951. SOBOLEVA, EKATERINA. Microscopy investigation of the surface of some modern magnetic materials. 2021. Diss.

952. MOHAMMADI ASL, REZA. Improved state observers and robust controllers for non-linear systems with special emphasis on robotic manipulators and electro-hydraulic servo systems. 2021. Diss.

953. VIANNA NETO, MÁRCIO RIBEIRO. Synthesis and optimization of Kraft process evaporator plants. 2021. Diss.

954. MUJKIC, ZLATAN. Sustainable development and optimization of supply chains. 2021. Diss.

955. LYYTIKÄINEN, JOHANNA. Interaction and barrier properties of nanocellulose and hydrophobically modified ethyl(hydroxyethyl)cellulose films and coatings. 2021. Diss.

956. NGUYEN, HOANG SI HUY. Model based design of reactor-separator processes for the production of oligosaccharides with a controlled degree of polymerization. 2021. Diss.

957. IMMONEN, HEIKKI. Application of object-process methodology in the study of entrepreneurship programs in higher education. 2021. Diss.

958. KÄRKKÄINEN, HANNU. Analysis of theory and methodology used in determination of electric motor drive system losses and efficiency. 2021. Diss.

959. KIM, HEESOO. Effects of unbalanced magnetic pull on rotordynamics of electric machines. 2021. Diss.

960. MALYSHEVA, JULIA. Faster than real-time simulation of fluid power-driven mechatronic machines. 2021. Diss.

961. SIEVINEN, HANNA. Role of the board of directors in the strategic renewal of later-generation family firms. 2021. Diss.

962. MENDOZA MARTINEZ, CLARA. Assessment of agro-forest and industrial residues potential as an alternative energy source. 2021. Diss.

963. OYEWO, AYOBAMI SOLOMON. Transition towards decarbonised power systems for sub-Saharan Africa by 2050. 2021. Diss.

964. LAHIKAINEN, KATJA. The emergence of a university-based entrepreneurship ecosystem. 2021. Diss.

ISBN 978-952-335-663-4
ISBN 978-952-335-664-1 (PDF)
ISSN-L 1456-4491
ISSN 1456-4491
Lappeenranta 2021